2.5S.1 Basic Geologic and Seismic Information

The geological and seismological information presented in this section was developed from a review of previous reports prepared for the existing units, published geologic literature, interpretation of aerial photography, a subsurface investigation, and an aerial reconnaissance conducted for preparation of this STP 3 & 4 application. Previous site-specific reports reviewed include the STP 1 & 2 FSAR, Revision 13 (Reference 2.5S.1-7). A review of published geologic literature and seismologic data supplements and updates the existing geological and seismological information. A list of references used to compile the geological and seismological information presented in the following pages is provided at the end of Subsection 2.5S.1.

It is intended in this section of the STP 3 & 4 FSAR to demonstrate compliance with the requirements of 10 CFR 100.23 (c).

Presented in this section is information of the geological and seismological characteristics of the STP 3 & 4 site region, site vicinity, site area, and site. Subsection 2.5S.1.1 describes the geologic and tectonic characteristics of the site region and site vicinity. Subsection 2.5S.1.2 describes the geologic and tectonic characteristics of the STP 3 & 4 site area and site. The geological and seismological information was developed in accordance with NRC guidance documents RG-1.206 and RG-1.208.

2.5S.1.1 Regional Geology (200 mile radius)

Using Texas Bureau of Economic Geology Terminology, this subsection discusses the physiography, geologic history, stratigraphy, and tectonic setting within a 200 mi radius of the STP 3 & 4 site. The regional geologic map and explanation (Figure 2.5S.1-5 [References 2.5S.1-8, 2.5S.1-9, 2.5S.1-10 and 2.5S.1-11]) contains information on the geology, stratigraphy, and tectonic setting of the region surrounding the STP site. Summaries of these aspects of regional geology are presented to provide the framework for evaluation of the geologic and seismologic hazards presented in the succeeding sections.

2.5S.1.1.1 Regional Physiography and Geomorphology

The STP 3 & 4 site lies within the Coastal Prairie subsection of the Gulf Coastal Plain Physiographic Province (Figure 2.5S.1-1 [References 2.5S.1-2 and 2.5S.1-3]). The region within a 200 mi radius of the site encompasses parts of the three subsections of the Gulf Coastal Plain Province (Coastal Prairies, Interior Coastal Plains, and Blackland Prairies) (Figure 2.5S.1-6 [Reference 2.5S.1-12]) and a portion of the Edwards Plateau Physiographic province as well as parts of the Llano (Central Texas) Uplift, the Texas-Louisiana Shelf, and the Texas-Louisiana Slope. Each of these physiographic provinces is described briefly in the following sections.

The physiographic provinces in the site region are shown in Figure 2.5S.1-1 (References 2.5S.1-2 and 2.5S.1-3). A map showing the physiographic provinces of Texas as depicted by the Texas Bureau of Economic Geology (BEG) is shown in Figure 2.5S.1-6 (Reference 2.5S.1-12).

2.5S.1.1.1.1 Gulf Coastal Plain Physiographic Province

The Gulf Coastal Plain Physiographic Province (Figure 2.5S.1-6 [Reference 2.5S.1-12]) extends southeast and east from the edge of the Edwards Plateau, (Figure 2.5S.1-6 [Reference 2.5S.1-12]), 200 to 300 mi to the shore of the Gulf of Mexico. The Gulf Coastal Plain has been divided into three sub-provinces: the Coastal Prairies, the Interior Coastal Plains, and the Blackland Prairie.

The Coastal Prairie sub-province begins at the edge of the Gulf of Mexico and extends to the northwest for approximately 50-75 miles. The land surface has an almost negligible slope to the southeast. The sediments are composed of young (Pleistocene and Holocene) unconsolidated deltaic sands, silts, and clays incised by meandering streams that discharge into the Gulf of Mexico. Approximately 26,000 ft of unconsolidated Cenozoic sediments underlie the surface of this sub-province, the details of which are presented in Subsection 2.5S.1.1.3.5. The elevation ranges from sea level to approximately 300 ft, and it is approximately 30 ft MSL at the STP site.

The four periods of continental glaciation that comprise the Pleistocene are reflected by the rising and falling sea levels both along the Gulf and world-wide (eustatic) changes in sea level. Rivers draining the continental interior flowed across the Gulf Coastal Plains and built deltas as they discharged into the Gulf. The most recent of these events, the Wisconsinan Glacial Stage of the late Pleistocene, resulted in the deposition of the Beaumont Formation, which forms the present surface of the Coastal Prairie sub-province. Post-Beaumont erosion and deposition has created terraces within incised channels. These sediments comprise the undifferentiated Deweyville Terrace Deposits.

A rise in sea level beginning approximately 18,000 years ago initiated the geomorphic process of longshore drift sand deposits and deposition of those sands as barrier islands and lagoons. The barrier islands are separated from the mainland by narrow lagoons. Previous high sea level stands can be identified by a series of late Pleistocene ridges (former barrier bars) on the north side of the lagoons. Smaller rivers have discharged sediments into the lagoons nearly filling them.

The Interior Coastal Plains begin at or near the contact between Quaternary and Tertiary sediments (Figures 2.5S.1-1 [References 2.5S.1-2 and 2.5S.1-3], 2.5S.1-5 [References 2.5S.1-8, 2.5S.1-9, 2.5S.1-10, 2.5S.1-11], and 2.5S.1-6 [Reference 2.5S.1-12]) and extend to the northwest 75-150 miles. The sediments are resistant uncemented sands and clays. Down-to-the-coast normal fault systems parallel the coast. Sediments consist of thin red and brown sand and clay. Elevation ranges from 300 ft. MSL to 800 ft. MSL. Underlying the surface sediments are several thousand feet of unconsolidated Cenozoic-age sands and clays. These sediments are described in detail in Subsection 2.5S.1.1.3.5.

The Blackland Prairies (Balcones Escarpment) is the innermost of the Gulf Coastal Plains sub-provinces and consists of upper Cretaceous chalk and marls. Soils consist of fertile, deep, black clay. The surface is gently rolling and agriculturally developed. Elevations range from 450 ft. MSL to 1000 ft. MSL (Reference 2.5S.1-12).

2.5S.1.1.1.2 Edwards Plateau Physiographic Province

The Edwards Plateau is bounded on the south and east by the Balcones Escarpment (Figure 2.5S.1-6 [Reference 2.5S.1-12]). The Balcones Escarpment traces a series of normal faults that follow the Ouachita Tectonic Front, an extension of the Appalachian Front that is present along the entire length of the Eastern seaboard of the United States. The rocks of the Edwards Plateau consist mainly of limestones and dolomites in which caverns and sinkholes are common. Hard and soft strata have created stair-step topography. Streams have eroded the surface by as much as 1800 ft. Elevations range from 450 ft. to 3000 ft. in the principal part of the province, higher in the Stockton Plateau which is the western portion of the Edwards Plateau (Reference 2.5S.1-12).

2.5S.1.1.1.3 Texas-Louisiana Shelf

The continental shelf off the Texas Gulf Coast is termed the Texas-Louisiana Shelf by Coleman et al. (Reference 2.5S.1-13). It has experienced a net progradation (seaward movement) during the Tertiary and Quaternary periods. Clastic materials derived from the uplands to the north have spread across the shelf as the seas transgressed for more than 66 million years. This depositional pattern has been present in the Gulf of Mexico since the Jurassic, and the shelf has prograded approximately 186.4 mi in that time (Reference 2.5S.1-13).

The offshore Texas-Louisiana Shelf is a broad nearly featureless plain. Thin Holocene sediments cover a late Pleistocene fluvial plain. Entrenched stream channels are common, but are filled by Holocene sediments. Carbonate banks occur in places, including true algal-reefs off Galveston, Texas (Reference 2.5S.1-13).

2.5S.1.1.1.4 Texas-Louisiana Slope

The continental slope known as the Texas-Louisiana Slope off the shore of Texas covers 46,332 sq. mi of knoll-and-basin sea floor (Reference 2.5S.1-13). The average gradient is less than 1° but slopes greater than 20° are found near knolls and basins. The extreme change in relief is the result of salt diapirs that have moved upward from the deeper Jurassic-age beds (Reference 2.5S.1-13). Because of rapid sedimentation, growth faults are common and tend to accentuate the shelf-edge break.

2.5S.1.1.2 Regional Geologic History

The geologic and tectonic setting of the STP 3 & 4 site region is the product of a complex history of continental collisions and rifting which spanned a period of more than one billion years. Continental collision more than a billion years ago and continental rifting in the Jurassic followed by deposition of sediments in the newly formed Gulf of Mexico Basin shaped the south Texas terrain.

Major tectonic events in the site region include three compressional deformational events (orogenies) and at least two major extensional events. Direct evidence for most of these events is largely buried beneath the coastal plain sediments in the site region.

2.5S.1.1.2.1 Grenville Orogeny

The earliest of the orogenies recorded in the rocks of the region is the Grenville Orogeny that occurred during the Middle to Late Precambrian (Proterozoic) time, approximately one billion years ago (1000 mya) as a result of continent-to-continent impact along the edge of Laurentia, the ancestral North America. Some reconstructions show only the ancestral African continental mass impacting on the eastern edge of Laurentia, but evidence indicates that Amazonia, the ancestral South American continent, impacted Laurentia along the southern coastal area (References 2.5S.1-14 and 2.5S.1-15).

Rocks of Grenville age are poorly exposed in Texas, occurring only in the Llano Uplift in central Texas, in the Franklin Mountains, and the West Texas Uplifts in west Texas. Based on a few oil and gas borings, Renfro et al. (Reference 2.5S.1-16) indicated that large areas of the state have granitic basement related to the Llano Uplift. The basement beneath STP is believed to be continental crust material (Reference 2.5S.1-17), which is overlain by approximately 40,000 ft. of sedimentary section.

According to Mosher (Reference 2.5S.1-14), Grenville rocks along the southern edge of Laurentia record more than 300 million years of tectonic activity, including both arc-continent and continent-continent collision.

2.5S.1.1.2.2 Late Proterozoic Laurentian Rifting

Following the Grenville Orogeny, late Proterozoic crustal extension and rifting occurred, causing the separation of Laurentia and Gondwanaland, creating the ancestral African continent and the proto-Atlantic (Iapetus) Ocean. In the region of the Gulf of Mexico, shallow seas transgressed across the wide area between Alabama and Texas as the land subsided, possibly over a period of more than 200 million years. Thomas (Reference 2.5S.1-18) suggests that this period included early extension, pervasive rifting and late-stage rifting. Failed rifts (aulocagens) formed graben systems (Reelfoot Rift, South Oklahoma, and Rome Trough), located in the northeastern region of the Gulf of Mexico, indicate late crustal extension along the rift margin (Reference 2.5S.1-18) (Figure 2.5S.1-7 [Reference 2.5S.1-19]).

From the Cambrian to the Early Mississippian periods, the region between the southern Appalachians and the Marathon embayment in west Texas was covered by shallow seas whose deposits record periods of transgression and regression. The early Paleozoic Continental Margin was well inland from the present STP site. According to Thomas (Reference 2.5S.1-18), the STP site area received sediments of the pre-orogeny Ouachita facies - shale, chert, micrite, and sandstone. These sediments have an estimated total thickness of approximately 4000 ft., but no data are available to confirm that these sediments overlie Precambrian basement because this contact is estimated to be some 40,000 ft. below the surface.

2.5S.1.1.2.3 Ouachita Orogeny

From the Middle Mississippian to the Permian periods, the tectonics in the southern edge of Laurentia changed from the spreading (extensional) phase to a closing

(compressed) phase. This is equivalent to the Allegany Orogeny along eastern Laurentia and the Ouachita Orogeny along southern Laurentia when ancestral Africa collided with Laurentia, resulting in the closing of the proto-Atlantic (Iapetus) Ocean.

Rates of deposition were high in the pre-orogenic Ouachita trough (Reference 2.5S.1-20). As the Ouachita orogenic belt developed, thrusting of the sediments in the fore-arc basin toward the north and northwest forming the Ouachita Orogen in North America. There is evidence that this tectonic event began in the Devonian because isotopic ages from metamorphic clasts in the Haymond boulder beds south of the Marathon Region indicate Devonian deformation and metamorphism (References 2.5S.1-20 and 2.5S.1-21). These boulders must have originated from a source south of the Ouachita trough, as Devonian deformation is not known to have affected rocks from the Laurentia side of the proto-Atlantic Ocean.

After late Paleozoic (Late Pennsylvanian-Permian) thrusting created the Ouachita Mountains, the closing of the proto-Atlantic Ocean and the assembly of Pangea was complete.

2.5S.1.1.2.4 Mesozoic Rifting (Opening of the Gulf of Mexico and the Atlantic)

Although there was some sort of basin developed as the proto-Gulf of Mexico prior to the Cretaceous period, there was no connection to the Atlantic Ocean until the Early Cretaceous period. Jurassic-age salt deposits were derived from the evaporation of Pacific seawater that came over the Mexico-Central American region (Reference 2.5S.1-22). No Triassic rocks are known to have been deposited in the region of the present Gulf of Mexico, and the first indication of marine deposition in the present Gulf of Mexico Region are extensive salt deposits of the Middle Jurassic about the time the initial breakup of Pangea began. Salvador (Reference 2.5S.1-22) states that the salt was deposited over continental or transitional crust and that the thick salt suggests that subsidence kept pace with salt deposition.

The initial rifting and crustal extension probably began in the Late Triassic and continued into the Middle to late Jurassic periods. By the Late Jurassic, the emplacement of new oceanic crust in the Gulf of Mexico basin had ended and the new crust cooled and subsided. There still was no connection with the Atlantic Ocean because the Florida and Yucatan Platforms were above sea level during the Jurassic and probably connected to each other (Reference 2.5S.1-22). The proto-Gulf of Mexico and Atlantic Ocean had not been connected.

By the Early Cretaceous period, the Gulf of Mexico Basin was tectonically stable. The Florida Platform had been covered by a transgressing sea and the connection to the Atlantic Ocean had been made. The deposition of sediments from the North American continent had begun in the northern part of the basin brought to the Gulf by the ancestral Mississippi River.

2.5S.1.1.2.5 The Laramide Orogeny

The lithology of deposits along the western and northwestern flanks of the Gulf of Mexico Basin indicates that the Laramide Orogeny began in the Late Cretaceous

period (Reference 2.5S.1-22). In addition, volcanism was occurring in the Balcones fault zone in central and south Texas and offshore Louisiana. The principal effect that the Laramide Orogeny had on the Gulf of Mexico was providing a western source of clastic sediments (the Rocky Mountains) and reducing the connection between the Pacific Ocean and the Gulf of Mexico (Reference 2.5S.1-22). Subsidence continued in the central part of the Gulf of Mexico Basin while there was uplift in the Mississippi Embayment.

2.5S.1.1.2.6 Cenozoic History

Early Cenozoic (Paleocene and early Eocene) rocks and geologic structures record the final thrust faulting and folding of the Laramide Orogeny. Along with the uplift of the Cordillera came an influx of clastic sediments originating from the new terrestrial source. Subsidence of the Gulf of Mexico basin previously due to cooling of newly emplaced oceanic crust now was primarily due to loading of the crust by prograding wedges of sediments. In addition to the loading of the crust, these rapidly accumulating sediments contributed to the development of growth faults, and salt and shale diapirs in the Jurassic salt and lower Cenozoic over-pressured shales respectively (Reference 2.5S.1-22). The location of the depositional centers changed over time. The thickest accumulations during the Paleocene and early Eocene were in northeast Texas, northeast Louisiana, southeast Arkansas, and western Mississippi. During the late Eocene and early Oligocene, the depocenter moved to south Texas, then towards southwest Louisiana. The Pliocene and Pleistocene occurred depocenters west of the Mississippi delta then south of south Texas (Reference 2.5S.1-22). While volcanic materials are found in the Cenozoic sediments of the Gulf Coastal Plain, these are derived from areas in Mexico and other western areas, not within the Coastal Plain Province itself. Marine deposits record sequences of transgression (sea-level rise) and regression (fall) throughout the Cenozoic, but especially during the Pleistocene when continental glaciations held huge volumes of water as icecaps which, when melted during the interglacial periods, caused sea levels to rise world-wide.

2.5S.1.1.3 Regional Stratigraphy

This subsection contains information on the regional stratigraphy within the Coastal Plain Physiographic Province. Figure 2.5S.1-8 (Reference 2.5S.1-23) contains a regional cross section illustrating the regional stratigraphy.

2.5S.1.1.3.1 Basement Rock

Because the Cenozoic section below the Coastal Plain Physiographic Province is thick and the petroleum industry considers the sediments below the Triassic to be barren, few borings that penetrate the full Cenozoic section have been drilled. As a result, there is sparse data on the Pre-Cenozoic sediments overlying basement rock.

The history of investigations of the Gulf of Mexico basin contains contradictory views on the origin and crustal type present beneath the marine and non-marine sediments that are known to be present. As late as 1967, some geologists favored the concept that the basin had been formed at the end of the Precambrian period and existed then as it is today (Reference 2.5S.1-22). Recent interpretation of geophysical (seismic)

survey data suggests that the crust beneath the Jurassic sediments is continental and could not be older than Middle or Late Jurassic (Reference 2.5S.1-22).

2.5S.1.1.3.2 Paleozoic Stratigraphic Units

Little is known about the Paleozoic strata that are away from the structural rim of the Gulf of Mexico Basin. Un-metamorphosed Paleozoic rocks are exposed in the southern Appalachian Mountains, in the Ouachita Mountains, in the Llano Uplift, and in the Marathon Uplift of west Texas, plus two small areas on the eastern edge of the Sierra Madre Oriental in Mexico. The thick sequence of Cenozoic sediments effectively conceals the Paleozoic "basement" around the rim, and virtually no wells have penetrated below the Mesozoic in the deeper part of the basin (Reference 2.5S.1-24).

Between 45,000 ft. and 52,000 ft. of Paleozoic rocks are exposed in the Ouachita Mountains, with approximately 75% of this sequence late Mississippian through mid-Pennsylvanian. The Paleozoic section is thinner in the Marathon Uplift area, with a total of about 18,000 ft. of which about two-thirds are upper Mississippian to mid-Pennsylvanian sandstones and shales with some interbedded limestones. At the Llano Uplift, the Paleozoic section is thinner with only 3500 ft. of sandstones, shale, and limestone.

As recently as 1991, no wells in southern Texas (Reference 2.5S.1-24) had been drilled deep enough to reach Paleozoic rocks. Only two wells had been drilled on the structural rim that penetrated Ouachita facies rocks. The scarcity of wells penetrating the Paleozoic sediments in the south Texas Gulf basin makes it difficult to interpret the paucity of stratigraphic data as well as the geophysical (seismic) data.

The absence of Late Paleozoic and early Mesozoic marine sediments in the Coastal Plain (Reference 2.5S.1-24) surrounding the Gulf of Mexico suggests that this was a positive, stable area until the mid Jurassic. Rifting that accompanied the opening of the Atlantic and the Gulf of Mexico opened depositional basins for mid-Jurassic salt deposits, as noted in the discussion of Mesozoic rifting above (Subsection 2.5S.1.1.2.4).

2.5S.1.1.3.3 Mesozoic Stratigraphic Units

Geologic and geophysical evidence indicates that the present Gulf of Mexico was part of Pangea, a supercontinent landmass at the beginning of the Mesozoic (Reference 2.5S.1-22). The development of the Gulf of Mexico basin occurred with the breakup of Pangea and the opening of the Atlantic Ocean. Sediments from North America began to fill the newly formed basin. The text that follows discusses the opening of the basin and the deposition of approximately 40,000 ft. of sediments above the bedrock crust. A generalized Mesozoic stratigraphic column is shown on Figure 2.5S.1-9 (Reference 2.5S.1-25).

2.5S.1.1.3.3.1 Triassic Stratigraphic Units

The Triassic was a period of tectonic activity comprising rifting in the Gulf of Mexico Basin and breakup of Pangea. Redbeds of Triassic-Jurassic ages are found in the Mesozoic rift basins; however, there are no outcrops of Triassic stratigraphic units

within the STP region (Reference 2.5S.1-26). Redbeds have been encountered in petroleum exploration wells in the Eagle Mills Formation in northeastern Texas. This formation is predominantly composed of red, greenish, or mottled shales and siltstones, which are similar to strata present in the Newark Basin and other Triassic grabens of the Appalachian Mountains. Diabase dikes and sills also are present in the Gulf of Mexico Basin and have been dated from Early to Middle Jurassic by isotopic methods.

2.5S.1.1.3.3.2 Jurassic Stratigraphic Units

The Gulf of Mexico Basin did not appear as a structural feature until the mid-Jurassic period (Reference 2.5S.1-22). Stratigraphic evidence within the region indicates that approximately 200 mya (Figure 2.5S.1-9) the mid-Jurassic Louann Salt forms the basal Jurassic unit, except for the Eagle Mills in the rift basins on the fringes of the basin. The thickness of Cenozoic sediments effectively conceals the Mesozoic strata from investigation in the STP region, although a few petroleum exploration borings have reached the mid-Jurassic salt. These few wells and seismic investigations are the source of data on the salt. The seawater that was evaporated to form the “mother” salt beds originated in the Pacific Ocean and entered the shallow Gulf of Mexico depression across the Mexico platform.

The Louann Salt is mainly coarsely crystalline halite, with anhydrite as the chief additional mineral, but making up at most 10% of the rock (Reference 2.5S.1-26). The Louann Salt is inferred to be present in the STP region, as petroleum wells do not reach depths below the Cenozoic, but there are salt domes in the region, as shown in Figures 2.5S.1-10 (Reference 2.5S.1-27),and 2.5S.1-11 (References 2.5S.1-28, 2.5S.1-29, and 2.5S.1-30). The salt thickness varies with location. The original thickness may have ranged from more than 3300 ft. in east Texas, North Louisiana, and Mississippi salt basins to as much as 13,000 ft. in the Texas-Louisiana Gulf of Mexico slope area (Reference 2.5S.1-26).

Over most of the Gulf, migration of the salt has formed diapirs. Borehole and geophysical data indicate that the base of the salt shows little deformation and unconformably overlies the underlying rocks (Reference 2.5S.1-26).

Following the deposition of the mid-Jurassic Louann Salt, the region was covered by a marine transgression (Reference 2.5S.1-26), which was continuous through the Upper Jurassic. The Middle Jurassic Norphlet Formation represents the basal coarse clastic stratum in the United States, extending from the Florida Panhandle to northeastern Mexico. It is mainly composed of sandstones and conglomerate sandstones with a thickness less than 100-200 ft. in the site region (Reference 2.5S.1-26).

The Upper Jurassic sediments generally form a transgressive and conformable sequence with each successive unit pinching out further landward. This sequence has been interpreted as coastal on-lap due to eustatic sea-level rise. The Upper Jurassic section does not crop out in the U.S. part of the Gulf of Mexico Basin (Reference 2.5S.1-26). However, the Upper Jurassic sediments outcrop in Mexico. This information is based on stratigraphic data from petroleum wells.

In the Gulf of Mexico Basin the Upper Jurassic is predominately marine, with non-marine fluvial and deltaic clastic sediments present in the northern and northwestern basin margins (Reference 2.5S.1-26). The ancestral Mississippi River appears to have contributed clastics to the Gulf in the Late Jurassic - perhaps 150 mya.

The Upper Jurassic sediments do not show evidence of large scale tectonics. The strata are relatively uniform in lithology and do not abruptly change in thickness. The Upper Jurassic was affected by (a) contemporaneous movement of regional tensional normal fault zones, (b) the flow of the underlying Middle Jurassic salt, (c) fluctuations of sea level, and (d) pre-existing topography (Reference 2.5S.1-26).

The Smackover Formation conformably overlies the Norphlet Formation and is composed mainly of carbonates and calcareous shales. The lower unit is a dark-colored carbonate mudstone deposited in a low energy environment while the upper unit is a high-energy oolitic carbonate which is a reservoir rock for oil and gas fields. Thickness of the Smackover Formation may reach as much as 1600 ft. in the STP site region (Reference 2.5S.1-26).

The middle stage of the Upper Jurassic, known as the Kimmeridgian, is not as defined as the lower, or Oxfordian, stage due to the vertical and lateral lithologic variability. In the U.S. Gulf Coastal Plain, the Kimmeridgian is composed of clastics, carbonates, and evaporites. The term “Buckner” has been applied to the lower evaporite section and the overlying, predominately clastic section has been called “Haynesville.” The “Gilmer” Limestone identifies the limestone equivalent of the “Haynesville.” Salvador (Reference 2.5S.1-26) uses the “Haynesville” terminology to describe the entire section between the Oxfordian Smackover Formation and the base of the younger Cotton Valley Group. The Buckner and Gilmer become members of the Haynesville Formation. It seems appropriate for the discussion of these units in the STP region to accept the grouping proposed by Salvador.

The Buckner is characterized by white, pink, or gray massive or nodular anhydrite in thick, massive beds with thinner interbeds of dolomite, argillaceous limestone, anhydritic limestone, and anhydritic or dolomitic mudstone (Reference 2.5S.1-26). Downdip, the Buckner Evaporites seem to grade into oolitic limestone similar to those in the Oxfordian Smackover Formation. In the STP region, the upper part of the Haynesville Formation is the carbonate Gilmer Member. The Haynesville Formation may be more than 1600 ft. thick in the STP region (Reference 2.5S.1-22).

As discussed previously, there is no evidence that the Gulf of Mexico had a connection to the Atlantic Ocean until the deposition of the Buckner Evaporate. Throughout the region, the Buckner represents low energy, hypersaline coastal lagoons overlying the high energy, shallow water marine upper portions of the Smackover Formation (Reference 2.5S.1-26). In the eastern part of the basin, the upper Haynesville Formation is composed of terrigenous clastics, but in the STP region, the influx of clastics was not as strong and the Gilmer Limestone was deposited in high energy, shallow marine conditions.

The upper stage of the Upper Jurassic is called Tithonian. Along the northern part of the basin, the Tithonian consists of a thick wedge of coarse clastics, while on the western and southwestern flanks the Tithonian section is thinner and composed of fine clastics with non-clastics sediments (shales, calcareous shales, and argillaceous limestones (Reference 2.5S.1-26). In the U.S., the northern section is called the Cotton Valley Group and is further divided into Schuler Formation, a nonmarine unit in the upper Cotton Valley, and the Bossier Formation, a predominately marine shale lower unit. In the STP 3 & 4 site region, the Cotton Valley is shaly becoming increasingly sandy in a landward direction.

The Bossier Formation is composed of dark gray to black marine shales and calcareous shales with occasional thin bed of fine-grained sandstone. The Bossier Formation is time transgressive and in the deeper portions of the Gulf of Mexico Basin is time-equivalent to the upper part of the Smackover and Haynesville Formations, and most of the Cotton Valley Group (Reference 2.5S.1-26). The Schuler Formation is composed of a variety of clastics including mudstones, shales, siltstones sandstones, and conglomerates. The coarse clastics give way basin-ward to finer grained sediments that are shades of red and maroon while the coarser clastics shoreward are greenish gray to white. The maximum thickness of the Tithonian sediments in south Texas is between 1600 ft. and 2300 ft. (Reference 2.5S.1-22). The stratigraphic data indicate that the Gulf of Mexico was connected to the Atlantic Ocean during this last stage of the Upper Jurassic period.

2.5S.1.1.3.4 Cretaceous Stratigraphic Units

Through most of Early Cretaceous time, the Gulf of Mexico Basin was the site of continental and marine deposition surrounded by the Appalachian and Ouachita Uplands on the north, and the Llano and Marathon Uplifts to the northwest (Reference 2.5S.1-31). There were marine connections to both the Atlantic and Pacific Oceans. The basin was tectonically stable, although growth faults occurred on the margins related to the influx of terrestrial clastics as the basin center continued to subside.

The thickness of the Lower Cretaceous section varies from 8000 to 11,000 ft. along the northern shelf, thinning to less than 6000 ft. toward the central part of the basin (Reference 2.5S.1-31). In the STP region, the Lower Cretaceous section is primarily carbonates with thin shales and calcareous shales. The upper Cotton Valley Group forms the first stage of the Lower Cretaceous section.

The second stage of the Lower Cretaceous is represented by the Trinity Group, which is composed of the Hosston, Sligo, Pearsall, Glen Rose, and Stuart City Formations. The estimated total thickness of the Trinity Group in the site region is about 2000 ft. (Reference 2.5S.1-31).

In the STP site region, the Hosston Formation unconformably overlies the Cotton Valley strata. In the east, where streams drain the southern Appalachians and the continental interior, the Hosston Formation consists of fine-to-coarse clastics. In the STP site region, the Hosston becomes finer grained and includes a large amount of chert (Reference 2.5S.1-31). Across the northern shelf, the Hosston interfingers with the argillaceous limestones of the Sligo Formation.

The Pearsall Formation conformably overlies the Sligo Formation. The lower part of the Pearsall Formation is called the Pine Island Shale and consists of dark shale interbedded with gray, thin limestones. The James Limestone (also known as the Cow Creek in the site region) overlies the Pine Island from south Texas to Florida (Reference 2.5S.1-31). The James Limestone is a dense non-porous gray limestone interbedded with shale. Overlying the James Limestone is the Bexar Shale forming the upper member of the Pearsall Formation.

Conformably overlying the Pearsall Formation are the limestones of the Glen Rose Formation. In south Texas, these rocks are gray argillaceous dolomite with anhydrite layers. Downdip toward the basin the Glen Rose shelf carbonates interfingers with reef limestones containing rudists, corals, mollusks, and other shallow water bank fauna. This mappable lithology has been named the Stuart City Formation.

Unconformably overlying the Glen Rose Limestone are the shelf limestones of the Fredericksburg Group. In the STP site region, this group includes the Edwards Limestone, which is subdivided in the transgressive West Nueces Limestone, the overlying McKnight Evaporite, and McKnight Limestone. Downdip, the Fredericksburg Group interfingers with the Stuart City Formation, which in turn grades into the basinal micrites and shales of the Atascosa Formation (Reference 2.5S.1-31).

The deposition of Fredericksburg Group strata came to a halt as the land gradually rose and the shoreline regressed at the beginning of Washita Group deposition. The Washita Group includes from older to younger: the upper Cretaceous Georgetown, the upper Cretaceous Del Rio, and upper Cretaceous Buda Limestone. The Georgetown limestone grades basinward into the reef facies of the Stuart City Formation. The Del Rio Formation is thin calcareous shale that is covered by the onlapping Buda Limestone.

During the Lower Cretaceous, the ancestral Gulf of Mexico was connected with the Atlantic and Pacific Oceans as well as the Continental Interior Seaway. The surrounding platforms were stable and were covered with shallow seas. Clastics were brought in along the northern margin by major streams that drained the southern Appalachian Mountains. Long-shore currents flowed westward carrying these clastics away from the deltas. The maximum extent of carbonate deposition took place during the end of the Lower Cretaceous.

In the Gulf of Mexico Basin, the Upper Cretaceous was a period of generally high sea levels that supported the deposition of a continuous cover of Upper Cretaceous rocks. These rocks thicken down-dip (basinward) to a shelf edge that is postulated to follow the reef of the Early Cretaceous period (Reference 2.5S.1-22). In the northern shelf areas, clastic sediments were derived from the southern Appalachian Mountains as they had been in the early Cretaceous. However, toward the end of the period, clastics from a western source, possibly from the nascent Laramide uplift make a more pronounced contribution. The thickest Upper Cretaceous sections are found in the major embayments with as much as 5500 ft. in the Rio Grande Embayment (Figure 2.5S.1-12 [Reference 2.5S.1-32]).

The middle of the Upper Cretaceous occurs within the Washita Group, but there is no major physical discontinuity that defines this contact. The base of the “Gulfian Series” occurs at the the physical break in the mid-Cenomanian, the lowermost stage in the Upper Cretaceous (Reference 2.5S.1-33). The magnitude of the disconformity varies within the Gulf of Mexico Basin and is much less pronounced in the southern part of the basin, suggesting that section has had a different structural history than the northern part (Reference 2.5S.1-33).

The lowermost rocks of the upper Cretaceous, the Del Rio and Buda Limestones, have been discussed as part of the Wichita Group in the Lower Cretaceous.

The Woodbine Formation is the first Upper Cretaceous Unit deposited above the disconformity. In general, this unit is a fluvio-deltaic to marginal marine sequence that is highly variable and complicated. The Woodbine Formation thins south of the type area in east Texas, and the sand content decreases. The outcrop area consists of black noncalcareous shales that are the upper part of the Woodbine Formation (Reference 2.5S.1-33). The shale thins southward and pinches out on the San Marcos Arch.

The Eagle Ford Group is the fine-grained phase of terrestrial deposition that began with the coarse-grained deposits of the Woodbine in north Texas. By the time the Eagle Ford reaches the STP/San Marcos Arch Region, the strata are thin and consist of fissile, calcareous, carbonaceous black shale with interbeds of dark limestone. The Woodbine/Eagle Ford thins or is locally absent over the San Marcos Arch, and it may reach a thickness of about 225 ft. in south Texas (Reference 2.5S.1-32).

The Austin Group disconformably overlies the Eagle Ford Group of strata and reflects a change in depositional environment in many areas from clastics to limestone. In the STP 3 & 4 site region, the Austin Group (undifferentiated) consists of a lower chalk and a limestone that become calcareous shale and overlying limestone. The undifferentiated group of strata can be 980 ft. thick toward the Rio Grande Embayment, thinning over the San Marcos Arch. The thickness of this unit at the STP site region is unknown due to absence of petroleum targets below the thick Cenozoic Strata.

The Anacacho Limestone disconformably overlies the Austin Group. The Anacacho Limestone is mainly a clayey, bioclastic limestone interbedded with clay and marl and can be as much as 800 ft. thick. Downdip, the Anacacho Limestone grades into shelf mudstones of the Upson Formation. The Upson Formation can be as much as 500 ft. of fossiliferous dark to greenish gray clay (Reference 2.5S.1-33). Outcrops of the Upson Formation are limited, in part due to erosion, but it is commonly recognized in the subsurface where it is conformably overlain by the San Miguel Formation (Reference 2.5S.1-33). The San Miguel Formation consists of as much as 400 ft. (in outcrop) of fossiliferous sands and sandy limestones interbedded with gray clays. The lithology of the San Miguel Formation in the subsurface is similar and as much as 1150 ft. have been identified (Reference 2.5S.1-33). The San Miguel Formation probably was deposited in a wave-dominated deltaic system that was transitional from the underlying Upson Formation, a shallow water shelf deposit (Reference 2.5S.1-33) and transitional to the overlying Olmos Formation. All of these strata are truncated against

the San Marcos Arch. In some areas of south Texas, there was uplift and erosion so that the San Miguel and Upson Formations are missing and the Escondido Formation (uppermost Cretaceous) disconformably overlies the Anacacho Limestone directly. This uplift may be related to the early stages of the Laramide Orogeny, which probably contributed to deposition of the clastics in the San Miguel Deltaic Complex.

The Laramide Orogeny continued to create a source for clastics in the upper Cretaceous. In the area of the San Marcos Arch, the claystone, chalky marls, and sandy strata of the east Texas Navarro Group give way to coarser clastics of the Olmos Formation. In outcrop, the Olmos Formation is mainly non-marine, irregularly bedded clays, shales and sandstones, accompanied by seams of coal, lignite, fire clay, and carbonaceous shales (Reference 2.5S.1-33). The Olmos Formation ranges between 400-500 ft. in outcrop, but thickens to more than 1300 ft. in the Rio Grande Embayment subsurface.

The Olmos Formation is transitional to the Escondido Formation, the uppermost Cretaceous unit in south Texas. The lower three-quarters of the formation consist of bioturbated mudstones interbedded with sandstones and coquina beds (Reference 2.5S.1-33). Some sandstones contain ripple marks or cross-bedding that indicates a shallow-water depositional environment. The upper quarter consists of inner-shelf deposits of sandy mudstone, siltstone and impure limestone. In outcrop, the Escondido Formation is about 800 ft. in Texas, thickening gulfward to approximately 1300 ft. (Reference 2.5S.1-33).

Along the northern Gulf of Mexico Coast, Tertiary sediments lie disconformably on upper Cretaceous strata (Reference 2.5S.1-33). Basal Paleocene units contain reworked Cretaceous fossils along with those from the Paleocene in most areas. However, in the Rio Grande Embayment and the Brazos River Sequence in Central Texas, deposition may have been continuous from the Cretaceous through the Paleocene. This is largely due to the continued uplift in the Cordillera resulting from the Laramide Orogeny (Reference 2.5S.1-33). The connection between the Gulf of Mexico and the Western Interior Seaway was probably cut in the Upper Cretaceous time frame (Reference 2.5S.1-33).

2.5S.1.1.3.5 Cenozoic Stratigraphic Units

The western section of the Gulf Coastal Plain has a different Cenozoic history than the northeastern section due to the continued structural impact of the Laramide Orogeny during the Paleocene and Eocene. The large volumes of clastics that began to accumulate created an offlapping depositional style that continued throughout the Cenozoic in Texas (Reference 2.5S.1-34). Growth faults developed in the Wilcox and Yegua Sequences. Subsidence of the basin was mainly due to sedimentary loading and, in the Pleistocene, the variation of ice volumes which had a eustatic effect on sea levels. Figure 2.5S.1-13 (Reference 2.5S.1-25) contains a generalized Cenozoic stratigraphic column.

Not much is known about the stratigraphy beneath the Cenozoic in the STP area as oil exploration is generally limited to the units above the depth of 13,000 ft. Groundwater is obtained from the Coastal Lowlands Aquifer System, which has a lower bound in the

Catahoula Confining System at depths of 5000-6000 ft. It is estimated that there is approximately 25,500 ft. of Mesozoic and Paleozoic sediments below the site. The Precambrian Basement is believed to be continental or oceanic crustal rocks (Reference 2.5S.1-35).

2.5S.1.1.3.5.1 Paleocene

The Midway Group contains the basal Cenozoic sediments along the Gulf Coastal Plain and overlies Upper Cretaceous strata in disconformable contact. The Kinkaid Formation, the basal unit of the Midway Group, is mostly composed of limestone, calcareous sand, and sandstone and is usually less than 100 ft. thick. The Wills Point Formation is present throughout the area and represents the bulk of the Midway Group. The thickness of the Wills Point is more than 2500 ft. in southern Texas. The Wills Point Formation is mainly a dark-gray to black, micaceous clay (Reference 2.5S.1-36).

The Lower Wilcox Group reflects the first Cenozoic episode of major deltaic offlap, largely east of the modern Guadalupe River in Texas with the Rockdale Delta and the Holly Springs Deltaic System in Mississippi. These were the first systems to contribute to growth faulting and salt mobilization (Reference 2.5S.1-34) through application of Lithostatic pressure developed by the large volume of sediments deposited in the delta. In south Texas, a strandline-shelf system developed that generally covered that same area as the Cretaceous limestone platforms. The sands were reworked from the deltaic lobes and were transported southwestward along the coast. The sands grade into shelf mud toward the Gulf of Mexico.

The Wilcox Group is undifferentiated in Texas where it lacks regionally mappable units (Reference 2.5S.1-36). It has a maximum thickness of 1200 ft. in the Mississippi Embayment, becomes thousands of feet thick toward the Gulf and is estimated to be 2000 ft. thick beneath the STP site. The Wilcox Group typically consists of sandy-clayey deposits; lignite is common and is characterized by coarser sandy, deltaic and nonmarine sediments.

2.5S.1.1.3.5.2 Eocene

In the Early Eocene, the sediment distribution systems established in the Paleocene generally continued (Reference 2.5S.1-34). Sediments eroded from the Laramide Uplift prograded into the western Gulf basin as much as 20 miles. A broad alluvial coastal plain derived from fluvial systems flowing from the continent extended along the central and south Texas coast. The sediments constitute the Carrizo Sandstone of the Claiborne Group (Figure 2.5S.1-13 [Reference 2.5S.1-25]) and are overlain by the Reklaw Shale.

The Carrizo Sand is the basal Claiborne Unit in Texas. Deposited unconformably on the Wilcox Formation, the Carrizo Sand varies in thickness, ranging from 100 ft. to 1200 ft. in Texas and is estimated to be approximately 800 ft. thick beneath the STP site, based on oilfield logs.

The Reklaw Formation conformably overlies the Carrizo Sand and is composed largely of dark shales and sands. The lower part of the Reklaw Formation is glauconitic and partly nonmarine (Reference 2.5S.1-36).

In the Middle Eocene, the Queen City and the Sparta Sands were deposited in two depositional episodes. During the Sparta depositional period, a wave-dominated barrier island complex extended from the present coast of Mexico northward to the Houston Embayment. The outer shelf, slope, and deep basin remained sediment starved (Reference 2.5S.1-34).

The Queen City Sand is predominately light-gray to grayish-brown very fine to medium quartz sand with interbeds of dark carbonaceous shale, silt and lignite. Beneath the STP site, the Queen City Sand thickness is estimated to be approximately 100 ft. based on oilfield logs.

The Weches Formation underlies the Sparta Sand and overlies the Queen City Sand. It is predominately glauconitic and has been mined as an iron ore where leaching of the glauconite has concentrated the iron. The sands are highly crossbedded, and interbedded with dark-gray to black glauconitic clay and shale (Reference 2.5S.1-36). The Weches Formation is highly fossiliferous which distinguishes it from the units above and below.

The Sparta Sand overlies the Weches formation and is composed of very fine to medium unconsolidated quartz sand with interbeds of sandy clay and clay. Lignite is common. The Sparta Sand is about 100 ft. thick at the outcrop to more than 1000 ft. thick in the subsurface near the Mississippi Embayment Axis (Reference 2.5S.1-36). The thickness of the Sparta Sand beneath the STP site is estimated at 100 ft., based on oil field logs.

The Cook Mountain Formation overlies the Sparta Sand in what may be a gradational contact (Reference 2.5S.1-36). The formation in south Texas has a large proportion of sandy clay and sand containing disseminated glauconite. Interbedded clays are bluish gray to black and become the dominant lithologic type as the formation thickens downdip. In the site area, the Cook Mountain Formation is estimated to be 300-400 ft. thick, based on oilfield logs.

The Yegua Formation is composed of massive laminated and crossbedded, fine to medium grained sand. Sandy clay and clay, thin lignite beds and glauconitic sands are present in some places. The maximum thickness of the Yegua Formation is more than 1800 ft. Beneath the STP site the formation thickness is estimated to be 800-1000 ft. based on oil field logs.

Volcanic ash in the Yegua Sediments reflects the uplift and crustal heating in the Mexican Cordillera and western Gulf of Mexico. Areas in the western Gulf were uplifted, and the area of active deposition of mud extended eastward (Reference 2.5S.1-34). The Gulf Margin prograded as much as 15 miles during this time.

The Jackson Group was deposited during the late Eocene. Stratigraphic equivalents are present throughout the Gulf Coastal Plain. The presence of volcanic ash and

coarser volcanic-derived clastics in the Jackson Group reflects volcanic activity in Mexico and southwestern United States. This group and its stratigraphic equivalents were deposited during the last major marine transgression that covered the Coastal Plain and occupied the Mississippi Embayment (Figures 2.5S.1-9 [Reference 2.5S.1-25] and 2.5S.1-13 [Reference 2.5S.1-25]). Jackson sediments conformably overlie the Yegua Formation deposits of the underlying Claiborne Group.

The lowermost unit of the Jackson Group is the Caddell Formation. The lower part of the Caddell Formation is typically a marine deposit and is composed of gray calcareous sandstone and greenish calcareous clays. The upper part exhibits fewer marine characteristics and locally contains lignite and thin chocolate shales and interbedded sands. The lower part of the Caddell Formation commonly contains gray calcareous sands, and some glauconite. The Caddell Formation ranges from 30 ft. to 300 ft. in thickness (Reference 2.5S.1-36).

The Wellborn Sandstone, which overlies the Caddell Formation, is massive gray sandstone with interbedded marine clay units. The middle part is a highly fossiliferous marine facies consisting of sandy, marly clays. The upper part is a massive gray to white clayey sandstone. The entire Wellborn Sandstone is between 100 ft. and 300 ft. thick (Reference 2.5S.1-36).

The Manning Clay, consisting of carbonaceous, dark brown clay alternating with two beds of gray sandstone, overlies the Wellborn Sandstone. The clay is essentially nonmarine, but some marine shale beds are present locally. The thickness of the Manning Clay is between 250 ft. and 350 ft. (Reference 2.5S.1-36).

The Whitsett Formation, the uppermost unit in the Jackson Group, is mainly nonmarine crossbedded sandstone interbedded with tuffaceous shale and fine sandy tuff (Reference 2.5S.1-36). The sands are generally fine to medium grained but may be very coarse and conglomeratic in places. The Whitsett Formation is about 135 ft. thick.

2.5S.1.1.3.5.3 Oligocene

During the Oligocene multiple fluvial systems developed resulting in an influx of sediments from Mexico and southwestern United States. The Norias Delta on the Rio Grande Axis merged with the Norma Delta to the south. A third system developed along the Houston Embayment while the fourth developed along the Central Mississippi Margin (Reference 2.5S.1-34). The eastern Gulf of Mexico continued to receive a minimum of clastics. Clastics consisted of the Vicksburg Group and the overlying Catahoula Sandstone (tuff).

The Vicksburg Group is composed of a variety of marine sediments, varying from sandstones and clays to marl and limestone (Reference 2.5S.1-36). The Frio Clay (not to be confused with the Frio Formation) is probably time-equivalent with the Vicksburg Group (Reference 2.5S.1-36). The Frio Clay is typically composed of massive dark, greenish-gray, red, and blue gypsiferous clay interbedded with sandy clay, sand, and sandstone.

The Catahoula Sandstone (or tuff) consists of three units which are identified only in the subsurface. These are, from oldest to youngest: the Frio Formation, the Anahuac Formation, and the Upper part of the Catahoula Tuff. The Catahoula Formation consists of approximately 60% volcanic material, mainly airborne ash from Mexican volcanoes and 30% sand (Reference 2.5S.1-37). The Catahoula Sandstone thickens down-dip to thousands of ft. The thickness at the site is estimated from oilfield logs to be at least 3000 ft. with the top at approximately -5350 ft. MSL. The age of the Catahoula Sandstone is uncertain, but the U.S. Geological Survey (USGS) designates the unit as both Oligocene and Miocene (Reference 2.5S.1-37).

2.5S.1.1.3.5.4 Miocene

The Miocene was a fairly stable period. Uplift of the Edwards Plateau and the adjacent areas is demonstrated by the increased presence of Cretaceous limestone clastics in the Miocene fluvial deposits. The Fleming Formation overlies the Oakville Sands. In the STP 3 & 4 site area, the Fleming Formation is largely variegated yellow, green red, pink blue, purplish gray, or greenish gray clay (Reference 2.5S.1-36). The strata may be calcareous and contain thin chalky limestone as well as cross-bedded sands. The upper part of the Fleming Formation may be sandy, and it forms the lower portion of the Evangeline Aquifer (Subsection 2.4S.12). The Fleming Formation is about 200 ft. thick in outcrop and can be thousands of feet thick in the subsurface. The estimated thickness of the Fleming Formation beneath the site is 3200 ft.

The Oakville Sandstone is a sandy facies in the lower part of the Fleming Formation (Reference 2.5S.1-36) in the vicinity of the site. It is composed of non-marine, irregularly bedded clastics consisting of coarse sands and interbedded clay. The Fleming Formation and the Oakville Sandstone are similar lithologically, but the Oakville Sandstone is much sandier. The thickness of the Oakville Sandstone ranges from about 200 to about 500 ft. regionally. At the site, the thickness is estimated to be 250 ft., based on oil field geophysical logs, with the top at an estimated elevation of -2100 ft. MSL.

During the middle Miocene epoch the Corsair Delta developed in the region of the Colorado River, an area which had not previously been a depocenter. The Corsair Delta Apron formed a sandy depositional element on the Gulf floor (Reference 2.5S.1-34).

2.5S.1.1.3.5.5 Pliocene

By the early Pliocene, sediment supply and accumulation had shifted to the Mississippi depositional axis. Sediments were carried east and west from the delta, forming shore deposits which were thin veneers, compared with previous deposits (Reference 2.5S.1-34).

In the late Pliocene, the three central Gulf fluvial systems, the Red River, Central Mississippi and Eastern Mississippi formed a composite delta system, in which the Red River continued to dominate the sediment supply (Reference 2.5S.1-34). The fluvial systems of the western and northwestern Gulf were dormant.

The influence of the continental ice sheet during the interglacial periods occurred in the late Pliocene epoch (Reference 2.5S.1-34).

The Goliad Sand was the dominant unit deposited during the Pliocene epoch. The Goliad Sand ranges from a basal strata of coarse undivided sediments to indurated units whitish to pinkish gray, ranging in grain size from very fine to coarse. The cement is typically calcium carbonate. Clay interbeds are grayish and may be calcareous. The bedding suggests that the Goliad Sand was deposited as river-bottom sediments (Reference 2.5S.1-36). Based on oil field logs, the estimated thickness of the Goliad Sand beneath the site is 800 ft.

2.5S.1.1.3.5.6 Pleistocene

The Pleistocene depositional record shows pulses of sandy outwash during glacial retreats and cyclic sea level changes. The inland Mississippi and Red River Fluvial Systems were separate inland but coalesced on the depositional coastal plain. The Rio Grande Delta was reactivated and the Colorado/Brazos Delta became minor features.

The Lissie Formation is in unconformable contact with the underlying Goliad Sand. The sediments are partially flood plain deposits and partially deltaic sands, silts, and muds. The sediments are described as reddish, orange, and gray fine-to-coarse grained, cross bedded sands with the base of the formation often indicated by caliche (Reference 2.5S.1-37).

The surface sediments at the STP site belong to the Beaumont Formation. From the Louisiana/Texas border to the Rio Grande, the Beaumont Formation is recognized as a delta that formed during the last eustatic sea level high. Sediments in the STP area are attributed to the Colorado/Brazos Fluvial Systems, which today are the largest systems in Texas (Figure 2.5S.1-14 [Reference 2.5S.1-38]). The thickness of the Beaumont varies, and it is difficult to distinguish between the underlying Lissie and the Beaumont in the subsurface because of the similarity of the sediments.

2.5S.1.1.4 Regional Tectonic Setting

In 1986, the Electric Power Research Institute (EPRI) developed a seismic source model for the Central and Eastern United States (CEUS), which included the STP 3 & 4 site region (Reference 2.5S.1-39). The CEUS is a stable continental region (SCR) characterized by low rates of crustal deformation and no active plate boundary conditions. The EPRI source model included the independent interpretations of six Earth Science Teams (ESTs) and reflected the general state of knowledge of the geoscience community as of 1986. The seismic source models developed by each of the six teams were based on the tectonic setting and the occurrence, rates, and distribution of historical seismicity. The original seismic sources identified by EPRI (Reference 2.5S.1-39) are thoroughly described in the (Reference 2.5S.1-39) reports and are summarized in Subsection 2.5S.2.2.

Since 1986 additional geological, seismological, and geophysical studies have been completed in the CEUS and in the STP 3 & 4 site region. The purpose of this section is to summarize the current state of knowledge on the tectonic setting and tectonic

structures in the site region and to highlight new information acquired since 1986 that is relevant to the assessment of seismic sources.

A global review of earthquakes in SCRs shows that areas of Mesozoic and Cenozoic extended crust is positively correlated with large SCR earthquakes. Nearly 70% of SCR earthquakes with moment magnitudes **M** ≥ 6 occurred in areas of Mesozoic and Cenozoic extended crust (Reference 2.5S.1-40). Additional evidence shows an association between Late Proterozoic rifts and modern seismicity in eastern North America (References 2.5S.1-40; 2.5S.1-41; and 2.5S.1-42). Proterozoic and Mesozoic extended crust underlies at least part of the site region (Figure 2.5S.1-15 [References 2.5S.1-43, 2.5S.1-44, and 2.5S.1-45] and Figure 2.5S.1-16 [References 2.5S.1-44, 2.5S.1-46, 2.5S.1-47, and 2.5S.1-48]). As discussed in this subsection, however, there is no positive evidence for late Cenozoic seismogenic activity or any tectonic feature or structure in the site region (References 2.5S.1-49 and 2.5S.1-50). Although research during the last two decades has modified interpretations of the tectonic evolution and processes in the Gulf Coastal Plain and Gulf of Mexico, no new structures or features have been identified in the STP site region since 1986 that show clear evidence of seismogenic potential greater than what was recognized and incorporated in the EPRI (Reference 2.5S.1-39) seismic source model.

2.5S.1.1.4.1 Regional Tectonic History of the STP 3 & 4 Site

2.5S.1.1.4.1.1 Overview

The STP 3 & 4 site lies within the Gulf Coastal Plain Physiographic Province (Figure 2.5S.1-1 [References 2.5S.1-2 and 2.5S.1-3]), which extends from Mexico on the west and southwest to Florida on the east. The Coastal Plain developed as part of the geologic and physiographic evolution of the Gulf of Mexico (Reference 2.5S.1-51), an ocean basin that opened in the Triassic along the trend of the Ouachita Orogenic belt (Reference 2.5S.1-20), a largely buried Paleozoic mountain chain. Exposures of the Ouachita Belt are located in the Ouachita Mountains of eastern Oklahoma and western Arkansas, and in the Marathon Mountains of western Texas. Between these widely separated exposures, the Ouachita Orogenic Belt extends continuously beneath Mesozoic and Tertiary marine sediments that fringe the northern margin of the Gulf Coastal Plain (References 2.5S.1-52, 2.5S.1-53, and 2.5S.1-20). The Ouachita Belt records orogenic events related to the opening and closing of a Paleozoic ocean basin along the southeastern margin of ancestral North America. The tectonic events associated with the formation of the Ouachita Belt have significantly influenced the structure of the crust in the STP 3 & 4 site region, and they are summarized in the following sections.

2.5S.1.1.4.1.2 Late Proterozoic and Paleozoic Plate Tectonic History

The Ouachita Orogenic Belt formed in Paleozoic time along with the Appalachian Orogenic Belt, which trends northeast-southwest along the length of the eastern United States and Canada (Reference 2.5S.1-52). A comprehensive synthesis of the Appalachian Orogen can be found in Reference 2.5S.1-54. The ancestral North American continent that predated the Appalachian and Ouachita Orogenies is known as Laurentia. Exposures of Proterozoic Laurentian Basement are present in the Llano

Uplift at the northwest margin of the STP 3 & 4 site region (Reference 2.5S.1-55) (Figure 2.5S.1-5 [References 2.5S.1-8, 2.5S.1-9, 2.5S.1-10, and 2.5S.1-11], Figure 2.5S.1-10 [Reference 2.5S.1-27]).

In late Precambrian to Cambrian time, Laurentia broke up along a series of NNE-SSW-trending rifts that led to sea-floor spreading and development of an ocean basin known as Iapetus (References 2.5S.1-54 and 2.5S.1-20). In general, the rift system along the eastern margin of Laurentia was approximately coincident with the present Appalachian Mountain Belt (Reference 2.5S.1-54). The locus of rifting stepped abruptly westward at about the latitude of Alabama and Mississippi along a WNW-ESE-trending transform fault zone (Reference 2.5S.1-56). This transform fault zone terminated to the west at the northern end of a NNW-SSE-trending rift system that was located approximately between the Sabine Arch (Figure 2.5S.1-17) and the Fort Worth Basin (Reference 2.5S.1-57). Figure 2.5S.1-10 (Reference 2.5S.1-27) illustrates the location of the Ft. Worth Basin and the Sabine Arch. The transform fault system formed a jog in the ancestral continental margin that roughly parallels the northern rim of the present Gulf Coastal Plain (Reference 2.5S.1-20). Two failed rift basins, or aulocogens, developed along Laurentia's southern margin (Reference 2.5S.1-19). One of the aulocogens is known as the Reelfoot Rift, which trends northeast-southwest and underlies the Mississippi Embayment. The other failed rift basin is known as the Oklahoma Aulocogen, which trends west-northwest-east-southeast along the border between southern Oklahoma and northeastern Texas (References 2.5S.1-19 and 2.5S.1-20).

The rifted southern margin of Laurentia in early Paleozoic time included structures typical of passive margins, such as grabens and fault-bounded basins open to the ocean (References 2.5S.1-57 and 2.5S.1-20). As rifting ceased, shallow-water shelf environments emerged along the developing passive margin and are recorded in sequences of early to middle Paleozoic marine clastic and carbonate deposits (Reference 2.5S.1-20). Progressive subsidence of the Laurentian passive margin and Iapetus basin in Late Ordovician through Early Mississippian time is indicated by deep-water siliceous chert and shale overlying the older clastic and carbonate rocks (Reference 2.5S.1-20).

The onset of collisional tectonics and closing of the Iapetan Ocean during the Carboniferous are marked in the stratigraphic record by the abrupt appearance of coarse clastic deposits over the older deep-water deposits. The general model proposed by Viele and Thomas (Reference 2.5S.1-20) for the development of the Ouachita Belt, invokes progressive closure of the Iapetus Ocean along a subduction zone that dipped south beneath an island arc located off the southern coast of Laurentia. The collision is interpreted to be oblique, which resulted in diachronous, westward-propagating closure of the Iapetus basin (Reference 2.5S.1-57). As the ocean basin was consumed, rocks of the accretionary prism above the subduction zone were thrust northward over deposits of the Laurentian passive margin. The passive margin strata subsequently were caught up in the deformation and thrust northward as the island arc overrode the continental margin, forming the ancestral Ouachita Mountains (see Reference 2.5S.1-58 for a lithospheric-scale model of the collisional orogen east of the STP 3 & 4 site determined from a synthesis of seismic,

borehole, and gravity data). Growth of the Ouachita Mountains loaded the Laurentian continental crust, forming a series of broad arches and basins in the foreland region north and west of the orogenic belt (References 2.5S.1-59 and 2.5S.1-60). Examples of these foreland structures that are relatively proximal to the STP 3 & 4 site include the Kerr Basin, Llano Uplift, and Fort Worth Basin (Reference 2.5S.1-61) (Figure 2.5S.1-10 [Reference 2.5S.1-27]).

2.5S.1.1.4.1.3 Mesozoic and Cenozoic Geology

The development of the Ouachita Belt in late Paleozoic time marked the end of a complete Wilson Cycle, during which Laurentia was rifted, Iapetus formed, and then the ocean basin was consumed during a continent-continent collision. The opening of the modern Gulf of Mexico beginning in the Mesozoic represents the commencement of another Wilson Cycle. Formation of the Gulf of Mexico began in Late Triassic time with renewed rifting approximately along the trend of the Ouachita Belt (References 2.5S.1-22 and 2.5S.1-62). Detailed modeling of gravity data suggests that the locus of rifting and crustal extension occurred south of the main Ouachita collisional orogen, approximately beneath the present continental shelf and rise in the offshore region of the Gulf of Mexico (Reference 2.5S.1-59).

Rifting lasted from Late Triassic to Late Jurassic and caused both the extension of pre-rift continental crust and the formation of new oceanic crust. Sawyer et al. (Reference 2.5S.1-44) describes four classifications of crust within the STP 3 & 4 site region related to the effect of rifting on the crust (Figure 2.5S.1-15 [References 2.5S.1-43, 2.5S.1-44, and 2.5S.1-45] and Figure 2.5S.1-16 [References 2.5S.1-44, 2.5S.1-46, 2.5S.1-47, and 2.5S.1-48]): (1) extended continental crust, (2) extended thick transitional crust, (3) extended thin transitional crust, and (4) Mesozoic oceanic crust. The locations of the boundaries between these crustal classifications is debated within the literature (e.g., References 2.5S.1-63, 2.5S.1-64, 2.5S.1-65, 2.5S.1-66, 2.5S.1-44, and 2.5S.1-48), but the tectonic significance of each classification, as described below, is generally accepted.

The initial stages of rifting occurred during the Late Triassic and Early Jurassic and are thought to have occurred along preexisting crustal weaknesses and sutures from the earlier Precambrian rifting and late Paleozoic Ouachita Orogeny (Reference 2.5S.1-44). Most rifting occurred in the Middle Jurassic and created the divisions between continental, thick transitional and thin, transitional crust (References 2.5S.1-66 and 2.5S.1-44). The thick transitional crust underwent moderate thinning with post-extension crustal thicknesses ranging between 12.4 miles and 21.7 miles. This variable thinning occurred along gulf-perpendicular trends (Reference 2.5S.1-44) and is proposed by some to have influenced the formation of the gulf-perpendicular basement highs and lows that form the alternating arches and embayments of the Gulf coastal margin (e.g., Sabine Arch, Houston Embayment, San Marcos Arch, Rio Grande Embayment) (Reference 2.5S.1-67 and Figures 2.5S.1-10 [Reference 2.5S.1-27] and 2.5S.1-17 [Reference 2.5S.1-27]).

The thin transitional crust underwent considerably more thinning with post-extension crustal thicknesses of 4.9 mi and 9.3 mi (References 2.5S.1-68 and 2.5S.1-44).

Sawyer et al. (Reference 2.5S.1-44) hypothesized that the contrast in thinning is due to the thin transitional crust having originally been weaker due to locally elevated crustal temperatures. In contrast to the thick transitional crust, the major crustal thickness variations in the thin transitional crust are parallel to the Gulf margin (Figure 2.5S.1-18 [References 2.5S.1-26, 2.5S.1-43, and 2.5S.1-45]) (Reference 2.5S.1-44). Throughout the period of rifting significant accumulations of non-marine clastic rocks, volcanic rocks, and salt were deposited in fault-bounded basins (References 2.5S.1-22, 2.5S.1-62, and 2.5S.1-44). In particular, thick deposits of Mesozoic salt accumulated in long-lived basins along the continually developing rift margin.

The oceanic crust is thought to have been formed during the Middle and Late Jurassic (References 2.5S.1-66 and 2.5S.1-44). The extent of oceanic crust within the Gulf of Mexico is limited (Figure 2.5S.1-15 [References 2.5S.1-43, 2.5S.1-44, and 2.5S.1-45] and Figure 2.5S.1-16 [References 2.5S.1-44, 2.5S.1-46, 2.5S.1-47, and 2.5S.1-48]) compared to the total relative plate motion reflecting the observation that over 50% of the relative plate motion during rifting occurred as crustal extension as opposed to sea floor spreading (Reference 2.5S.1-64). The thickness of the oceanic crust is difficult to determine in all regions due to the presence of thick, overlying sediments and salt, but there is considerable structural variation observed within the oceanic crust thought to be related to variations in spreading initiation, duration, and rate (Reference 2.5S.1-44).

After the rapid phase of continental extension and rifting ended, a long period of tectonic quiescence ensued during which the newly passive margin subsided and thick deposits of Late Jurassic and Cretaceous marine sediments accumulated (References 2.5S.1-22 and 2.5S.1-62). Enormous volumes of terrigenous sediment were deposited along the northern and northwestern margins of the ancestral Gulf of Mexico by streams draining the interior of North America, causing flexural loading of the crust and progressive southward migration of the shoreline toward the axis of the basin (Reference 2.5S.1-33). The long-term migration of the shoreline is marked by bands of offlapping marine strata in the Gulf Coastal Plain, which are progressively younger from north to south (Figure 2.5S.1-19 [Reference 2.5S.1-38] and Figure 2.5S.1-5 [References 2.5S.1-8, 2.5S.1-9, 2.5S.1-10, and 2.5S.1-11]).

Ewing (Reference 2.5S.1-51) subdivided the Gulf of Mexico basin into two main zones that roughly parallel the geographic trend of the Coastal Plain. The Interior Zone is the more landward of the two zones, and is primarily associated with broad, relatively shallow Mesozoic embayments that locally host diapir provinces overlying Paleozoic basement. According to Ewing (Reference 2.5S.1-51), the principal structures of the Interior Zone are Mesozoic-age rift faults associated with opening of the Gulf of Mexico. South of the Interior Zone is the Coastal Zone, which is characterized by a very thick (6.2 mi to 9.3 mi) section of late Mesozoic to Cenozoic strata that bury highly-extended Paleozoic crust and Mesozoic oceanic crust (Reference 2.5S.1-51). The boundary between the Interior and Coastal Zones lies along a trend of Lower Cretaceous reefs within the Coastal Plain section (Figure 2.5S.1-10 [Reference 2.4S.1-27]). The location of this reef trend is interpreted as a hinge zone reflecting the transition between thick and thin transitional crust and the increased subsidence of the

thin transitional crust due to sedimentary loading in the basin to the south (References 2.5S.1-44 and 2.5S.1-51).

Strata of the Gulf Coastal Plain have been deformed by diapiric rise of salt bodies and by growth faults, which have formed in response to sedimentary compaction, subsurface migration of salt, and down-to-the-basin slumping of the Coastal Plain section (References 2.5S.1-51, 2.5S.1-22, and 2.5S.1-62). Stratigraphic relationships in the Coastal Plain section document salt-related deformation and growth fault activity beginning in Mesozoic time and continuing to the Recent. Growth faults occur almost exclusively in the Coastal Zone (according to Reference 2.5S.1-51) of the Coastal Plain, within the thickest section of Mesozoic to Cenozoic strata. Growth faults terminate against or sole into bodies of salt or detachment horizons within the Coastal Plain section (Reference 2.5S.1-69). These structures do not penetrate the crystalline basement rocks beneath the Coastal Plain strata, and thus are characterized as “Class B” structures by the USGS (Reference 2.5S.1-70); i.e., faults that “might not extend deeply enough to be a potential source of significant earthquakes” (References 2.5S.1-49 and 2.5S.1-50).

Broad epeirogenic uplift is interpreted to have occurred in west-central Texas and New Mexico during the Miocene, coeval with development of the Rio Grande Rift and the Basin and Range Province to the west (see summary discussion in Reference 2.5S.1-55). This uplift resulted in widespread erosion of Paleocene and Upper Cretaceous strata in central Texas, and was accompanied by down-to-the-southeast flexure of the Interior Zone along a NE-SW-trending hinge line. The relatively uplifted area northwest of the hingeline is known as the Edwards Plateau, and it is characterized by generally horizontal bedded rocks of the Cretaceous Edwards Limestone. The NE-SW-trending Balcones and Luling Fault Zones are spatially associated with the hingeline and geomorphic transition from the Edwards Plateau to the Interior Zone of the Coastal Plain (Reference 2.5S.1-55; Figure 2.5S.1-17 [Reference 2.5S.1-27]). The Balcones and Luling Fault Zones are interpreted to extend through the Coastal Plain strata and either terminate against the upper surface of the Paleozoic basement (Reference 2.5S.1-71), or continue downward into the Ouachita rocks (Reference 2.5S.1-55). Major activity on the Balcones and Luling Faults is interpreted to have occurred in late Oligocene or early Miocene time (Reference 2.5S.1-72), and possibly was driven by crustal flexure and tilting along the hingeline associated with sedimentary loading of the Gulf of Mexico.

The long-term southward migration of the Gulf shoreline continued into the late Quaternary but has been overprinted with relatively minor marine regressions and transgressions associated with sea-level changes during glacial and interglacial periods. Within the greater site vicinity, some of these glacial cycles are recorded in the deposition of the Beaumont and Lissie Formations, the major Pleistocene formations within the site vicinity. Both of these formations were originally deposited as alluvial fan-delta deposits (Reference 2.5S.1-38) (Figure 2.5S1-19). The Lissie Formation is the older of the two with a depositional age between 1.4 million and 400,000 years ago (Reference 2.5S.1-38). The closest Lissie Formation outcrop to the site is approximately 42 miles (68 km) north of the site (Reference 2.5S.1-30). The Beaumont Formation underlies the site (Figure 2.5S.1-11 and Figure 2.5S.1-27) and

varies in age between approximately 350,000 and 100,000 based on thermoluminescence ages from three distinct valley fills identified in the Colorado river basin (Figure 2.5S.1-14) (Reference 2.5S.1-38). The site lies on the youngest valley fill, the Bay City fill, which was deposited between 100,000 to 150,000 years ago. Subsequent to the deposition of the Beaumont Formation, falling sea levels resulted in the incision of coastal plain rivers (e.g., Colorado) into the Beaumont Formation.

2.5S.1.1.4.2 Tectonic Stress

Earth science teams (ESTs) that participated in the EPRI (Reference 2.5S.1-39) evaluation of intra-plate stress found that tectonic stress in the CEUS region is primarily characterized by northeast-southwest-directed horizontal compression. In general, the ESTs concluded that the most likely source of tectonic stress in the mid-continent region was ridge-push force associated with the Mid-Atlantic Ridge, transmitted to the interior of the North American plate by the elastic strength of the lithosphere. Other potential forces acting on the North American plate were judged to be less significant in contributing to the magnitude and orientation of the maximum compressive principal stress.

In general, the ESTs focused on evaluating the state of stress in the mid-continent and Atlantic seaboard regions, for which stress indicator data were relatively abundant. Fewer stress indicator data were available for the Gulf of Mexico, Gulf Coastal Plain, and Western Great Plains, and thus these areas received less scrutiny in the EPRI studies (Reference 2.5S.1-39). Notably, the Dames & Moore, Law, and Bechtel ESTs observed that the orientation of maximum horizontal compression in the Gulf Coastal Plain and west Texas may be perturbed from the regional northeast-southwest orientation that characterizes much of the CEUS.

Since 1986, an international effort to collate and evaluate stress indicator data culminated in publication of a new World Stress Map in 1989 (References 2.5S.1-74 and 2.5S.1-75) that has been periodically updated (Reference 2.5S.1-76). Plate-scale trends in the orientations of principal stresses were assessed qualitatively based on analysis of high-quality data (Reference 2.5S.1-77), and previous delineations of regional stress provinces were refined. Statistical analyses of stress indicators confirm that the trajectory of the maximum compressive principal stress is uniform across broad continental regions at a high level of confidence (Reference 2.5S.1-78). In particular, the northeast-southwest orientation of principal stress in the CEUS inferred by the EPRI ESTs is statistically robust and is consistent with the theoretical orientation of compressive forces acting on the North American Plate from the Mid-Atlantic Ridge (Reference 2.5S.1-77).

According to the continental United States stress map of Zoback and Zoback (Reference 2.5S.1-74), the STP 3 & 4 site is located within the Gulf Coast Stress Province, which generally coincides with the belts of growth faults in the coastal regions of Texas, Louisiana, Mississippi, Alabama, and northwestern Florida. The Gulf Coast Stress Province is characterized by north-south-directed tensile stress (Reference 2.5S.1-74) and is spatially associated with down-to-the-Gulf extension and slumping of the Coastal Plain stratigraphic section. Because these strata are

deforming above subhorizontal detachment faults and/or large bodies of Jurassic salt, gravitational tensile stress driving growth faulting is confined to the sedimentary section, and thus decoupled mechanically from the state of stress in the underlying crystalline basement.

The state of stress in the crystalline basement underlying the Coast Plain strata is very poorly constrained by data (Reference 2.5S.1-79) and may be affected by flexural loading of the lithosphere due to rapid and voluminous sedimentation in the Gulf of Mexico during the Pleistocene. Detailed numerical modeling of flexural deformation associated with sedimentary loading in the Gulf (Reference 2.5S.1-80) suggests that large bending stresses may be present in the crust and systematically vary from north-south tension in the Coastal Plain, to north-south compression in an approximately 60-mile-wide zone in the northern offshore region directly adjacent to the coast, to north-south tension at distances of greater than 60 miles from the coast.

North of the Coastal Plain Stress Province, the generalized continental U.S. Stress Map of Zoback and Zoback (Reference 2.5S.1-74) shows a northwest-trending boundary between two major crustal stress provinces in central Texas:

- The Mid-Plate Stress Province, which includes the CEUS and is characterized by northeast-southwest horizontal compression; and
- The Southern Great Plains Stress Province, which is characterized by northeast-southwest to NNE-SSW horizontal tension.

Zoback and Zoback (Reference 2.5S.1-74) interpret the Southern Great Plains Province to be a transition between tensile stress and active extension in the Basin and Range to the west, and compressive stress in the tectonically stable mid-continent to the east. The boundary between the Mid-Plate and Southern Great Plains Stress Provinces is shown as approximately located by Zoback and Zoback (Reference 2.5S.1-74), which reflects the paucity of stress indicator data to precisely constrain the location of the boundary. Zoback and Zoback observed that the Southern Great Plains Province “generally coincides with the major topographic gradient (about 100 miles) separating the thermally elevated western Cordillera from the mid-continent area” (Reference 2.5S.1-74). If this correlation obtains in Texas, then the boundary between the Mid-Plate and Southern Great Plains Stress Provinces probably is located near the eastern foot of the mountains in west Texas, west of the STP 3 & 4 site.

In addition to better documenting the orientation of stress, research conducted since 1986 has addressed quantitatively the relative contributions of various forces that may be acting on the North American Plate to the total stress within the plate. Numerical models by Richardson and Reding (Reference 2.5S.1-79), Lithgow-Bertelloni and Guynn (Reference 2.5S.1-81), and Humphreys and Coblentz (Reference 2.5S.1-82) of lithospheric stress have generally considered the contribution to total tectonic stress in the lithosphere from three classes of forces:

- Horizontal stresses that arise from gravitational body forces acting on lateral variations in lithospheric density. These forces commonly are called buoyancy forces. Richardson and Reding (Reference 2.5S.1-79) emphasized that what is

commonly called “ridge-push” force is an example of this class of force. Rather than a line-force that acts outwardly from the axis of a spreading ridge, ridge-push arises from the pressure exerted by positively buoyant, young oceanic lithosphere near the ridge against older, cooler, denser, less buoyant lithosphere in the deeper ocean basins (Reference 2.5S.1-83). The force is an integrated effect over oceanic lithosphere ranging in age from about zero to 100 million years (Reference 2.5S.1-84). The ridge-push force is transmitted as stress to the interior of continents by the elastic strength of the lithosphere.

- Shear and compressive stresses transmitted across major plate boundaries (strike-slip faults and subduction zones).

- Shear tractions acting on the base of the lithosphere from relative flow of the underlying asthenospheric mantle.

Richardson and Reding (Reference 2.5S.1-79) concluded that the observed northeast-southwest trend of principal stress in the Mid-Plate Stress Province of the CEUS dominantly reflects ridge-push body forces associated with the Mid-Atlantic Ridge. They estimated the magnitude of these forces to be about 7 to 10 x 10^8 tons/ft. (i.e., the total vertically integrated force acting on a column of lithosphere 1 ft. wide), which corresponds to average equivalent stresses of about 417 tsf to 627 tsf distributed across a 30-mile-thick elastic plate.

The tensile stress regime in the Southern Great Plains Stress Province is interpreted by Humphreys and Coblentz (Reference 2.5S.1-82) to arise from positive buoyancy forces associated with the high potential energy of the elevated Cordilleran topography to the west. Essentially, the tensile stress in the western Cordillera and, in the Southern Great Plains along its southeastern flank, is an on-land version of the ridge-push buoyancy force. The magnitude of the positive buoyancy force and resulting tensile stress decays eastward in the Southern Great Plains Province, coincident with the eastward decrease in topography and potential energy from the southern Rocky Mountains to the interior of the continent, as noted by Zoback and Zoback (Reference 2.5S.1-74).

Richardson and Reding (Reference 2.5S.1-79) found that the fit of the model stress trajectories to data was improved by adding compressive stress (about 52 to 105 tsf) acting on the San Andreas Fault and Caribbean Plate boundary structures. The fit of the model stresses to data further indicates that shear stresses acting on these plate boundary structures must also be in the range of 52 to 105 tsf. Humphreys and Coblentz (Reference 2.5S.1-82) also found that the fit of numerical stress models for the North American Plate was improved by imposing large compressive stresses on the San Andreas Fault and Caribbean Plate boundary structures.

Richardson and Reding (Reference 2.5S.1-79) noted that the general northeast-southwest orientation of principal stress in the CEUS also could be reproduced in numerical models that assume horizontal shear tractions acting on the base of the North American Plate. Richardson and Reding (Reference 2.5S.1-79) did not favor this as a significant contributor to total stress in the mid-continent region because their

model would require an order-of-magnitude increase in the horizontal compressive stress from the eastern seaboard to the Great Plains. Using numerical models, Humphreys and Coblentz (Reference 2.5S.1-82) also evaluated the contribution of shear tractions on the base of the North American lithosphere to intra-continental stress, and concluded that:

- There is a viscous drag or resisting force acting on the cratonic root of North America as it moves relative to the asthenospheric mantle and that this drag supports part of the ridge-push force acting from the east and creates a stress shadow for the western United States, and

- Shear tractions on the base of North America from flow of the underlying asthenospheric mantle are a minor contribution to stress in the mid-continental lithosphere. Humphreys and Coblentz (Reference 2.5S.1-82) concluded that the dominant control on the northeast-southwest orientation of the maximum compressive principal stress in the CEUS is ridge-push force from the Atlantic basin.

To summarize, research on the state of stress in the continental United States since publication of the EPRI studies (Reference 2.5S.1-39) have confirmed observations that stress in the CEUS is characterized by relatively uniform northeast-southwest compression and that this regional trend may be perturbed in the vicinity of the STP 3 & 4 site due to the influence of buoyancy forces in the uplifted Cordillera to the west and flexure of the crust due to sedimentary loading of the Gulf of Mexico. Very little new data have been reported since the EPRI study (Reference 2.5S.1-39) to better determine the orientations and relative magnitudes of the principal stresses in the STP 3 & 4 site region. Given that the current interpretation of the orientation of principal stress is similar to that adopted in EPRI (Reference 2.5S.1-39), a new evaluation of the seismic potential of tectonic features based on a favorable or unfavorable orientation to the stress field would yield similar results. Thus, there is no significant change in the understanding of the static stress in the Gulf Coastal Plain since the publication of the EPRI source models in 1986, and there are no significant implications for existing characterizations of potential activity of tectonic structures.

2.5S.1.1.4.3 Regional Gravity and Magnetic Data

The primary sources of gravity data reviewed for the STP 3 & 4 COL application are the compilation of on-land Bouguer gravity anomalies and offshore free-air gravity anomalies published by the Geological Society of America (Reference 2.5S.1-45) available through the National Geophysical Data Center (Reference 2.5S.1-43), the on-land Bouguer gravity anomalies of Lyons et al. (Reference 2.5S.1-85), the on-land Bouguer gravity anomalies of Keller (Reference 2.5S.1-86), and the offshore free-air gravity anomalies of Sandwell and Smith (Reference 2.5S.1-87) available from the Scripps Institution of Oceanography (Reference 2.5S.1-88). The gravity data of the Geologic Society of America is shown in Figure 2.5S.1-20 (References 2.5S.1-43 and 2.5S.1-45), Figure 2.5S.1-21 (References 2.5S.1-43, 2.5S.1-45, and 2.5S.1-89), Figure 2.5S.1-22, Figure 2.5S.1-15 (References 2.5S.1-43, 2.5S.1-44, and 2.5S.1-45), and Figure 2.5S.1-18 (References 2.5S.1-26, 2.5S.1-43, and 2.5S.1-45). The primary

sources of magnetic data reviewed for the STP 3 & 4 COL application are by Bankey et al. (References 2.5S.1-46 and 2.5S.1-47) and Keller (Reference 2.5S.1-86). The data from Bankey et al. (References 2.5S.1-46 and 2.5S.1-47) within the STP 3 & 4 site area is shown in Figure 2.5S.1-23 (References 2.5S.1-46 and 2.5S.1-47), Figure 2.5S.1-22, and Figure 2.5S.1-16 (References 2.5S.1-44, 2.5S.1-46, 2.5S.1-47, and 2.5S.1-48). With the exception of the Sandwell and Smith (References 2.5S.1-87 and 2.5S.1-88) free-air gravity anomaly data, each of the magnetic and gravity anomaly datasets are primarily composed of compiled data from other sources that have been in some cases reprocessed. Details of the compilations are given within the reference for each dataset. The free-air gravity anomaly of Sandwell and Smith (References 2.5S.1-87 and 2.5S.1-88) is an original dataset derived from satellite measurements.

The grid spacing of the potential field datasets is generally less than 6 miles, making the data useful in identifying and assessing gravity and magnetic features with wavelengths on the order of tens of miles or greater. Most of these features within the site region of STP 3 & 4 are due to three major tectonic events discussed in Subsection 2.5S.1.1.4.1:

- Late Precambrian to Cambrian rifting that lead to the break up of Laurentia and the opening of the Iapetus ocean basin (References 2.5S.1-54 and 2.5S.1-20),
- The Paleozoic Ouachita Orogeny that marked the close of the Iapetus basin (Reference 2.5S.1-20), and
- Mesozoic rifting that formed the present-day Gulf of Mexico (References 2.5S.1-62 and 2.5S.1-90).

Both rifting episodes and the Ouachita Orogeny have contributed to creating a complicated modern day basement structure beneath the Gulf Coastal Plain and Gulf of Mexico expressed in the gravity and magnetic anomaly data as long-wavelength features subparallel to the modern coastline (Figure 2.5S.1-23 [References 2.5S.1-46 and 2.5S.1-47] and Figure 2.5S.1-20 [References 2.5S.1-43 and 2.5S.1-45]). As discussed in Subsection 2.5S.1.1.4.3.1 and Subsection 2.5S.1.1.4.3.2, there is some uncertainty in the interpretations of what basement features are causing any particular gravity and magnetic anomaly (e.g., References 2.5S.1-61, 2.5S.1-63, 2.5S.1-69, 2.5S.1-91, 2.5S.1-92, 2.5S.1-59, 2.5S.1-65, 2.5S.1-93, 2.5S.1-94, and 2.5S.1-95). Part of this uncertainty is due to the difficulty in collecting seismic data within the Gulf of Mexico and the gulfward regions of the Coastal Plain where thick deposits of sediments and salt make it challenging to accurately image basement structure (Reference 2.5S.1-44).

The expression of these three tectonic events within the site region as gravity and magnetic anomaly features was recognized at the time of the 1986 EPRI study (References 2.5S.1-65, 2.5S.1-96, 2.5S.1-91, 2.5S.1-97, 2.5S.1-98, 2.5S.1-99, 2.5S.1-100, and 2.5S.1-101). As such, higher quality gravity and magnetic anomaly datasets postdating the 1986 EPRI study have refined the interpretation and identification of features related to these main tectonic events (References 2.5S.1-59, 2.5S.1-63, 2.5S.1-92, 2.5S.1-93, 2.5S.1-94 2.5S.1-95, and 2.5S.1-102). However,

these datasets have not generally led to the identification of new basement faults that were unidentified after the 1986 EPRI study.

2.5S.1.1.4.3.1 Gravity Data

Gravity anomaly data encompassing the STP 3 & 4 site region are shown in Figure 2.5S.1-20 (References 2.5S.1-43 and 2.5S.1-45). The data are a compilation of on-land Bouguer gravity anomalies and offshore free-air gravity anomalies published by the Geological Society of America (Reference 2.5S.1-45) available through the National Geophysical Data Center (Reference 2.5S.1-43). A profile of the gravity anomaly along profile B to B' through STP 3 & 4 and perpendicular to the regional structural trend is shown in Figure 2.5S.1-22.

The longest wavelength variations in the on-land Bouguer gravity anomalies correlate to the thickness of the Mesozoic sediments deposited after the opening of the Gulf of Mexico discussed in Subsection 2.5S.1.1.4.4.3. Figure 2.5S.1-18 (References 2.5S.1-26, 2.5S.1-43, and 2.5S.1-45) show this correlation with the gravity anomaly data overlain by contours of basement depth (Reference 2.5S.1-26) where basement is defined as the base of Mesozoic sediments (Reference 2.5S.1-44). As apparent in Figure 2.5S.1-18 (References 2.5S.1-26, 2.5S.1-43 and 2.5S.1-45), long-wavelength gravity lows correlate with regions of deep basement and thick sedimentary sequences as seen in the Houston Embayment and Rio Grande Embayment (Figure 2.5S.1-10 [Reference 2.5S.1-27]), and long-wavelength gravity highs correlate to regions of shallow basement and thin sedimentary sequences as in the San Marcos Arch and Sabine Arch (Figure 2.5S.1-10 [Reference 2.5S.1-27]). As discussed in Subsection 2.5S.1.1.4.1.3, these arches and embayments were probably formed due to a combination of variable crustal thinning during Jurassic rifting and east-west compression related to the Laramide Orogeny (References 2.5S.1-44 and 2.5S.1-103). The correlation between sediment thickness and gravity is due to the lower density of the Mesozoic sediments relative to the pre-Mesozoic basement. Within the offshore region the free-air gravity anomaly correlates less with basement depth (Figure 2.5S.1-18 [References 2.5S.1-26, 2.5S.1-43 and 2.5S.1-45]) than with bathymetry (Figure 2.5S.1-21 [References 2.5S.1-43, 2.5S.1-45 and 2.5S.1-89]) due to the inability of free-air gravity anomalies to account for variable water depths.

In addition to these long-wavelength variations there are ten individual features within the gravity data, referred to as Gravity Features A through J, that are described below and shown in Figures 2.5S.1-22 and 2.5S.1-15 (References 2.5S.1-43, 2.5S.1-44, and 2.5S.1-45).

Gravity Feature A

Gravity Feature A refers to a prominent gravity high to the northwest of Austin and north of San Antonio. In Figure 2.5S.1-15 (References 2.5S.1-43, 2.5S.1-44, and 2.5S.1-45), the feature appears as a roughly 50-mile wide circular region of high gravity. In Figure 2.5S.1-22, the feature appears as approximately 15 mgal gravity high on the northwest end of the profile. This feature correlates to the Llano Uplift discussed in detail in the UFSAR for STP 1 & 2 (Reference 2.5S.1-7) and here in Subsections 2.5S.1.1.2.3 and

2.5S.1.1.4.1. The high gravity anomaly of this feature is likely due to the relatively high density of the Proterozoic crystalline rocks comprising the core of the uplift (References 2.5S.1-15, 2.5S.1-104, and 2.5S.1-105).

Gravity Feature B

Gravity Feature B refers to a distinct arcuate gravity low adjacent and to the south-southeast of Gravity Feature A that passes through San Antonio, Austin, and Waco (Figure 2.5S.1-15 [References 2.5S.1-43, 2.5S.1-44 and 2.5S.1-45]). In Figure 2.5S.1-22, Gravity Feature B is apparent as an approximately 50 mile-wide gravity low adjacent to Gravity Feature A. The negative anomaly of Gravity Feature B has been attributed to the presence of low-density sediments within foreland basins, in some cases been overridden by thrusts sheets that formed during the Ouachita Orogeny (see discussion in Subsections 2.5S.1.1.4.4.2 and 2.5S1.1.4.1.2) (References 2.5S.1-94 and 2.5S.1-99).

Gravity Feature C

Gravity Feature C refers to a prominent gravity high directly south and southeast of Gravity Feature B (Figure 2.5S.1-15 [References 2.5S.1-43, 2.5S.1-44, and Reference 2.5S.1-45]). In Figure 2.5S.1-22, Gravity Feature C appears as an approximately 25-mile wide gravity high adjacent to the gravity low of Gravity Feature B. The high of Gravity Feature C has been attributed to a variety of sources (Reference 2.5S.1-94), but gravity modeling studies have suggested that the dominant signal is due to a major transition in basement structure from unextended continental crust to thick transitional crust that formed during Mesozoic rifting as discussed in Subsections 2.5S.1.1.4.1.3 and 2.5S.1.1.4.4.3 (Figure 2.5S.1-15 [References 2.5S.1-43, 2.5S.1-44 and 2.5S.1-45]) (References 2.5S.1-61, 2.5S.1-94 and 2.5S.1-99). Locally the anomaly may be enhanced by the intrusion of igneous rocks associated with Mesozoic rifting (Reference 2.5S.1-99).

Gravity Feature D

Gravity Feature D refers to the broad regional increase in gravity extending outward from Gravity Feature C to approximately 30 miles seaward of the coastline. In Figure 2.5S.1-22, this feature is apparent as an approximately 40 mgal increase in gravity over 250 miles. This feature is commonly interpreted as representing a regional scale thinning of the crust and is apparent throughout much of the Gulf Coastal Plain (Figure 2.5S.1-18 [References 2.5S.1-26, 2.5S.1-43, and 2.5S.1-45])(References 2.5S.1-59, 2.5S.1-94, 2.5S.1-99, and 2.5S.1-58). The thinned crust has been hypothesized to be a preserved feature of the Paleozoic continental margin (see Subsections 2.5S.1.1.4.4.2 and 2.5S.1.1.4.1.2), the signature of the transition between thick transitional and thin transitional crust formed during Mesozoic rifting (see Subsection 2.5S.1.1.4.4.3 and 2.5S.1.1.4.1.3) (Figure 2.5S.1-15 [References 2.5S.1-43, 2.5S.1-44 and 2.5S.1-45]), or a combination of the two (Reference 2.5S.1-94).

Gravity Feature E

Gravity Feature E refers to the short wavelength gravity variations overprinting the regional gravity increase of Gravity Feature D. In Figure 2.5S.1-22, the variations are apparent as 5 to 10 mgal oscillations in gravity superimposed on the regional increase. The exact cause of each variation is not well documented, but many of them are thought to be associated with horst and graben structures formed during Mesozoic rifting (see Subsections 2.5S.1.1.4.4.3 and 2.5S.1.1.4.1.3) that preferentially thinned some regions and created local deposition centers for low-density sediments (Reference 2.5S.1-99). Rifting related volcanism may also contribute to some of the positive gravity anomalies (Reference 2.5S.1-99).

Gravity Feature F

Gravity Feature F refers to the prominent gravity high offshore and subparallel to the coastline (Figure 2.5S.1-15 [References 2.5S.1-43, 2.5S.1-44 and 2.5S.1-45]). In Figure 2.5S.1-22, the feature is apparent as an approximately 10 mgal increase in gravity at the apex of the regional gravity increase of Feature D. Gravity Feature F is interpreted as an outer marginal basement high (Figure 2.5S.1-18 [References 2.5S.1-26, 2.5S.1-43 and 2.5S.1-45]) related to variations in crustal thickness within the thin transitional crust that formed during Mesozoic rifting (see Subsections 2.5S.1.1.4.4.3 and 2.5S.1.1.4.1.3) with the more extended crust occurring gulfward of the high (Reference 2.5S.1-91).

Gravity Feature G

Gravity Feature G refers to the broad regional decrease in gravity directly gulfward of Gravity Feature F (Figure 2.5S.1-15 [References 2.5S.1-43, 2.5S.1-44, and 2.5S.1-45]). In Figure 2.5S.1-22, the feature is apparent as an approximately 70 mgal decrease in gravity. Gravity Feature F reflects the effect of the increasing water depth with distance from the coast in the Gulf of Mexico (Reference 2.5S.1-3) on the free-air gravity anomaly (Figure 2.5S.1-21 [References 2.5S.1-43, 2.5S.1-45 and 2.5S.1-89]). Bouguer gravity anomaly maps for the Gulf of Mexico that correct for the increasing water depth show a continuation of the regional gravity increase of gravity of Feature D. This increase in the Bouguer gravity anomaly most likely indicates the continued thinning of the crust and positive relief on the Moho postulated to cause Gravity Feature D (References 2.5S.1-91, 2.5S.1-65, 2.5S.1-106, and 2.5S.1-93).

Gravity Feature H

Gravity Feature H refers to the short-wavelength gravity anomalies overprinted on the regional gravity decrease of Feature G (Figure 2.5S.1-15 [References 2.5S.1-43, 2.5S.1-44 and 2.5S.1-45]). In Figure 2.5S.1-22, this feature is apparent as 5 to 10 mgal variations in gravity. The exact source of each of these variations is not well documented, but the variations are likely due to a combination variations in bathymetry, crustal thickness, and crustal composition created during Mesozoic extension and rifting (see Subsections 2.5S.1.1.4.4.3 and 2.5S.1.1.4.1.3) (References 2.5S.1-65, 2.5S.1-91, 2.5S.1-99, and 2.5S.1-102).

Gravity Feature I

Gravity Feature I refers to the abrupt increase in gravity anomaly in the southeastern portion of Figure 2.5S.1-15 (References 2.5S.1-43, 2.5S.1-44, and 2.5S.1-45). In Figure 2.5S.1-22, the feature is apparent as an approximately 50 mgal increase in gravity anomaly. A spatially correlated bathymetric high (Reference 2.5S.1-3) likely causes a portion of the gravity increase (Figure 2.5S.1-21 [References 2.5S.1-43, 2.5S.1-45 and 2.5S.1-89]). However, a postulated basement high caused by a Late Jurassic mantle plume (i.e., “hot spot”) may also influence the gravity increase of Gravity Feature I (Reference 2.5S.1-63).

Gravity Feature J

Gravity Feature J reflects the numerous, short-wavelength (on the order of miles), low-magnitude (several mgal) anomalies that are present throughout the Texas Coastal Plain as small depressions in Figure 2.5S.1-20 (References 2.5S.1-43 and 2.5S.1-45). The exact source of each of these anomalies is not well documented. However, this style of feature is frequently due to the presence of salt diapirs (e.g., Reference 2.5S.1-107), and many diapirs are associated with these features (Figure 2.5S.1-10 [Reference 2.5S.1-27] and Figure 2.5S.1-17 [Reference 2.5S.1-27]) (Reference 2.5S.1-51).

2.5S.1.1.4.3.2 Magnetic Data

Magnetic anomaly data encompassing the STP 3 & 4 site region is shown in Figure 2.5S.1-23 (References 2.5S.1-46 and 2.5S.1-47). The data are from aeromagnetic surveys reported by Bankey et al. (References 2.5S.1-46 and 2.5S.1-47). A profile of the magnetic anomaly along profile B to B' through STP 3 & 4 and perpendicular to the regional structural trend is shown in Figure 2.5S.1-22. There are six major features present within the magnetic data, referred to as Magnetic Features A through F, which are described in detail below and shown in Figure 2.5S.1-16 (References 2.5S.1-44, 2.5S.1-46, 2.5S.1-47 and 2.5S.1-48).

Magnetic Feature A

Magnetic Feature A refers to the irregular pattern of distinct magnetic highs and lows in the region of the Llano Uplift (Figure 2.5S.1-16 [References 2.5S.1-44, 2.5S.1-46, 2.5S.1-47 and 2.5S.1-48] and Figure 2.5S.1-17 [Reference 2.5S.1-27]). In Figure 2.5S.1-22, this feature is apparent as a series of approximately 175 nanotesla variations in magnetic anomaly at the northwest end of the profile. Magnetic Feature A is likely due to variations in magnetism within the Proterozoic igneous intrusions comprising the core of the Llano Uplift (see Subsections 2.5S.1.1.2.3, 2.5S.1.1.4.1.2 and 2.5S.1.1.4.4.1) (References 2.5S.1-104 and 2.5S.1-42), which correlates with the Ouachita Orogeny as discussed in Subsection 2.5S.1.1.4.1.2. Magnetic Feature A is spatially correlated with Gravity Feature A.

Magnetic Feature B

Magnetic Feature B refers to a subtle, arcuate magnetic low adjacent and to the south-southeast of Magnetic Feature A (Figure 2.5S.1-16 [References 2.5S.1-44, 2.5S.1-46, 2.5S.1-47 and 2.5S.1-48]). In Figure 2.5S.1-22, this feature is apparent as an approximately 100 nanotesla decrease in magnetic anomaly.

Magnetic Feature B is spatially associated with the same foreland basins of the Ouachita system as Gravity Feature B and is proposed to indicate the presence

of deep sedimentary basins formed during the Ouachita Orogeny (see discussion in Subsections 2.5S.1.1.4.4.2 and 2.5S.1.1.4.1.2) (References 2.5S.1-94 and 2.5S.1-99).

Magnetic Feature C

Magnetic Feature C refers to a subtle magnetic high immediately south and southeast of Magnetic Feature B trending subparallel to Magnetic Feature B (Figure 2.5S.1-16 [References 2.5S.1-44, 2.5S.1-46, 2.5S.1-47 and 2.5S.1-48]). In Figure 2.5S.1-22, Magnetic Feature C is seen as an approximately 25-mile wide magnetic high of approximately 150 nanoteslas. This feature is spatially associated with Gravity Feature C. The more subdued nature of Magnetic Feature C relative to Gravity Feature C has been suggested to indicate that the source of the magnetic feature is at considerable depth (Reference 2.5S.1-94). As with Gravity Feature C, Magnetic Feature C is thought to represent a major transition in basement structure from unextended continental crust to thick transitional crust that formed during Mesozoic rifting as discussed in Subsections 2.5S.1.1.4.1.3 and 2.5S.1.1.4.4.3 (Figure 2.5S.1-16 [References 2.5S.1-44, 2.5S.1-46, 2.5S.1-47 and 2.5S.1-48]) (References 2.5S.1-61, 2.5S.1-94, and 2.5S.1-99). Locally the anomaly may be enhanced by the intrusion of igneous rocks associated with Mesozoic rifting (Reference 2.5S.1-99).

Magnetic Feature D

Magnetic Feature D refers to the prominent magnetic high inland of the coastline passing through Houston (Figure 2.5S.1-16 [References 2.5S.1-44, 2.5S.1-46, 2.5S.1-47 and 2.5S.1-48]). In Figure 2.5S.1-22, this feature is apparent as an approximately 100-mile-wide magnetic high with an overall increase in magnetic anomaly of approximately 300 nanoteslas. This feature is referred to as the “Houston magnetic anomaly” and is hypothesized to reflect the presence of a mafic dike complex injected into the thin transitional crust during Mesozoic rifting, the presence of ultramafic rocks emplaced during the Ouachita Orogeny, or a combination of both (Reference 2.5S.1-91).

Magnetic Feature E

Magnetic Feature E refers to the increase in magnetic anomaly approximately 50 miles south of the coastline (Figure 2.5S.1-16 [References 2.5S.1-44, 2.5S.1-46, 2.5S.1-47, and 2.5S.1-48]). In Figure 2.5S.1-22, this feature is apparent as an abrupt, approximately 175 nanotesla increase in magnetic anomaly. This feature has been attributed to a significant contrast in magnetism within the thin transitional crust (Reference 2.5S.1-91) and is likely due to variations in the amount of rift related intrusions.

Magnetic Feature F

Magnetic Feature F refers to the distinct magnetic highs located in the southeast of Figure 2.5S.1-16 (References 2.5S.1-44, 2.5S.1-46, 2.5S.1-47,

and 2.5S.1-48). This feature is spatially associated with Gravity Feature I. Magnetic Feature F potentially reflects the presence of mafic rocks intruded into the crust during passage of a Late Jurassic mantle plum (Reference 2.5S.1-63).

2.5S.1.1.4.4 Principal Tectonic Structures

In the sections below, specific tectonic features (Figure 2.5S.1-17 [Reference 2.5S.1-27] and Figure 2.5S.1-10 [Reference 2.5S.1-27]) and the evidence for activity published since the EPRI (Reference 2.4S.1-39) study are discussed. No new information has been published since 1986 on any tectonic feature within the STP 3 & 4 site region that would cause a significant change in the EPRI seismic source model.

The principal tectonic structures within the STP site region are divided into five categories based on their age of formation or most recent reactivation. These categories include Late Proterozoic, Paleozoic, Mesozoic, Tertiary, and Quaternary. Late Proterozoic, Paleozoic, and Mesozoic to early Tertiary structures are related to major plate tectonic events and are mapped regionally on the basis of geological and/or geophysical data. Late Proterozoic structures include normal faults active during rifting and formation of the Iapetan passive margin. Paleozoic structures include thrust and reverse faults active during the Ouachita collisional orogeny. Mesozoic structures include normal faults and other structures active during formation of the Gulf of Mexico.

Tertiary and Quaternary structures within the STP 3 & 4 site region are related to the tectonic environment of the Gulf of Mexico passive margin. This passive margin environment is characterized by southwest-northeast-oriented horizontal principal compressive stress (see discussion in Subsection 2.5S.1.1.4.2), large-scale basinward slumping of the Coastal Plain section, and vertical crustal motions. The vertical crustal motions are associated with flexural loading of the coastal plain and offshore sedimentary basins (Reference 2.5S.1-51), and erosion and exhumation of the Great Plains.

2.5S.1.1.4.4.1 Late Proterozoic Tectonic Structures

No significant Late Proterozoic structures are mapped within the 200-mile STP 3 & 4 site region. The only exposures of Proterozoic rocks in the site region are in the erosional window through Mesozoic strata across the axis of the Llano Uplift (Figure 2.5S.1-17 [Reference 2.5S.1-27] and Figure 2.5S.1-10 [Reference 2.5S.1-27]). The Proterozoic rocks in the Llano Uplift show evidence for multiple phases of penetrative ductile deformation that predate late Proterozoic rifting of Laurentia and formation of the Iapetan Margin (References 2.5S.1-104 and 2.5S.1-15). These rocks are also thought to cause the unique gravity and magnetic anomaly spatially correlated with the Llano Uplift described in Subsection 2.5S.1.1.4.3 (Figures 2.5S.1-20 [References 2.5S.1-43 and 2.5S.1-45] and 2.5S.1-22). Normal faults and fault-bounded basins associated with Late Proterozoic to Early Paleozoic rifting of Laurentia are inferred to lie beneath overthrust rocks of the Late Paleozoic Ouachita Orogenic Belt and Mesozoic and Tertiary Coast Plain Strata (References 2.5S.1-51 and 2.5S.1-20), but

these structures are not exposed in central Texas, and they are not well documented in peer-reviewed geologic literature.

2.5S.1.1.4.4.2 Paleozoic Tectonic Structures

The major Paleozoic tectonic structures in the STP site region are associated with the Late Paleozoic Ouachita Orogeny. These structures can be divided into two main groups: (1) structures of the Ouachita Orogenic Belt, and (2) basins and arches developed in the foreland of the Ouachita Orogenic Belt.

As discussed in Subsection 2.5S.1.1.4.1, the Ouachita Belt in central Texas is completely buried by Mesozoic and Tertiary strata of the Gulf Coastal Plain, and thus faults, folds, and other structures that developed during the Late Paleozoic Ouachita Orogeny are not exposed at the surface (Reference 2.5S.1-20). Based on analysis of borehole and other subsurface data from the Gulf Coastal Plain, the Ouachita Belt in central Texas is divided into a 20- to 39-mi-wide frontal zone, consisting primarily of rocks of the Paleozoic passive margin sequence that were transported northward and westward along low-angle thrust faults, and an interior metamorphic belt consisting of intensely deformed fragments of accreted granitic basement overlain by sandstone and marble, all subjected to weak to low-grade regional metamorphism (References 2.5S.1-20, 2.5S.1-57 and 2.5S.1-108). The southern boundary of the interior metamorphic belt has not been penetrated by drill holes, but is assumed to be down structural dip to the south beneath the Coastal Plain Strata (Reference 2.5S.1-108). Total minimum width of the Ouachita Belt in the subsurface of east Texas is about 50 miles (Reference 2.5S.1-20).

Like the better-exposed and better-studied Appalachian Orogenic Belt, workers have interpreted the Ouachita Belt to be underlain by a major décollement that dips south and separates the allochthonous Ouachita rocks from the autochthonous crust of the Laurentian Margin (Reference 2.5S.1-53). The autochthonous rocks below the décollement probably range from a full thickness of ancestral North American continental crust beneath the northwestern part of the Ouachita Belt, to transitional crust and oceanic crust farther to the south and southeast. The upper surface of the Ouachita rocks beneath the basal Mesozoic unconformity is a low-relief erosion surface that dips 1° or less toward the Gulf of Mexico (Reference 2.5S.1-53).

The boundary between the frontal belt and interior metamorphic belt was called the “Luling Front” by Flawn et al. (Reference 2.5S.1-109) and interpreted as an overthrust fault (i.e., the “Luling Thrust;” Reference 2.5S.1-20). Subsequent work has established that the “Luling Front” probably is not a single fault, but rather a zone of distributed thrust deformation that is up to several miles wide and locally difficult to define with precision (Reference 2.5S.1-108). Cullotta et al. (Reference 2.5S.1-71) interpreted a deep seismic reflection profile along the NNW-SSE-trending San Marcos Arch to image the Luling Thrust as a folded, south-dipping structural contact between deformed autochthonous rocks of the frontal zone and accreted rocks of the interior zone. It is important to note that the “Luling Front” or “Luling Thrust” is a structure of the buried Ouachita Belt inferred from analysis of subsurface data. This structure is

distinct from the Luling Fault Zone, which is a Tertiary fault mapped at the surface in the northern Gulf Coastal Plain in central Texas (Subsection 2.5S.1.1.4.3.4.3).

The Kerr Basin and Fort Worth Basin, located to the southwest and northeast of the Llano Uplift, respectively (Figure 2.5S.1-17 [Reference 2.5S.1-27] and Figure 2.5S.1-10 [Reference 2.5S.1-27]), are late Paleozoic marine basins that the developed in the foreland of Ouachita Orogenic Belt. These foreland basins are buried by strata of the Coastal Plain, and are known from subsurface data gathered during oil and gas exploration (e.g., References 2.5S.1-21 and 2.5S.1-61). The basins primarily formed by flexural loading of the crust as the Ouachita Orogen developed structural and topographic relief. Data from other parts of the Ouachita foreland indicate that these basins typically subsided along down-to-the-south normal faults, which in some cases were overthrust by the frontal zone thrust sheets during the latter stages of the Ouachita Orogeny (References 2.5S.1-20 and 2.5S.1-21). The most prominent basins are apparent in regional gravity data as discussed in Subsection 2.5S.1.1.4.3.1. Although comparable late Paleozoic foreland basin faults may be present beneath the Coastal Plain section in the STP 3 & 4 site region, they are not extensively documented in the peer-reviewed literature (e.g., Reference 2.5S.1-10).

2.5S.1.1.4.4.3 Mesozoic Tectonic Structures

Major Mesozoic structural features in the STP 3 & 4 site region include faults that accommodated renewed crustal rifting in the Triassic, structures associated with sea-floor spreading in the young Gulf of Mexico, Jurassic basins that formed in the early stages of the opening of the Gulf of Mexico, structures related to the movement of Jurassic salt deposits, and large basement-involved uplifts and arches that are hypothesized to have developed coeval with the Late Cretaceous-early Tertiary Laramide Orogeny to the west.

The initial stages of rifting related to the breakup of Pangea occurred in the Late Triassic and accommodated relatively little of the overall extension and thinning that formed the modern Gulf of Mexico (Reference 2.5S.1-44). This stage of rifting is characterized by the formation of grabens and half-grabens filled with nonmarine sediments, commonly referred to as red beds, and rift-related volcanics (References 2.5S.1-22, 2.5S.1-90, and 2.5S.1-44). These basins ring the modern day Gulf of Mexico, but are primarily concentrated along the western Gulf in Mexico and the north to northeastern Gulf from Texas to northern Florida (References 2.5S.1-22 and 2.5S.1-90).

The closest known red beds to STP 3 & 4 occur within the East Texas Basin (Figure 2.5S.1-10 [Reference 2.5S.1-27]), suggesting that this basin initially formed as part of the breakup of Pangea (Reference 2.5S.1-22). After the red bed deposition, the East Texas Basin accumulated thick deposits of salt in the late Middle Jurassic, followed by a large influx of clastic deposits during the Late Jurassic and Early Cretaceous (Reference 2.5S.1-51). The Jurassic salt deposits along the northeast-trending axis of the basin were mobilized beginning in Late Jurassic time to form numerous diapirs by Early Cretaceous time; these structures now comprise the East Texas Diapir Province (Reference 2.5S.1-51). Presently the East Texas Basin is bounded on the west and

north by the Mexia-Talco Fault System, on the east by the Late Cretaceous to early Tertiary Sabine Uplift, and on the southeast by a south-facing homocline (Reference 2.5S.1-51).

As discussed in Subsection 2.5S.1.1.4.1.3, the bulk of the rifting associated with the opening of the Gulf of Mexico occurred in the Middle to Late Jurassic and was accommodated almost equally as extension of continental crust and, at a later stage, by seafloor spreading (Reference 2.5S.1-64). The extension occurred as thinning within the now thin transitional crust and to a lesser degree within the now thick transitional crust (Reference 2.5S.1-44) (Figure 2.5S.1-15 [References 2.5S.1-43, 2.5S.1-44, and 2.5S.1-45] and Figure 2.5S.1-16 [References 2.5S.1-44, 2.5S.1-46, 2.5S.1-47, and 2.5S.1-48]). Basement block bounding faults formed during the extensional episode have been interpreted within both the thick and thin transitional crust based on combinations of gravity, magnetic, and seismic data (see Subsection 2.5S.1.1.4.3 for the identification of rift structures based on gravity and magnetic data) (e.g., References 2.5S.1-9, 2.5S.1-68, 2.5S.1-94, 2.5S.1-103, 2.5S.1-111, and 2.5S.1-112). However, the locations of these faults and their geometry are difficult to determine given the thick accumulations of younger sedimentary rocks. While the existence of any such faults within the STP site region is unknown for these reasons, no seismicity within the STP site region has been attributed to movement on these style of basement faults (References 2.5S.1-113, 2.5S.1-114 and 2.5S.1-115).

The kinematics of the Middle and Late Jurassic oceanic crust formation within the Gulf of Mexico (Figure 2.5S.1-15 [References 2.5S.1-43, 2.5S.1-44, and 2.5S.1-45] and Figure 2.5S.1-16 [References 2.5S.1-44, 2.5S.1-46, 2.5S.1-47, and 2.5S.1-48]) is poorly understood due to the relatively small extent of the oceanic crust and the thick accumulations of sedimentary rocks and salt overlying the crust (References 2.5S.1-66 and 2.5S.1-44). Accordingly there is no consensus regarding plate reconstruction models for the opening of the Gulf of Mexico (e.g., References 2.5S.1-63, 2.5S.1-64, 2.5S.1-66, 2.5S.1-92, 2.5S.1-116, and 2.5S.1-117). Common to all models are large transform faults accommodating the variations in spreading rate.

Following from the uncertainty associated with such plate reconstruction models in general and the lack of a consensus model, the position of any such transform faults within the STP 3 & 4 site region is unknown. Because the potential location of such faults is limited to the oceanic crust, the closest such faults could approach to the site is approximately 100 miles (Figure 2.5S.1-15 [References 2.5S.1-43, 2.5S.1-44, and 2.5S.1-45] and Figure 2.5S.1-16 [References 2.5S.1-44, 2.5S.1-46, 2.4S.1-47, and 2.5S.1-48]). No seismicity within the STP site region has been attributed to these postulated structures (References 2.5S.1-113, 2.5S.1-114, and 2.5S.1-115).

Mesozoic fault systems of the Gulf of Mexico region are thought to be related to bodies of Jurassic salt at depth. These fault systems include the Mexia-Talco, Milano, Charlotte-Jourdanton, Karnes, and Mt. Enterprise-Elkhart Graben Fault Zones (Figure 2.5S.1-17 [Reference 2.5S.1-27] and Figure 2.5S.1-10 [Reference 2.5S.1-27]). In general, these faults systems lie updip of and sole into salt pinchouts or welds, and motion on the faults is related to the salt migration that ultimately caused the formation of the welds and pinchouts (References 2.5S.1-69 and 2.5S.1-118).

The Mexia-Talco Fault System, which bounds the western and northern margins of the East Texas Basin, is mapped continuously from the northeastern flank of the San Marcos Arch in central Texas to the Arkansas border (Reference 2.5S.1-17) (Figure 2.5S.1-17 [Reference 2.5S.1-27] and Figure 2.5S.1-10 [Reference 2.5S.1-27]). In detail, the fault system is divided into three segments: the Talco Fault Zone in northeastern Texas, the Mexia Fault Zone in north-central Texas, and the Milano Fault Zone in central Texas. The Mexia-Talco Fault System is characterized by a series of asymmetric grabens ranging from 5 to 8 miles in width that are linked by left-stepping, down-to-basin (i.e., down-to-the-south) normal faults. Upper Jurassic and Lower Cretaceous strata systematically thicken within the grabens, indicating that movement began in the Jurassic. Stratigraphic relations also demonstrate that movement continued through the Mesozoic and into Paleocene to Eocene time (Reference 2.5S.1-17). Data cited in the UFSAR for STP 1 & 2 (Reference 2.5S.1-7) indicates movement on the Mexia-Talco Fault System also occurred in Late Oligocene or Early Miocene.

Seismic reflection and borehole data document that the Mexia-Talco Fault System is located directly updip of the pinchout of Jurassic salt in the subsurface of the East Texas Basin and that individual graben segments typically develop where salt pinchout parallels strike (References 2.5S.1-51 and 2.5S.1-119). A structural cross section across the Mexia Fault Zone by Locklin (Reference 2.5S.1-120), reproduced in Ewing (Reference 2.5S.1-17), shows the fault zone terminating downward at a depth of about 9000 ft. to 10,000 ft. at the unconformity between the Louann Salt at the base of the Mesozoic Coastal Plain section and the top of the Paleozoic Ouachita rocks. These relationships strongly suggest that activity of the Mexia-Talco Fault System is related to movement of salt and does not involve the underlying crystalline basement (Reference 2.5S.1-119).

The Charlotte-Jourdanton Fault Zone lies along the northeastern margin of the Rio Grande Embayment (Figure 2.5S.1-10 [Reference 2.5S.1-27]) and is interpreted by some as the southwestern continuation of the Mexia-Talco Fault System (see discussion in UFSAR for STP 1 & 2 [Reference 2.5S.1-7]). The Karnes Fault Zone (Figure 2.5S.1-10 [Reference 2.5S.1-27]) is included in the Charlotte-Jourdanton Fault Zone by some workers, and with the Milano Fault Zone, is interpreted to be a structural link with the Mexia-Talco Fault System (Reference 2.5S.1-51). Collectively, these structures are referred to as the Peripheral Graben System (References 2.5S.1-51 and 2.5S.1-7). Like the Mexia-Talco Fault System, the Charlotte-Jourdanton Fault Zone is comprised of a series of *en echelon*, graben-forming normal faults. Stratigraphic growth relations across faults of the Charlotte-Jourdanton Zone indicate that movement began in the Jurassic and continued into the early Tertiary. The youngest documented rocks displaced by the Charlotte-Jourdanton Fault Zone are undifferentiated strata of Paleocene-Eocene age (Reference 2.5S.1-7).

The Mt. Enterprise fault-Elkhart Graben (MEEG) fault system is a zone of normal faults that obliquely crosses the southeastern margin of the East Texas Basin, and extends eastward to the western flank of the Sabine Uplift (References 2.5S.1-51 and 2.5S.1-119). The MEEG fault system strikes east-northeast-west-southwest and extends for a total distance of about 90 miles from south of Carthage to the Trinity River near

Palestine, Texas (Figure 2.5S.1-17 [Reference 2.5S.1-27], Figure 2.5S.1-24 [References 2.5S.1-49 and 2.5S.1-121] and Figure 2.5S.1-25 [References 2.5S.1-121, 2.5S.1-122, and 2.5S.1-28]). At its closest approach, the MEEG is located about 194 miles northeast of the STP Site. Like the Mexia-Talco Fault System, the MEEG is a structurally complex series of grabens that are interpreted to root in Jurassic Louann Salt, and which were primarily active in Late Jurassic-Early Cretaceous (References 2.5S.1-51 and 2.5S.1-119). The UFSAR for STP 1 & 2 (Reference 2.5S.1-7) cites work indicating that activity on the MEEG fault system continued into the Eocene. Evidence for late Quaternary activity of the MEEG fault system is discussed in Subsection 2.5S.1.1.4.3.5.1 below.

The Gulf of Mexico Coastal Plain is partly characterized by a series of Mesozoic, gulf perpendicular, large-scale arches and basins including the Rio Grande Embayment, the San Marcos Arch, the Houston Embayment and East Texas Basin, and the Sabine Arch (Figure 2.5S.1-17 [Reference 2.5S.1-27] and Figure 2.5S.1-10 [Reference 2.5S.1-27]). The presence of these features is apparent in the regional gravity data (see Subsection 2.5S.1.1.4.3) and the depth to the base of Mesozoic sediments with greater depths associated with basins and shallower depths associated with arches (Figure 2.5S.1-18 [References 2.5S.1-26, 2.5S.1-43, and 2.5S.1-45]). The San Macros Arch, which lies between the Rio Grande Embayment and East Texas Basin, is a northwest-trending, southeast-plunging antiform with an axial trace greater than 250 miles long that crosses the northeast-southwest structural trend of the Ouachita Belt in the northwestern part of the STP 3 & 4 site region (Reference 2.5S.1-71). The Llano Uplift is the northern reach of the San Marcos Arch (Reference 2.5S.1-55). The Sabine Arch is the general term for the conglomeration of smaller north-, northeast-, and northwest-trending, doubly plunging anticlines that extend between the coast and the Sabine Uplift (Reference 2.5S.1-103). The more complicated shape of the Sabine Arch relative to the San Marcos Arch is due to the distortion of the overall arch shape due to local flexures and salt structures (Reference 2.5S.1-103).

Both the San Marcos and Sabine Arches are defined by broad, open folding of Paleozoic structures and strata, as well as Jurassic subcrop trends. Cretaceous units overlying the arches and intervening basins have gentle 0.2º-1º dips, and the structural relief between Lower Cretaceous rocks on the arches and in the basins is on the order of about 3000 ft. (Reference 2.5S.1-103). Ewing (Reference 2.5S.1-51) characterized the San Marcos Arch as a “broad area of lesser (Mesozoic) subsidence between the Rio Grande Embayment and East Texas Basin.” The onset of bending for both arches occurred in the Late Cretaceous (References 2.5S.1-51 and 2.5S.1-103); subsequent growth of the arches is indicated by thinning of Late Cretaceous marine strata across the axes of the structures (References 2.5S.1-51 and 2.5S.1-103).

The formation of the series of arches and basins along the Texas Gulf Coastal Plain was likely caused by the combination of Mesozoic rifting of Pangea and the Late Cretaceous Laramide Orogeny. As discussed in Subsection 2.5S.1.1.4.1.3 and above, thinning and rifting related to extension within the modern thick-transitional crust may have caused gulf-perpendicular trends in basement thickness that in turn allowed for variable subsidence of crustal blocks and the creation of variable amounts of accommodation space for sedimentation observed in the modern day arches and

embayments (Reference 2.5S.1-44). It has been proposed that the arches are genetically related to east-west compressive stresses during the Late Cretaceous to early Tertiary Laramide Orogeny that occurred further to the west along the edge of the proto North American continent (References 2.5S.1-51, 2.5S.1-103, and 2.5S.1-123).

2.5S.1.1.4.4.4 Tertiary Tectonic Structures

The Gulf Coastal Plain was tectonically quiescent throughout most of the Tertiary. Regional deformation during the Tertiary primarily is characterized by slow sedimentary loading near the coast and down-to-the-south flexure of the lithosphere, resulting in progressive southward migration of the Gulf shoreline. Sedimentary loading of deeply buried Jurassic salt, combined with basinward migration of the shelf margin, compaction of the Coastal Plain strata, and gravitational slumping toward the Gulf, all contributed to the development of diapir provinces and systems of growth faults that accommodate down-to-the-basin subsidence. Although stratigraphic relations indicate that salt migration and growth faulting began in the Cretaceous (Reference 2.5S.1-51), the evolution of these structures in the Tertiary has significantly affected patterns of deposition and geomorphic development of the Coastal Plain.

2.5S.1.1.4.4.4.1 Tertiary Salt Structures

Mobilization of Jurassic salt deposits in sub-basins that formed during the Mesozoic led to the development of distinct diapir provinces in the Gulf Coastal Plain Region. Major concentrations of salt diapirs in the STP site region include the East Texas, Rio Grande, and Houston Diapir Provinces (Figure 2.5S.1-17 [Reference 2.5S.1-27] and Figure 2.5S.1-10 [Reference 2.5S.1-27]). As discussed in Subsection 2.5S.1.1.4.3.1, some of these concentrations of salt diapirs are also apparent in the regional gravity data (Figure 2.5S.1-21 [References 2.5S.1-43, 2.5S.1-45, and 2.5S.1-89]). Ewing (Reference 2.5S.1-51) noted that individual diapir provinces are characterized by distinctive spatial clustering of salt bodies, as well as distinct patterns and styles of salt movement. Major zones of diapiric salt movement in the offshore Gulf of Mexico Region include the Northwest Slope and Perdido Provinces south of the site, and the much larger Texas-Louisiana Slope Provinces to the southeast of the site. Although initial movement of salt began in the Mesozoic, deformation continued locally on structures during the Tertiary (Reference 2.5S.1-33).

The UFSAR for STP 1 & 2 (Reference 2.5S.1-7) identified three salt domes associated within the site vicinity: the Big Hill Salt Dome, approximately 10 miles from STP 3 & 4; the Hawkinsville Salt Dome, approximately 15 miles from STP 3 & 4; and the Markham Salt Dome, approximately 14 miles from STP 3 & 4 (Figure 2.5S.1-11 [References 2.5S.1-28, 2.5S.1-29 and 2.5S.1-30]). These domes are part of the salt diapirism related to the Houston Embayment. Since publication of the UFSAR for STP 1 & 2 (Reference 2.5S.1-7), no previously undiscovered, large-scale salt domes have been identified within the STP 3 & 4 site vicinity (References 2.5S.1-124 and 2.5S.1-125).

2.5S.1.1.4.4.4.2 Tertiary Growth Faults

Syndepositional growth faults generally parallel the trend of the Gulf Coastline and are clustered in distinct spatial groups by age and structural style (Reference 2.5S.1-69)

(Figure 2.5S.1-17 [Reference 2.5S.1-27], Figure 2.5S.1-24 [References 2.5S.1-49 and 2.5S.1-121] and Figure 2.5S.1-10 [Reference 2.5S.1-27]). According to Ewing (Reference 2.5S.1-51), the locations of individual growth fault zones are related to positions of the clastic Gulf shelf margin as it progressively stepped basinward during the Late Cretaceous, Tertiary, and Quaternary. From north to south, the major growth fault systems within the STP 3 & 4 site region include the Wilcox Fault Zone, the Yegua Fault Zone, the Vicksburg Fault Zone, and the Frio Fault Zone (Figure 2.5S.1-17 [Reference 2.5S.1-27] and Figure 2.5S.1-10 [Reference 2.5S.1-27]). The next major growth fault zone to the south in the offshore region is the Corsair or Brazos Fault Zone. The common characteristic of all growth faults is that they sole into or terminate against low-angle detachment horizons within the Gulf Coastal Plain section. These detachments are variously bodies of Jurassic salt and/or shale horizons (References 2.5S.1-69 and 2.5S.1-118). Growth faults do not extend through the Coastal Plain section into the basement. Characteristics of the major growth fault zones in the STP 3 & 4 site region are summarized in greater detail below.

- The Wilcox Fault Zone is Paleocene-Eocene in age and related to the shelf-margin progradation marked by the deposition of the deltaic Wilcox Group strata in south Texas and Louisiana (Reference 2.5S.1-126). Interpretation of a deep seismic reflection profile along the San Marcos Arch suggests that the Wilcox Fault Zone is localized along the buried edge of a Cretaceous reef system (Reference 2.5S.1-57), which marks the boundary between the Interior Zone and Coastal Zone of the Coastal Plain (Reference 2.5S.1-51). The Wilcox Fault Zone consists of about 5 to 10 closely spaced, moderately to steeply dipping faults that terminate against or are rooted in a detachment in highly pressured Cretaceous strata at depth (Reference 2.5S.1-51). Wilcox faults that cross the Houston Diapir Province north of STP 3 & 4 are both localized above pre-existing salt pillows, and deformed by salt diapirs (References 2.5S.1-69 and 2.5S.1-126).

- The Yegua Fault Zone is associated with middle to late Eocene southward progradation of the clastic shelf margin (Reference 2.5S.1-126), and is best expressed in the Houston Embayment east-northeast of the San Marcos Arch (Figure 2.5S.1-17 [Reference 2.5S.1-27] and Figure 2.5S.1-10 [Reference 2.5S.1-27]). The Yegua Fault Zone is characterized by a series of fault-bounded blocks that are rotating domino-style against a low-angle detachment or detachments at depth, which may in part be inherited from structures of the older Wilcox System.

- The Vicksburg Fault Zone is associated with an early Oligocene deltaic progradation (Reference 2.5S.1-127). The Vicksburg Fault Zone is best developed west-southwest of the San Marcos Arch, but some growth faults of early Oligocene (Vicksburg) age are observed in southeast Texas. In contrast to the domino-style faulting of the hanging wall observed in the Yegua Fault Zone, the Vicksburg growth faults are characterized by “escalator-style glide faults,” in which the hanging wall moves down as a relatively intact block and is continuously buried by large bodies of syntectonic sediment (Reference 2.5S.1-51). The detachment for the Vicksburg Fault Zone soles out into shales of the upper part of the Eocene Jackson Group (Reference 2.5S.1-127).

- The Frio Fault Zone, which is the closest growth fault system to the STP 3 & 4 site, developed in response to late Oligocene shelf progradation in Texas and Louisiana (Reference 2.5S.1-126). The Frio Fault Zone is about 37 miles wide and characterized by moderately dipping sinuous normal faults spaced at 3 to 6 mi intervals that root in a deep detachment system (Reference 2.5S.1-126). The hanging walls of the major south-dipping normal faults contain roll-over anticlines (Reference 2.5S.1-128) and some antithetic, north-dipping normal faults (Reference 2.5S.1-51). Variations in structural style along the Frio growth fault trend are attributed to the relative influence of salt tectonism and associated structures (salt domes, salt-cored anticlines, and salt-withdrawal features), and shale tectonism (e.g., shale diapirs and ridges), and the depositional environment of the Frio-aged strata involved in the deformation (Reference 2.5S.1-126).

- The Corsair Fault Zone south of the STP 3 & 4 site formed in response to middle Miocene shelf progradation. Like the Vicksburg Fault Zone, the Corsair Fault Zone is an escalator-style glide-fault system (Reference 2.5S.1-51).

2.5S.1.1.4.4.4.3 Tertiary Basement-Involved Faults

The Balcones and Luling Fault Zones strike northeast-southwest, subparallel to the trend of the buried Ouachita Orogenic Belt, and are exposed on the San Marcos Arch southeast of the Llano Uplift (Figure 2.5S.1-17 [Reference 2.5S.1-27] and Figure 2.5S.1-10 [Reference 2.5S.1-27]). Both of these structures are discussed in detail in the UFSAR for STP 1 & 2 (Reference 2.5S.1-7). The Balcones Fault Zone is dominated by down-to-southeast normal faults with maximum displacements up to 1640 ft., and the Luling Fault Zone is dominated by down-to-the-northwest normal faults with a cumulative throw of about 1000-2000 ft. (Reference 2.5S.1-51). Together, the Balcones and Luling Fault Zones form a 730 mile-wide graben system (Reference 2.5S.1-51). Displacements on the faults diminish to the northeast and southwest with distance from the axis of the San Marcos Arch (Reference 2.5S.1-17).

Initial movement on the Balcones and Luling Fault Zones may have occurred in the Mesozoic because Late Cretaceous volcanic rocks of the Balcones Igneous Province generally are exposed along the trend of the fault zones, and in some cases volcanic centers are aligned along the faults (Reference 2.5S.1-51). Most of the displacement on the Balcones Fault Zone is thought to have occurred in the late Oligocene and early Miocene (Reference 2.5S.1-129).

The down-dip geometry of the Luling Fault Zone was imaged in a deep seismic reflection profile acquired by the Consortium for Continental Reflection Profiling (COCORP) along the axis of the San Marcos Arch. Cullotta et al. (Reference 2.5S.1-71) interpreted the COCORP data to show the Luling Fault terminating at a depth of 0.6-1.2 miles against the unconformity between Cretaceous limestones and underlying Paleozoic rocks of the Ouachita orogenic belt. The Ouachita rocks beneath the Luling Fault Zone are associated with an antiformal pattern of reflectors that Cullotta et al. (Reference 2.5S.1-71) interpret as an antiformal structural duplex of Ouachita-age thrust sheets.

Cullotta et al. (Reference 2.5S.1-71) proposed that the Tertiary Luling Fault Zone may represent localized reactivation of south-dipping Ouachita structures in response to flexure along the subsiding Gulf Margin. They speculated that the location and magnitude of flexure, and thus the Balcones and Luling Fault Zones, may be controlled in part by pre-existing structures in the Ouachita orogenic belt. Ewing (Reference 2.5S.1-130) suggested that extension represented by these faults may be the shallow expression of down-to-the-basin motion on reactivated south-dipping thrust faults in the Ouachita Belt, which may have acted as glide planes. Alternatively, the graben formed by the Balcones and Luling Fault Zones may be a “keystone graben” formed along the early Miocene hingeline that accommodated sedimentary loading and flexure of the lithosphere (Reference 2.5S.1-130).

The Balcones Fault Zone is associated with the southeast-facing Balcones Escarpment, a prominent geomorphic feature in central Texas (Reference 2.5S.1-131). Rocks exposed on the up-thrown side of the fault zone are dominantly Lower Cretaceous carbonates, which are relatively resistant to erosion, whereas strata on the downthrown side are non-resistant Upper Cretaceous chalk and mudrocks (Reference 2.5S.1-132). The Balcones Escarpment is a fault-line scarp produced by differential erosion of these units.

2.5S.1.1.4.4.5 Quaternary Tectonic Structures

The site region is part of a tectonically stable continental margin. No capable tectonic faults were identified within the STP 3 & 4 site region during the 1986 EPRI studies (Reference 2.5S.1-39), and the UFSAR for STP 1 & 2 (Reference 2.5S.1-7) concluded that there were no capable tectonic faults within the site region. The Gulf Region in general, and site region in particular, is characterized by very low rates of background seismicity (Subsection 2.5S.2.1).

Evidence for potential Quaternary activity on the Mt. Enterprise Fault, the Balcones Fault Zones and the New Madrid Fault Zone, beyond the site region, are discussed below.

2.5S.1.1.4.4.5.1 Mt. Enterprise-Elkhart Graben System

The Mt. Enterprise-Elkhart Graben (MEEG) system is described in the UFSAR for STP 1 & 2 (Reference 2.5S.1-7), which concluded that the most recent movement was likely Eocene in age or younger. As noted in publications that predate the 1986 EPRI studies, several lines of evidence document Quaternary motion and active creep along the MEEG:

- Three faults at the western end of the MEEG fault zone in the Trinity River Valley near Palestine, Texas, displace late Quaternary (37,000 year old) deposits overlying Eocene Claiborne Strata (Reference 2.5S.1-121) (Figure 2.5S.1-25 [References 2.5S.1-121, 2.5S.1-122 and 2.5S.1-28]). Maximum normal displacement of the Eocene strata on the faults at this site is 46.5 inches, with maximum offset of the overlying Quaternary gravels of 26 inches. Based on an estimated age of 37 ka for the late Quaternary gravels (Reference 2.5S.1-121), the

implied average, late Quaternary separation rate across the fault is about 0.0007 in/yr.

- Geodetic leveling data showing a relative movement of about 5 inches across the geographic center of the MEEG in a 30-year period between 1920 and the mid-1950s, with a down-to-the-south displacement across the southern margin of the MEEG system (Reference 2.5S.1-121) (Figure 2.5S.1-25 [References 2.5S.1-121, 2.5S.1-122, and 2.5S.1-28]). If this motion is due to slip on normal faults of the MEEG, then the average vertical separation rate is 0.17 in/yr.

- Historical and instrumentally located seismicity is spatially associated with the MEEG, including: the 1891 Rusk Earthquake (**M** 4.0, location and magnitude estimated from felt effects); four earthquakes in 1957 (**M** 3.0 to **M** 4.7, estimated from felt effects); and the 1981 Center (m_b 3.0) and Jacksonville (m_b 3.2) Earthquakes (References 2.5S.1-113 and 2.5S.1-115) (Figure 2.5S.1-25 [References 2.5S.1-121, 2.5S.1-122, and 2.5S.1-28]).

As discussed in Subsection 2.5S.1.1.4.4.3, seismic reflection data suggest that the MEEG is rooted in the Jurassic Louann Salt at maximum depths of 3 to 4 mi (References 2.5S.1-119 and 2.5S.1-133). This suggests that observed late Quaternary displacement and contemporary creep across the MEEG may be driven by movement of salt at depth, indicating that the fault is not accommodating tectonic deformation and thus is not an independent source of moderate to large earthquakes. Presumably, this was the evaluation of the EPRI ESTs, which had access to the pre-1986 literature on the MEEG and did not specifically characterize it as a Quaternary tectonic fault and potentially capable structure. Notwithstanding, Ewing (Reference 2.5S.1-51) commented in a post-EPRI publication that “surface strata are displaced and seismicity suggests continuing deformation” on the MEEG.

Based on a review of post-EPRI scientific literature, no new data have been published to support an interpretation that the MEEG is a capable tectonic structure. Recent reviews of suspected Quaternary tectonic features in the CEUS by Crone and Wheeler (Reference 2.5S.1-49) and Wheeler (Reference 2.5S.1-50) did not identify or discuss the MEEG as a potential tectonic fault. Based on the documented association of the MEEG with Jurassic salt deposits and the high rate of active creep measured by geodetic methods, the preferred interpretation is that Quaternary activity of the MEEG is related to salt migration at depth. The separation rate of 0.17 in/yr. implied by the geodetic data is highly anomalous for a fault located in a stable continental block; if tectonic, deformation rates and fault slip rates of about 0.15-0.2 in/yr. are more characteristic of those associated with an active plate boundary. There is broad consensus within the informed geoscience community that the Gulf Coastal Plain is part of stable North America and not part of an active plate boundary. The high geodetic deformation rates, if accurate, are most simply explained by movement of salt at depth and do not reflect whole-crustal strain. In conclusion, there is no new information on the Quaternary activity of the MEEG faults requiring a revision of the EPRI seismic source characterization of the Coastal Plain Region.

2.5S.1.1.4.4.5.2 Balcones Fault Zone

As discussed in Subsection 2.5S.1.1.4.4.4.3, the Balcones Fault and Luling Fault Zones comprise an approximately east-west-trending graben system located about 140 miles northwest of the site. The major displacements on the Balcones Fault are interpreted to have occurred in the late Oligocene-early Miocene (Reference 2.5S.1-129). In a post-EPRI publication, Collins et al. (Reference 2.5S.1-134) reported that downward tapering, wedge-shaped fractures filled with weathered colluvium have been observed along individual faults of the Balcones Zone. Collins et al. (Reference 2.5S.1-134) speculated that the fractures may have formed during surface-rupturing events on the associated faults and subsequently filled with colluvial material. Based on the degree of weathering and soil profile development in the colluvium, Collins et al. (Reference 2.5S.1-134) inferred that the deposits are Pleistocene in age. If the wedges of colluvium are filling fractures that formed during surface-rupturing events on the Balcones Fault Zone, then the faults generated moderate to large earthquakes during the Quaternary. Collins et al. (Reference 2.5S.1-134) also noted, however, that strands of the Balcones Fault Zone are overlain by unfaulted Quaternary terrace deposits and that these relations suggest the fissure-fill deposits probably are not related to co-seismic faulting. Collins et al. (Reference 2.5S.1-134) concluded that detailed paleoseismic studies of the Balcones Fault Zone are needed to conclusively demonstrate activity or non-activity of the structure during the Quaternary.

Based on the review of post-EPRI literature, no data documenting Quaternary activity of the Balcones Fault Zone has been published since the EPRI (Reference 2.5S.1-39) study. The colluvial relations discussed by Collins et al. (Reference 2.5S.1-134) are equivocal evidence for late Cenozoic activity at best, and the stratigraphic relationships of unfaulted Quaternary terrace deposits overlying the Balcones Fault Zone are positive evidence for no Quaternary activity. There is no new post-EPRI information on the Balcones Fault Zone that requires a revision of the EPRI seismic source characterization of the Coastal Plain Region.

2.5S.1.1.4.4.5.3 New Madrid Seismic Zone

The New Madrid Seismic Zone extends from southeastern Missouri to southwestern Tennessee and is located more than 500 miles northeast of the STP site (Figure 2.5S.1-26 [Reference 2.5S.1-135]). The New Madrid Seismic Zone lies within the Reelfoot Rift and is defined by post-Eocene to Quaternary faulting with previous older seismic activity. Given its significant distance from the site, the New Madrid Seismic Zone did not contribute to 99% of the hazard at STP 1 & 2 in the original EPRI PSHA study (Reference 2.5S.1-17). This subsection presents discussion of the New Madrid Seismic Zone, however, because several recent studies provide significant new information regarding source zone parameters.

The New Madrid Seismic Zone is approximately 125 miles long and 25 miles wide. Research conducted since 1986 has identified three distinct fault segments embedded within the seismic zone, consisting of a southern northeast-trending dextral slip fault, a middle northwest-trending reverse fault, and a northern northeast-trending dextral strike-slip fault (Reference 2.5S.1-136). In the current east-northeast to west-southwest directed regional stress field, Precambrian and Late Cretaceous age

extensional structures of the Reelfoot Rift appear to have been reactivated as right-lateral strike-slip and reverse faults.

The New Madrid Seismic Zone produced a series of historical, large-magnitude earthquakes between December 1811 and February 1812 (Reference 2.5S.1-137). The December 16, 1811 earthquake is associated with strike-slip fault displacement along the southern part of the New Madrid Seismic Zone. Johnston estimates a magnitude of **M** 8.1±0.31 for the December 16, 1811 event (Reference 2.5S.1-138). However, Hough et al. re-evaluated the isoseismal data for the region and conclude that the December 16 event had a magnitude of **M** 7.2 to 7.3 (Reference 2.5S.1-137). Bakun and Hopper similarly conclude this event had a magnitude of **M** 7.2 (Reference 2.5S.1-139).

The February 7, 1812 New Madrid Earthquake is associated with reverse fault displacement along the middle part of the New Madrid Seismic Zone (Reference 2.5S.1-140). This earthquake most likely occurred along the northwest-striking Reelfoot Fault that extends approximately 43 mi from northwestern Tennessee to southeastern Missouri. The Reelfoot Fault is a northeast-dipping, southwest-vergent reverse fault. The Reelfoot Fault does not extend updip to the earth's surface, but a topographic scarp as has developed above the buried tip of the fault as a result of fault-propagation folding (References 2.5S.1-141, 2.5S.1-142, and 2.5S.1-143). Johnston estimated a magnitude of **M** 8.0±0.33 for the February 7, 1812 event (Reference 2.5S.1-138). However, Hough et al. re-evaluated the isoseismal data for the region and conclude that the February 7 event had a magnitude of **M** 7.4 to 7.5 (Reference 2.5S.1-137). More recently, Bakun and Hopper estimated a similar magnitude of **M** 7.4 (Reference 2.5S.1-139).

The January 23, 1812 earthquake is associated with strike-slip fault displacement on the East Prairie Fault along the northern part of the New Madrid Seismic Zone. Johnston estimated a magnitude of **M** 7.8±0.33 for the January 23, 1812, event (Reference 2.5S.1-138). Hough et al., however, re-evaluated the isoseismal data for the region and concluded that the January 23 event had a magnitude of **M** 7.1 (Reference 2.5S.1-137). More recently, Bakun and Hopper estimated a similar magnitude of **M** 7.1 (Reference 2.5S.1-139).

Because there is very little surface expression of faults within the New Madrid Seismic Zone, earthquake recurrence estimates are based largely on dates of paleoliquifaction and offset geological features. The most recent summaries of paleoseismologic data (References 2.5S.1-144, 2.5S.1-145, and 2.5S.1-146) suggest a mean recurrence time of 500 years, which was used in the 2002 USGS model (Reference 2.5S.1-147). This recurrence interval is half of the 1000-year recurrence interval used in the 1996 USGS hazard model (Reference 2.5S.1-148), and an order of magnitude less than the seismicity-based recurrence estimates used in the 1986 EPRI study (Reference 2.5S.1-135).

The upper-bound maximum values of M_{max} used in EPRI (1986) range from mb 7.2 to 7.9 (Reference 2.5S.1-39). Since the EPRI study, estimates of M_{max} have generally been within the range of maximum magnitudes used by the six EPRI models. The most

significant update of source parameters in the New Madrid Seismic Zone since the 1986 EPRI study is the reduction of the recurrence interval to 500 years.

2.5S.1.1.4.4.5.4 Quaternary Growth Faults

As discussed in Subsection 2.5S.1.1.4.1.3, evidence for Quaternary activity in the form of surface deformation has been documented on some growth faults in the Texas Coastal Plain. As noted by Wheeler (Reference 2.5S.1-70):

> The gulf-margin normal faults in Texas are assigned as Class B structures because their low seismicity (sic) and because they may be decoupled from underlying crust, making it unclear if they can generate significant seismic ruptures that could cause damaging ground motion.

The definition of a Class B structure, according to the USGS criteria (Reference 2.5S.1-50), is as follows:

Class B: Geologic evidence demonstrates the existence of Quaternary deformation, but either (1) the fault might not extend deeply enough to be a potential source of significant earthquakes, or (2) the currently available geologic evidence is too strong to confidently assign the feature to Class C but not strong enough to assign it to Class A.

Additionally, Wheeler (Reference 2.5S.1-50) defines Class A faults as tectonic faults with Quaternary slip, and Class C faults as having no evidence of being tectonic faults or having Quaternary slip.

The assessment of the USGS (Reference 2.5S.1-70) is consistent with the UFSAR for STP 1 & 2 (Reference 2.5S.1-7) and numerous studies published since the 1986 EPRI study (Reference 2.5S.1-39) (see discussion in Subsection 2.5S.1.1.4.3.4.2) that growth faults are confined to the Coastal Plain section and do not extend into the crystalline basement. The assessment of the USGS (Reference 2.5S.1-70) that growth faults may not generate significant seismic ruptures also is consistent with the conclusion of the UFSAR for STP 1 & 2 (Reference 2.5S.1-7) that the sediments involved in growth faulting do not have sufficient elastic strength to store strain energy that can be released in moderate to large earthquakes. The UFSAR for STP 1 & 2 (Reference 2.5S.1-7) discussed reports of microearthquake activity associated with growth faults in Brazoria County, Texas, and Percperdue, Vermillion Parish, Louisiana, but noted that no events with magnitudes larger than 1.5 have been reported.

To summarize, no new information has been published since the 1986 EPRI study (Reference 2.5S.1-39) that would require updating the characterization of growth faults in the Coastal Plain as tectonic features. The recent USGS assessment of growth faults (Reference 2.5S.1-70) supports the conclusion of the STP 3 & 4 FSAR regarding the seismic potential of growth faults. The contribution of growth faults to seismic hazard at the STEGS site is adequately captured by the EPRI source model (Reference 2.5S.1-39), as modified to reflect new information published since 1986 on background seismicity in the Gulf of Mexico (see discussion in Subsection 2.5S.2.1).

2.5S.1.2 Site Area Geology

2.5S.1.2.1 Site Area Physiography and Geomorphology

The STP 3 & 4 site covers an area of approximately 12,220 acres. The site is located in Matagorda County, Texas, approximately 12 miles southwest of Bay City and 10 miles north of Matagorda Bay. The site area is located within the Coastal Prairies sub-province of the Gulf Coastal Plains Physiographic Province. It is bordered by the Gulf of Mexico to the southeast and the Interior Coastal Plains to the northwest (Figure 2.5S.1-6 [Reference 2.5S.1-12]).

The site vicinity geologic map (Figure 2.5S.1-11 [References 2.5S.1-28, 2.5S.1-29, and 2.5S.1-30]) indicates that the terrain located approximately 18 miles east to northeast from the STP site is underlain by Holocene Alluvium. A Holocene alluvium unit also lies in the STP site area. This relatively narrow band of alluvium surrounds the Colorado River and correlates with recent fluvial sediment deposited on the river's floodplain (Figure 2.5S.1-14 [Reference 2.5S.1-38]). Most of what remains within the site vicinity is underlain by Beaumont Formation, which was deposited during the Late Pleistocene (Figure 2.5S.1-11 [References 2.5S.1-28, 2.5S.1-29, and 2.5S.1-30]). The Beaumont Formation is one of many featureless Pleistocene surfaces found trending parallel to the Texas Gulf Coast (Reference 2.5S.1-7). The Beaumont Formation sediments are predominantly a sequence of sands and clays deposited by ancestral Colorado River streams in a deltaic environment that existed during the last eustatic sea level high as discussed in Subsection 2.5S.1.2. The sands are indicative of channel lag deposits, while the clays represent deposition as natural levees and overbank deposits.

The site generally has less than 15 ft. of natural relief in the 4.5 miles distance from its northern to southern boundary. The northern portion of the site is at an elevation of approximately 30 ft. above MSL, while the southeastern section is at an elevation of approximately 15 ft. above MSL. The Colorado River flows along the site's southeastern boundary. There are also several unnamed drainage features within the site boundary, one of which feeds the manmade Kelly Lake. Figure 2.5S.1-27 (Reference 2.5S.1-149) shows the STP site area geologic map. The map shows the approximately 7000-acre MCR to be the predominant feature in the site area. This map shows the Holocene Alluvium Unit that borders the south to southeasterly course of the Colorado River in the site area to lie roughly 3 miles east of the site. The vast majority of sediment that lies west of these recent alluvium flood basin deposits consists of Beaumont Formation flood deposits and Beaumont Formation ridge deposits. Examination of the site geologic map (Figure 2.5S.1-28 [References 2.5S.1-6 and 2.5S.1-149]) shows the STP site itself to lie exclusively on top of Beaumont Formation flood deposits consisting of silt and clay with a few isolated areas lying northeast and southwest of the Power Block areas consisting of construction fill at their surface.

As stated in the STP 1 & 2 UFSAR, a number of small “pimple mounds” exist at the site, many of which have been modified through agricultural activities, such as plowing and re-grading (Reference 2.5S.1-7). These pimple mounds have been postulated to result from deposition followed by subsequent erosion during past flood stages at the

site. The STP 1 & 2 UFSAR concluded that there was no physical evidence to indicate that these pimple mounds were related in any way to seismic activity (Reference 2.5S.1-7). Since that time, no new evidence has emerged to indicate a different conclusion.

2.5S.1.2.2 Site Area Geologic History

Major tectonic events in the region surrounding the site include three compressional orogenies (Grenville, Ouachita, and Laramide) and a minimum of two major extensional events (Late Proterozoic Laurentian Rifting and Mesozoic Rifting). Subsection 2.5S.1.1.2 contains a detailed discussion of each of these events. The basement rock beneath the site is presently believed to be continental crustal material from the Grenville Orogeny overlain by approximately 40,000 ft. of sedimentary section.

Regional subsidence of the Gulf Coast basin occurred simultaneously with inland uplift of the Cordillera throughout the Quaternary. This newly uplifted terrestrial source provided a great influx of sediment and for the first time subsidence of the basin was primarily due to loading of the crust by prograding wedges of clastic sediment instead of cooling of new oceanic crust (Reference 2.5S.1-22). Subsection 2.5S.1.1.2.6 contains discussions of these events and their regional effects. A result of this sediment influx was the migration of the Gulf Coast depocenter toward the south to its current location approximately 70 miles southeast of Matagorda Bay (Reference 2.5S.1-7). This has led to the STP site being located on a thick wedge of clastic sediments with the formations that comprise it thickening toward the Gulf.

Four periods of glaciation followed by interglacial climatic episodes occurred during the Pleistocene that affected the geology of the site due to falling and rising sea levels along the Gulf Coast. During glacial periods, sea levels were lower causing the processes of valley cutting and widespread erosion to dominate the landscape. Interglacial periods were marked by higher sea levels along the Gulf Coast, which lead to the deposition of coalescing alluvial and deltaic plains by ancestral river systems (Reference 2.5S.1-7). The Willis, Lissie, and Beaumont Formations and the undifferentiated Deweyville terrace sediments were deposited following these interglacial episodes (Figure 2.5S.1-13 [Reference 2.5S.1-25]). As stated in Subsection 2.5S.1.2.1, the STP site is underlain by the Beaumont Formation (Figures 2.5S.1-27 [Reference 2.5S.1-149] and 2.5S.1-28 [References 2.5S.1-6 and 2.5S.1-149]). The Beaumont Formation, which was deposited during a short interglacial in the early Wisconsinan glacial stage of the late Pleistocene, was encountered in all STP site characterization boreholes.

2.5S.1.2.3 Site Area Stratigraphy

The STP site is located on Cenozoic Coastal Plain sediments estimated to be approximately 26,000 ft. thick, which in turn rest on older sediments estimated to be approximately 14,000 ft. thick. The basement on which the sediments rest is believed to be continental crust (Reference 2.5S.1-35). Figure 2.5S.1-29 describes the strata encountered during the STP 3 & 4 subsurface investigations. Figure 2.5S.1-29 also shows a correlation between geologic/geotechnical and hydrogeologic units discussed

in detail in FSAR Subsection 2.4S.12. These strata are described below as they occur from the ground surface down at the STP 3 & 4 site. The Beaumont Formation is the usual unit penetrated by borings drilled for the STP 3 & 4 COL; the two deeper borings (B-305 and B-405) may have penetrated into the underlying Lissie Formation. The subunits identified by letters are informal; site specific units based on the original Unit 1 & 2 site investigation and carried over for the Unit 3 & 4 investigation. Boring logs are included in Appendix 2.5-A. Figure 2.5S.1-27 (Reference 2.5S.1-149) shows the site area geologic map. Figure 2.5S.1-28 (References 2.5S.1-6 and 2.5S.1-149) shows the site geologic map.

The Texas Coastal Plain sediments are part of a thick sequence of sediments deposited in a subsiding basin. The surficial deposits at the site consist of the Pleistocene Beaumont Formation veneered by soil. The Beaumont Formation is a sequence of sand and clay deposited by ancestral Colorado River streams as a delta discharging into a sea that was at a higher elevation during that part of the Pleistocene than the present sea level. The Beaumont Formation is reported to be about 400 ft. thick beneath the site; however, because the contact between the Beaumont Formation and the underlying Lissie Formation is difficult to determine due to the similarity of the lithology of both formations, the exact thickness is unknown. The Lissie Formation and the Beaumont Formation are the two dominant subdivisions of the Pleistocene deltaic System.

For the purpose of capturing the site geology, subsurface information was collected from over 150 geotechnical borings and cone penetrometer tests (CPTs). Of these over 150 subsurface field testing locations, 119 are borings. Of the 119 borings drilled, 50 are located within the boundary of the future STP 3 Power Block (300-series borings) and 41 are located within the STP 4 Power Block (400-series borings) (Figure 2.5S.1-30). The remaining 28 borings (900-series borings) are strategically placed between and surrounding the STP 3 & 4 Power Blocks to provide subsurface stratigraphic control for the surrounding areas of the site. A more detailed discussion of the comprehensive geotechnical investigation employed to characterize the site subsurface is provided in Subsection 2.5S.4.

Site specific information regarding the stratigraphy underlying the STP 3 & 4 site is limited by the total depths of the various borings advanced during the site investigation. Of the 119 borings drilled as part of the investigations for the STP 3 & 4, two were advanced to the depth of 618 ft. below ground surface. The remaining 117 borings ranged from 30 ft. below ground surface (bgs) to 220 ft. bgs with an average of approximately 125 ft. bgs. This enabled investigators to gather detailed information about the near-surface structure and composition of sediments underlying the site as well as provide them with some information regarding subsurface materials at greater depths. The two deep borings (B-305DH/DHA and B-405DH) probably penetrated the entire Beaumont Formation beneath the site at about 400 ft. below ground surface. Information gathered from the regional investigation coupled with information gathered in deeper borings that were drilled as part of the STP 1 & 2 subsurface investigations strongly indicate that the stratigraphy found under STP 3 & 4 most likely follows the stratigraphic column presented in Figure 2.5S-13 (Reference 2.5S.1-25), which shows

the Beaumont Formation underlain by the Pleistocene Lissie Formation and Willis Formation.

A series of cross sections have been developed, using the information obtained from more than 150 geotechnical borings and CPTs and from correlations interpreted from a suite of geophysical boring logs. Figure 2.5S.1-31 shows the location and orientation of these cross sections at the site. Cross section A-A' trends southeast starting at the northeast corner of the STP 4 Power Block area and then continues across the STP 3 Power Block area (Figure 2.5S.1-32). This cross section has been extended through the STP 1 Power Block using data collected as part of the subsurface investigations for STP 1 & 2. The other two cross sections (B-B' and C-C') both trend northeast across the STP 3 & 4 Power Block areas only (Figures 2.5S.1-33 and 2.5S.1-34). The strata shown in Figures 2.5S.1-32, 2.5S.1-33 and 2.5S.1-34 are color-coded to show aquitard (dark green) and aquifers(yellow) within the Beaumont Formation.

The sediments encountered during the STP 3 & 4 investigations were divided into strata based on their material properties and were assigned designation names consistent with those used in the STP 1 & 2 UFSAR (Reference 2.5S.1-7). Structure contour maps were created for those strata that were penetrated by enough boreholes and CPTs in the STP 1 & 2 and the STP 3 & 4 investigations to provide adequate contour control. Each of the strata encountered is described and characterized below. The estimated thickness and elevations for each stratum was calculated as an average from the data collected during the STP 3 & 4 subsurface investigations only. Borings and CPTs were only used for thickness calculations of a particular stratum if they fully penetrated through the stratum. The reported thicknesses and elevations of each stratum pertain to the area inside the STP 3 & 4 Power Block area. A more detailed analysis of the strata, including additional information concerning their thickness, elevations and engineering properties in areas other than inside the Power Block area, can be found in FSAR Subsection 2.5S.4.2 and Table 2.5S.4-2.

Stratum A is typified as a yellowish red, brown, gray, and/or black clay with varying amounts of silt, sand, and/ or gravel. It is generalized as being a silty clay sediment, and it is encountered at the uppermost strata of all borings (Figures 2.5S.1-32, 2.5S.1-33, and 2.5S.1-34). However, in 31 of the 119 borings, clayey and/or gravelly soils suspected to be artificial fill were found within the upper few feet of Stratum A. Based on evidence from the borings coupled with data from CPTs, the thickness of Stratum A varies from 8 ft. to 29 ft. within the Power Block areas with an average thickness of 18 ft. Because the top of Stratum A is generally consistent with the site ground surface elevation, it is generally fairly level, with elevations at the time of the investigations ranging from approximately El. 24 ft. MSL to El. 32 ft. MSL and an average of approximately El. 30 ft. MSL (Figure 2.5S.1-35).

Below the Stratum A sediments, Stratum B sediments were found in all but 10 of the borings (B-307, B-312, B-313, B-412, B-427, B-433, B-434, B-908, B-928, and B-929) (Figures 2.5S.1-32, 2.5S.1-33, and 2.5S.1-34). Stratum B typically consisted of yellowish red, reddish brown and brown silt, silty sand, or clay. Designated as a clayey silt layer, the thickness of Stratum B varies from 0 ft. to 16 ft., with an average thickness of 7 ft. Where present, the top of Stratum B varies from below MSL to El. 23 ft. MSL,

with an average of El. 12 ft. MSL. As shown on the structure contour map in Figure 2.5S.1-36, the elevation of the top of Stratum B is highest in the STP 3 Power Block area. To the east and west of the STP 3 Power Block area, Stratum B gently dips before it again begins to ascend to the east of the STP 1 Power Block and to the west of the STP 4 Power Block area.

Taken together, Stratum A and Stratum B approximate the Upper Shallow Aquifer Confining Layer discussed and depicted in FSAR Subsection 2.4S.12 (Figure 2.5S.1-29). The combined thickness of Strata A and B combine for a thickness that ranges from 10 to 30 ft.

Stratum C sediments were encountered below Stratum B in most of the borings drilled across the site (Figures 2.5S.1-32, 2.5S.1-33, and 2.5S.1-34). Generically described as silty sand, Stratum C is characterized as a yellowish brown to dark brown sand with varying amounts of silt and/or clay also being present. Inside the STP 3 & 4 Power Block area, the thickness of Stratum C varies from 3 ft. to 30 ft. with an average thickness of approximately 20 ft., and the elevation where the stratum is first encountered varied from El. 9 ft. MSL to El. -14 ft. MSL with an average of El. 5 ft. MSL. This stratum dips from the northwest portion of the site, where the STP 3 & 4 Power Block areas are located, southeast toward the STP 1 Power Block, where it flattens out at an elevation of approximately El. -10 ft. MSL (Figure 2.5S.1-37). The top of Stratum C then seems to slowly rise in elevation heading due east away from the STP 1 Power Block. Stratum C correlates closely with the Upper Shallow Aquifer described in FSAR Subsection 2.4S.12 (Figure 2.5S.1-29).

Stratum D soils were encountered below Stratum C in a majority of the site borings (Figures 2.5S.1-32, 2.5S.1-33, and 2.5S.1-34). Described as silty clay, Stratum D is typified as a greenish gray, yellowish red, or reddish brown to dark brown clay with varying amounts of silt and/or sand, occasionally containing isolated thin lenses of silty sand. The thickness of Stratum D varied from 1.5 ft. to 34 ft. with an average thickness of approximately 22 ft. Power Block elevations representing the top of this stratum range from El. -24 ft. MSL to El. -6.0 ft. MSL with an average of El. -15 ft. MSL. Figure 2.5S.1-38 shows Stratum D to be slightly dipping south to southeast at the site. Stratum D correlates closely with the Lower Shallow Aquifer Confining Layer described in FSAR Subsection 2.4S.12 (Figure 2.5S.1-29).

Stratum E was found underlying Stratum D (Figures 2.5S.1-32, 2.5S.1-33, and 2.5S.1-34). Described as a gray or yellowish brown to dark brown sand, this layer also contained varying amounts of silt and/or clay. The thickness of Stratum E varied from 0 ft. to 36.5 ft. with an average thickness of 18 ft., and its top was found between El. -45 ft. MSL to El. -18 ft. MSL, with an average of El. -37 ft. MSL. The structure contour map presented in Figure 2.5S.1-39 demonstrates Stratum E as a nearly flat lying layer in and around the STP 3 & 4 Power Block area. Stratum E correlates closely with the Lower Shallow Aquifer discussed in detail in FSAR Subsection 2.4S.12 (Figure 2.5S.1-29).

Stratum F soils were encountered below Stratum E in a majority of the borings and CPTs made site-wide that terminated below Stratum E (Figures 2.5S.1-32, 2.5S.1-33,

and 2.5S.1-34). However, Stratum F was absent in a number of borings in and around the central to northern part of the STP 3 Power Block area, including Borings B-308DH, B-309, B-310, B-316, B-321, B-326, B-332, B-350, and B-430. Classified as silty clay, Stratum F is more fully described as consisting of reddish brown to dark grayish brown or greenish gray clay with varying amounts of silt and/or sand. The thickness of Stratum F varies from 0 ft. to 55 ft., with an average thickness of 16 ft. Borings containing Stratum F penetrated its upper boundary at elevations ranging from El. -72 ft. MSL to El. -43 ft. MSL with an average of El. -55 ft. MSL. Figure 2.5S.1-40 shows the top of Stratum F to undulate up and down in elevation in the vicinity of the STP 3 & 4 Power Block area while remaining relatively flat at approximately El. -60 ft. MSL to the southeast in and around the STP 1 Power Block.

Stratum H was penetrated during site investigations advanced to sufficient depths below Stratum F, except in Boring B-348 (Figures 2.5S.1-32, 2.5S.1-33, and 2.5S.1-34). Typically consisting of light yellowish brown to dark yellowish brown or grayish brown fine to medium sand with varying amounts of silt, clay, and/or gravel, Stratum H has been classified as being predominantly a silty sand. In the interior of the STP 3 & 4 Power Block area, the thickness of Stratum H varied from 0 ft. to 35.5 ft., with an average thickness of 17.5 ft. This stratum's top corresponded with elevations ranging from El. -93 ft. MSL to El. -48 ft. MSL, with an average of El. -68 ft. MSL. Stratum H is found at its highest elevations in the northernmost part of the STP 4 Power Block area (Figure 2.5S.1-41). Borings located progressively south, east, or west of this area tended to show the top of Stratum H occurring at progressively deeper elevations within and near the STP 3 & 4 Power Block area. This trend is consistent until well outside the STP 3 & 4 Power Block area to the east where the top of Stratum H seems to become relatively flat at an elevation of approximately El. -80 ft. MSL.

Stratum I was not used in the description of the subsurface conditions to avoid confusion between alphabetical designations and Roman numerals.

Stratum J soils were encountered below Stratum H in all borings drilled to sufficient depth (Figures 2.5S.1-32, 2.5S.1-33, and 2.5S.1-34). Only two borings completely penetrated through Stratum J. These two borings were B-305DH/DHA in the STP 3 Power Block area and B-405DH in the STP 4 Power Block area. Stratum J typically consisted of reddish brown to brown or greenish gray clay with interbedded sub-strata of sand and/or sandy silt and is generalized as being silty clay. The stratum has an estimated overall thickness of 92 ft. and was found at elevations ranging from El. -95 ft. MSL to El. -63 ft. MSL with an average of El. -87 ft. MSL.

When combined, Stratum F, Stratum H, and Stratum J comprise the silty clay and silt with discontinuous sand layers that separate the Lower Shallow Aquifer from the Deep Aquifer as discussed in FSAR Subsection 2.4S.12 (Figure 2.5S.1-29). Taken together, these strata have an approximate thickness of 100 to 150 ft.

Stratum K soils were encountered below Stratum J in borings B-305DH/DHA in the STP 3 Power Block area and B-405DH in the STP 4 Power Block area (Figures 2.5S.1-32 and 2.5S.1-33). Overall characterized as a sandy silt, Stratum K typically consisted of greenish gray to gray clay with varying amounts of sand, grading to a silty sand or

silt towards its base. The stratum has an estimated overall thickness of 50 ft. in the STP 3 & 4 Power Block area and was found at an average elevation of El. -174 ft. MSL.

Stratum L was found to underlie Stratum K in borings B-305DH/DHA in the STP 3 Power Block area and B-405DH in the STP 4 Power Block area (Figures 2.5S.1-32 and 2.5S.1-33). Stratum L is described as a red to brown silty clay with varying amounts of sand. Based on borings B-305DH/DHA and B-405DH, the thickness of Stratum L varied from 4.5 ft. to 5 ft., with an average thickness of 5 ft. The approximated top of Stratum L occurs at around El. -228 ft. MSL.

Stratum M soils were found to underlie Stratum K in borings B-305DH/DHA in the STP 3 Power Block area and B-405DH in the STP 4 Power Block area (Figures 2.5S.1-32 and 2.5S.1-33). Stratum M is silty sand whose thickness varied from 14.5 ft. to 15.5 ft., with an average thickness of 15 ft. The top of Stratum M occurs near El. -233 ft. MSL.

Stratum N is the lowest sediment layer encountered during the site characterization investigations performed for the STP 3 & 4 COL application (Figures 2.5S.1-32 and 2.5S.1-33). Designated as silty clay, Stratum N typically consisted of brown to greenish gray clay with varying amounts of sand and interbedded sub-strata of sand to silty sand. This stratum extended to depths greater than the maximum attained depth of 618 ft. below ground surface in borings B-305DH/DHA and B-405DH, so thickness for this stratum was not estimated. However, the top of Stratum N has been approximated to coincide with an elevation of around El. -248 ft. MSL.

The combined Stratum K, Stratum L, Stratum M, and Stratum N are interpreted to correlate with part of the Deep Aquifer discussed in FSAR Subsection 2.4S.12 (Figure 2.5S.1-29). The combined thickness of these strata is estimated to be greater than 500 ft.

2.5S.1.2.4 Structures Within the Site Area

2.5S.1.2.4.1 Basement Structure Beneath the Site Area

The site area is located within the Coastal Zone of the Gulf of Mexico basin (Reference 2.5S.1-51), and is underlain by approximately 6.8 miles to 7.4 miles of Mesozoic and Cenozoic strata above the crystalline basement (References 2.5S.1-62 and 2.5S.1-90). The basement below the STP 3 & 4 site is interpreted to be “thin transitional crust” between the tectonically thickened crust of the Paleozoic Ouachita orogenic belt to the northwest that was not significantly affected by Mesozoic rifting, and Mesozoic oceanic crust beneath the deep Gulf of Mexico basin to the southeast (Reference 2.5S.1-44). Although scientific literature published since the EPRI (Reference 2.5S.1-39) study has improved understanding of the crustal-scale structure along the buried rifted margin of the Gulf of Mexico, we conclude that there are no new data that indicate the presence of previously unknown discrete basement faults or basement structures beneath the site area.

2.5S.1.2.4.2 Growth Faults in the Site Area

The only geologic structures within the STP site area are buried growth faults that are associated with the Frio growth fault trend (Subsection 2.5S.1.1.4.3.4.2). The following sections summarize previous investigations of these features for the UFSAR for STP 1 & 2 (Reference 2.5S.1-7), then discuss new information developed on growth faults in the site area since preparation of the UFSAR. The UFSAR concluded that no growth faults project to the surface in the footprint of the STP 3 & 4. Data collected since preparation of the UFSAR and reviewed for this study are consistent with this conclusion.

2.5S.1.2.4.2.1 Previous Study of Growth Faults in the Site Area for the UFSAR for STP 1 & 2

Growth faults in the site area were extensively investigated and documented for the UFSAR for STP 1 & 2 (Reference 2.5S.1-7) via the following techniques:

- Interpretation of high-altitude imagery and stereo aerial photography
- Correlation of boring data and geophysical well logs
- Interpretation of petroleum industry seismic reflection profiles
- Field investigations

Based on analyses of these data (primarily the seismic reflection profiles), 10 growth faults were identified in the subsurface of the site area. (The following discussion summarizes work presented in the UFSAR for STP 1 & 2 [Reference 2.5S.1-7]). Structure contour maps of the growth faults were prepared from analysis of seismic reflection profiles. None of the growth faults identified in the UFSAR for STP 1 & 2 (Reference 2.5S.1-7) project to or intersect the earth's surface through the STP 3 & 4 site footprint. Seven of the 10 growth faults dip south, consistent with regional trends within the Frio Growth Fault Zone. Three of the 10 growth faults dip north and presumably are antithetic to the south-dipping faults.

The UFSAR for STP 1 & 2 (Reference 2.5S.1-7) concluded that seven of the 10 growth faults were buried below a minimum of 5000 ft. of undeformed sediments. Based on stratigraphic correlations, the UFSAR for STP 1 & 2 (Reference 2.5S.1-7) interpreted that deposits at a depth of 5000 feet are Miocene in age, and thus the seven growth faults overlain by these undeformed deposits have not been active since Miocene time or earlier.

The UFSAR for STP 1 & 2 (Reference 2.5S.1-7) concluded that three growth faults, informally named “A”, “I”, and “J”, deform sediments above 5000 ft. depth, and thus have been active since Miocene time. Deformation associated with growth fault “J” could be traced to a minimum depth of 3900 ft. and was interpreted to die out in sediments of probable Pliocene or Miocene age. Deformation associated with growth faults “A” and “I” was interpreted to extend to maximum depths of 500 ft. and 1000 ft., respectively. The UFSAR for STP 1 & 2 (Reference 2.5S.1-7) noted that these depths

were at the upper limits of resolution for the specific reflection lines across the “A” and “I” faults; thus, the “A” and “I” faults may deform shallower and thus younger strata above the minimum depth of seismic resolution. The “A” growth fault strikes west-northwest, dips toward the south-southwest and projects to the surface approximately 2.8 miles northwest of the STP site. The “I” growth fault strikes approximately east-west, dips south and projects to the surface in the vicinity of the southwestern corner of the cooling pond, approximately 3.8 miles south-southeast of the STP site.

The UFSAR for STP 1 & 2 (Reference 2.5S.1-7) evaluated lineaments identified from analysis of remote sensing imagery and aerial photos, and concluded that no linear features are associated with growth faults, nor are they the surface expression of growth fault activity. According to the UFSAR for STP 1 & 2 (Reference 2.5S.1-7), no topographic scarps, sag ponds, road pavement breaks, abrupt changes in ground surface elevation, or other features suggestive of fault displacement were observed during a field reconnaissance of the site area in December 1982. Based on analysis of seismic reflection data, the UFSAR for STP 1 & 2 (Reference 2.5S.1-7) inferred that that the updip surface projection of growth fault “I” is crossed by a 10-ft.- to 12-ft.-deep excavated channel that is presently occupied by relocated Little Robbins Slough. Exposures of Beaumont Formation deposits in the channel excavation were carefully examined in the field and logged, and the UFSAR for STP 1 & 2 (Reference 2.5S.1-7) concluded that a continuous sand-clay contact extends across the projection of fault “I” and is not deformed.

Based on results obtained from analysis of remote sensing imagery and borehole and geophysical subsurface data, the UFSAR for STP 1 & 2 (Reference 2.5S.1-7) concluded that there is no evidence of faults “A” or “I” at the ground surface and that the stratigraphic relations exposed in relocated Little Robbins Slough provide positive evidence for no post-Beaumont surface deformation associated with fault “I.”

2.5S.1.2.4.2.2 Updated Information on Growth Faults in the Site Area

2.5S.1.2.4.2.2.1 Current Information on Locations of Growth Faults in the Site Area

For this study, data were collated on locations of growth faults site vicinity about STP 3 & 4 (Figure 2.5S.1-42 [References 2.5S.1-29, 2.5S.1-124, 2.5S.1-150, 2.5S.1-151, 2.5S.1-152, and 2.5S.1-153]) from seven sources. The faults documented by these sources are listed in Table 2.5S.1-1. The locations of the faults that fall within the 5-mile site area are shown in Figure 2.5S.1-43 (References 2.5S.1-7, 2.5S.1-124, and 2.5S.1-151). The data sources include the following:

- White et al. (Reference 2.5S.1-29) identified the surface trace of four growth faults on Matagorda Peninsula. These faults have the prefix “Matagorda BW” in Table 2.5S.1-1 and “BW” in Figure 2.5S.1-42 (References 2.5S.1-29, 2.5S.1-124, 2.5S.1-150, 2.5S.1-151, 2.5S.1-152, and 2.5S.1-153).

- Geomap Company (Reference 2.5S.1-124) publishes structural contour maps of two prominent Miocene horizons that are deformed by growth faults in the site vicinity. These faults have the prefix “Matagorda GM” in Table 2.5S.1-1 and “GM” in Figure 2.5S.1-42 (References 2.5S.1-29, 2.5S.1-124, 2.5S.1-150, 2.5S.1-151,

2.5S.1-152, and 2.5S.1-153) and Figure 2.5S.1-43 (References 2.5S.1-7, 2.5S.1-124, and 2.5S.1-151).

- Dodge and Posey (Reference 2.5S.1-151) identified growth faults within of a series of structural cross sections for the Texas Gulf Coast. These faults have the prefix "Matagorda DP" in Table 2.5S.1-1 and "DP" in Figure 2.5S.1-42 (References 2.5S.1-29, 2.5S.1-124, 2.5S.1-150, 2.5S.1-151, 2.5S.1-152, and 2.5S.1-153) and Figure 2.5S.1-43 (References 2.5S.1-7, 2.5S.1-124, and 2.5S.1-151).

- Galloway et al. (Reference 2.5S.1-150) identified growth faults within a series of structural cross sections of the Texas Gulf Coast. These faults have the prefix "Matagorda G" in Table 2.5S.1-1 and "G" in Figure 2.5S.1-42 (References 2.5S.1-29, 2.5S.1-124, 2.5S.1-150, 2.5S.1-151, 2.5S.1-152, and 2.5S.1-153).

- Morton et al. (Reference 2.5S.1-152) identified growth faults within a series of structural cross sections offshore the Texas Gulf Coast. These faults have the prefix "Matagorda MJF" in Table 2.5S.1-1 and "MJF" in Figure 2.5S.1-42 (References 2.5S.1-29, 2.5S.1-124, 2.5S.1-150, 2.5S.1-151, 2.5S.1-152, and 2.5S.1-153).

- McGowen and Morton (Reference 2.5S.1-153) identified near surface growth faults on offshore geologic maps. These faults have the prefix "Matagorda MM" in Table 2.5S.1-1 and "MM" in Figure 2.5S.1-42 (References 2.5S.1-29, 2.5S.1-124, 2.5S.1-150, 2.5S.1-151, 2.5S.1-152, and 2.5S.1-153).

- The UFSAR for STP 1 & 2 (Reference 2.5S.1-7) identified growth faults within the site area from seismic reflection surveys. In the UFSAR for STP 1 & 2 (Reference 2.5S.1-7) these faults are referred to with single letter designations. These faults are referred to here using the prefix "Matagorda STP12" in Table 2.5S.1-1 and "STP12" in Figure 2.5S.1-43 (References 2.5S.1-7, 2.4S.1-124, and 2.5S.1-151).

Many of these data sources consist of growth fault locations observed at depth. These locations in conjunction with faults dips generated from the original sources were used to project the location of the growth faults to the surface. Given that growth faults are commonly observed to steepen updip, there is potential uncertainty in the projected growth fault locations shown in Figure 2.5S.1-42 (References 2.5S.1-29, 2.5S.1-124, 2.5S.1-150, 2.5S.1-151, 2.5S.1-152, and 2.5S.1-153) and Figure 2.5S.1-43 (References 2.5S.1-7, 2.5S.1-124, and 2.5S.1-151). Uncertainty may be as great as several miles, vary along strike of any individual fault, and vary between different faults. Details of each source are presented below.

Growth Faults of White et al. (Reference 2.5S.1-29)

White et al. (Reference 2.5S.1-29) mapped four faults on Matagorda Peninsula as part of a barrier island wetland habitat study. The faults were identified using aerial photographs from 2001. Surface expression of the visually most prominent fault, Matagorda BW2, can be seen in aerial photographs back to the 1970s as a distinct change in the vegetation related to the submergence of the downthrown side of the fault, but this vegetation change is not apparent in

photos from the 1950s. White et al. (Reference 2.5S.1-29) suggested that this temporal change in fault expression indicates that the fault has been activated within the past several decades. However, this change in temporal expression may simply indicate when fault slip occurring for an unknown period prior to the 1970s submerged the downthrown side to the point where vegetation was significantly influenced by saltwater encroachment. Figure 2.5S.1-42 (References 2.5S.1-29, 2.5S.1-124, 2.5S.1-150, 2.5S.1-151, 2.5S.1-152, and 2.5S.1-153) shows the surface traces of these growth faults as identified by White et al. (Reference 2.5S.1-29).

Growth Faults of Geomap Company (Reference 2.5S.1-124)

Geomap Company publishes proprietary structure contour maps of key stratigraphic horizons in the Gulf Coastal Plain derived from analysis of seismic reflection data and well logs. The maps show interpreted intersections of growth faults with these horizons. For this study, two sets of Geomap maps were obtained for the greater site area (Upper Texas Gulf Coast maps 328 and 329 [Reference 2.5S.1-124]). Each map set consists of two contoured horizons in the Frio formation: (1) an upper A horizon, and (2) a lower B horizon. For map 328, the A horizon is a Lower Miocene marker in part identified by the presence of *Marginulina indiomorpha*, and the B horizon is the base of the Miocene in part identified by the presence of *Textularia warreni, mississippiensis* and Lower Struma. For map 329, the A horizon is the top of the Frio and the Middle Miocene in part identified by the presence of *Amphistegina*, and the B horizon is Lower Frio in part identified by the presence of *Textularia mississippiensis* and *nodosaria*.

Figure 2.5S.1-42 (References 2.5S.1-29, 2.5S.1-124, 2.5S.1-150, 2.5S.1-151, 2.5S.1-152, and 2.5S.1-153) and Figure 2.5S.1-43 (References 2.5S.1-7, 2.4S.1-124, and 2.5S.1-151) show the approximate surface projections of the growth faults as determined for the STP 3 & 4 COL. Surface projections were made by using the depths of the faults within the two horizons mapped by Geomap to determine a dip for short (several miles long at most) growth fault segments and projecting those segments to the surface in a direction perpendicular to the fault strike using that dip. For each growth fault, smooth projected fault traces were created by hand drawing a single fault trace through the individual projected segments. Uncertainty in the location of the surface projection is estimated to be on the order of 0.6 miles (a kilometer) based on the projection technique and the smoothing of the fault trace.

Growth Faults of Dodge and Posey (Reference 2.5S.1-151)

Dodge and Posey (Reference 2.5S.1-151) published a series of structural cross sections of Texas Gulf Coast Tertiary strata. The purpose of these sections is to illustrate the gross regional sandstone and shale distribution, but they also indicate the presence of growth faults. The cross sections were constructed through the compilation of proprietary and publicly available data. Within the cross sections, numerous growth faults are identified by offsets in stratigraphic markers. The resolution of the sections is such that growth fault offset cannot be resolved above the Frio Formation. For the cross sections within the site vicinity, the top of the Frio occurs at depths of approximately 6000-7000 feet (Reference 2.5S.1-151).

Figure 2.5S.1-42 (References 2.5S.1-29, 2.5S.1-124, 2.5S.1-150, 2.5S.1-151, 2.5S.1-152, and 2.5S.1-153) and Figure 2.5S.1-43 (References 2.5S.1-7, 2.4S.1-124, and 2.5S.1-151) show the approximate surface projections of the growth faults as determined for the STP 3 & 4 COL. Surface projections were made by graphically extending the faults in cross section to the surface assuming a constant fault dip.

Growth Faults of Galloway et al. (Reference 2.5S.1-151)

Galloway et al. (Reference 2.5S.1-150) published a series of cross sections through the Paleogene section of the Texas Gulf Coastal Plain section. The primary purpose of these cross sections is to locate regional unconformities, condensed sections, and significant stratigraphic units; Galloway et al. (Reference 2.5S.1-150) also identified and interpreted growth faults. The sections are, in part, an update to the work of Dodge and Posey (Reference 2.5S.1-151). The cross sections were primarily constructed using correlations between well logs. The resolution of the sections is such that offset of horizons due to growth faulting cannot be resolved above the Frio-Lower Miocene boundary. For the cross sections within the site vicinity, this boundary is at depths on the order of 6000-8000 ft. (Reference 2.5S.1-150).

Figure 2.5S.1-42 (References 2.5S.1-29, 2.5S.1-124, 2.5S.1-150, 2.5S.1-151, 2.5S.1-152, and 2.5S.1-153) shows the approximate surface projections of the Galloway et al. (Reference 2.5S.1-150) growth faults as determined for the STP 3 & 4 COL. Surface projections were made by graphically extending the faults in cross section to the surface assuming a constant fault dip.

Growth Faults of Morton et al. (Reference 2.5S.1-152)

Morton et al. (Reference 2.5S.1-152) published a series of cross sections for near- and offshore regions of the Texas Gulf Coast. The purpose of these cross sections is to depict the offshore structural and stratigraphic framework of the Oligocene and Miocene sections. Growth faults are also identified within the cross sections. The cross sections were primarily constructed using commercially available, proprietary, and published well logs in addition to limited public and proprietary seismic profiles. The shallowest horizon identified in the cross sections is the top of the Miocene, which occurs at depths on the order of 1,000-2,000 ft. within the site vicinity (Reference 2.5S.1-152). Offsets of marker horizons above the top of the Miocene by growth faulting are not

shown in the cross sections, but some growth faults are shown to extend above this horizon.

Figure 2.5S.1-42 (References 2.5S.1-29, 2.5S.1-124, 2.5S.1-150, 2.5S.1-151, 2.5S.1-152 and 2.5S.1-153) shows the approximate surface projections of the Morton et al. (Reference 2.5S.1-152) growth faults as determined for the STP 3 & 4 COL. Surface projections were made by graphically extending the fault in cross section to the surface assuming a constant fault dip.

Growth Faults of McGowen and Morton (Reference 2.5S.1-153)

McGowen and Morton (Reference 2.5S.1-153) published a series of maps of the offshore regions of Texas. The maps are meant to characterize the geology and active geologic processes of the offshore region. As part of the maps, surface traces of potentially active growth faults were identified from ship-borne, acoustic geophysical surveys. McGowen and Morton (Reference 2.5S.1-153) classified potentially active growth faults as those having stratigraphic offsets within 50 feet of the seafloor surface. The surface traces of these faults are shown in Figure 2.5S.1-42 (References 2.5S.1-29, 2.5S.1-124, 2.5S.1-150, 2.5S.1-151, 2.5S.1-152, and 2.S5.1-153).

Growth Faults of UFSAR for STP 1 & 2 (Reference 2.5S.1-7)

As part of the UFSAR for STP 1 & 2 (Reference 2.5S.1-7), new seismic reflection surveys were conducted and existing seismic reflection data were reviewed to identify growth faults within the site area. In the UFSAR for STP 1 & 2 (Reference 2.5S.1-7) ten growth faults were identified at depth based on offset reflectors. Figure 2.5S.1-43 (References 2.5S.1-7, 2.5S.1-124, and 2.5S.1-151) shows the approximate surface projections of eight of these growth faults as determined for the STP 3 & 4 COL. Surface projections were made by graphically extending the fault in cross section to the surface assuming a constant fault dip. Two of the faults identified in the UFSAR for STP 1 & 2 (Reference 2.5S.1-7) were not projected due to their limited extent within the seismic sections.

2.5S.1.2.4.2.2.2 Current Information on Activity of Growth Faults in the Site Area

New air photo analyses were conducted for the STP 3 & 4 COL, as well as aerial and field reconnaissance to assess the surface expression or lack of surface expression associated with the growth faults described in Subsection 2.5S.1.2.4.1.2.2.1 (Figure 2.5S.1-44). Particular focus was given to growth faults Matagorda STP12 A and I because they were previously determined in the UFSAR for STP 1 & 2 (Reference 2.5S.1-7) to deform Miocene-Pliocene age (or younger) strata. This analysis included examination of stereo pairs of various sets of black and white, and color aerial photographs taken before, during, and after construction of STPEGS STP 1 & 2 to identify tonal lineaments and potentially anomalous geomorphic features. These features include closed depressions, vegetation lineaments, linear drainages, and subtle south-facing topographic breaks, some of which are spatially associated with growth faults Matagorda STP12 A and I (Figure 2.5S.1-45 [References 2.5S.1-7, 2.5S.1-124 and 2.5S.1-151]). In general, lineaments identified along growth fault

Matagorda STP12 I are more pronounced and obvious than other lineaments mapped in the 5-mile site area radius.

Aerial reconnaissance in a small, fixed-wing aircraft was conducted in February 2007 to further assess lineaments and geomorphic features identified on air photos, as well as growth faults identified by previous workers (Figure 2.5S.1-44). The latter included a series of geomorphically well-defined growth faults along the Matagorda Peninsula mapped by White et al. (Reference 2.5S.1-29), well outside the site area (Figures 2.5S.1-44 and 2.5S.1-45 [References 2.5S.1-7, 2.5S.1-124 and 2.5S.1-151]). The growth faults on Matagorda peninsula mapped by White et al. (Reference 2.5S.1-29) were discernable from the air as distinct vegetation lineaments and south-facing topographic breaks in the upper surface of the late Pleistocene Beaumont Formation. No other lineation or projected growth fault was observed during the aerial reconnaissance to have a distinct topographic break.

Field reconnaissance was conducted within the site vicinity in February 2007 to evaluate lineaments, geomorphic features interpreted in the aerial photography and observed during aerial reconnaissance, as well as the locations of growth fault surface projections (Figure 2.5S.1-45 [References 2.5S.1-7, 2.5S.1-124 and 2.5S.1-151]). The post-Beaumont Formation growth faults mapped on Matagorda Peninsula by White et al. (Reference 2.5S.1-29) are characterized by a subtle, discontinuous south-facing topographic break along which changes in vegetation are aligned. South-facing topographic breaks also were observed along parts of growth fault Matagorda GMO west of the STPEGS STP 1 & 2 MCR and near the surface projection of growth fault Matagorda STP12I. The spatial coincidence of these topographic breaks with the two growth faults as well as photolineaments and linear geomorphic features identified from interpretation of aerial photography suggests that the surface projections of growth fault Matagorda STP12I and GMO are from the same growth fault at depth. No scarps, topographic breaks, or other apparent offset of the surface of the Beaumont Formation was observed in association with any other mapped lineaments or growth faults within the 5-mile site area during aerial or field reconnaissance.

Four topographic profiles were surveyed across south-facing topographic breaks spatially associated with growth fault Matagorda STPI and GMO west of the STP MCR to characterize the potentially geomorphic expression of the growth fault. Locations of the profiles are shown in Figure 2.5S.1-45 (References 2.5S.1-7, 2.5S.1-124, and 2.5S.1-151), and the topographic profiles from the surveys are shown in Figure 2.5S.1-46. The surveys specifically document the magnitude and geometry of relief on the surface of the late Pleistocene Beaumont Formation. Profiles STP L2 and STP L3 are located outside the site area, and profiles STP L1 and STP L4 are located within the 5 mile site area radius (Figure 2.5S.1-45 [References 2.5S.1-7, 2.5S.1-124 and 2.5S.1-151]). The surveys of profiles STP L2 and STP L3 were conducted along graded surfaces adjacent to roads, and the surveys of profiles STP L1 and STP L4 were conducted through cultivated fields. To varying degrees all of the surveys reflect some cultural modification of the land surface. The profiles are presented in Figure 2.5S.1-46 and are discussed individually as follows:

Profile STP L1

This 1125-ft.-long profile was measured through a cultivated field just inside the site area. The short-wavelength, low-amplitude variability along the profile (i.e., changes in elevation of less than a foot over horizontal distances of tens of feet) is attributed to cultivation of the land surface (Figure 2.5S.1-46). The profile spans an approximately 4-ft.-high, south-facing break in the slope in the upper surface of the Beaumont Formation. The land surface both above (north of) and below (south of) the slope break is subhorizontal, which suggests that the slope break may be a discrete down-to-the-south displacement of an originally subhorizontal to very gently south-dipping surface. The gradient of the break in slope along the surveyed profile is relatively uniform across a horizontal distance of about 480 ft. to 500 ft. (i.e., approximately 4 ft./490 ft.), representing a 0.8% slope or an increase of about 0.5° in the southward dip of the land surface toward the Gulf of Mexico. The surface projection of growth fault Matagorda GMO coincides with the topographic break.

Profile STP L2

This approximately 2000-ft.-long profile was measured along the side of the north-south-trending paved County Road 1095, approximately 6 miles west of STP 3 & 4 (Figure 2.5S.1-45 [References 2.5S.1-7, 2.5S.1-124 and 2.5S.1-151]). Profile STP L2 is smoother and exhibits less short-wavelength variability than STP L1 due to grading and modification of the land surface associated with road construction (Figure 2.5S.1-46). The profile spans an approximately 6.5-ft.-high, south-facing break in the slope in the upper surface of the Beaumont Formation over a horizontal distance of approximately 875 ft. The average gradient of the south-facing slope break along the surveyed profile is about 0.7°, (6.5 ft./875 ft.), representing an increase of about 0.4° in the southward dip of the land surface toward the Gulf of Mexico. The profile documents a steepening of the slope break at a horizontal distance of about 500 ft., which is associated with a patch in the road surface. Based on conversations with Mark Woolridge of the Texas Department of Transportation, the patch repaired road damage caused by a drilling rig (Reference 2.5S.1-154). The profile crosses a small bridge over an irrigation canal just north of the slope break. The land surface is sub-horizontal between distances of about 1000 ft. and 1400 ft., then slopes toward the north, opposite the regional southward gradient toward the Gulf of Mexico. It is unknown to what extent the land surface was modified to create the drainage canal, and thus the true vertical height of the slope break is uncertain. The surface projection of growth fault Matagorda GMO coincides with the topographic break.

Profile STP L3

This profile is slightly over 600 ft. long and was measured along the side of the east-west-trending paved County Road 1095, approximately 7 miles west of STP 3 & 4 (Figure 2.5S.1-45 [References 2.5S.1-7, 2.5S.1-124 and 2.5S.1-151]). The smoothness and lack of short-wavelength irregularity reflects grading and preparation of the land surface for road construction (Figure 2.5S.1-46). The profile spans an approximately 1-ft.-high, south-southeast facing break in the slope in the upper surface of the Beaumont Formation. Given the east-west orientation of the road, the profile is oblique to the trend of

the slope break. The land surfaces above (northwest) and below (southeast) the slope break have similar gradients and are subhorizontal or gently sloping toward the southeast, which suggests that the slope break may represent down-to-the-south deformation of a surface that was originally graded to the Gulf of Mexico. The break in slope is relatively uniform across a horizontal distance of about 180 ft. between horizontal distances of about 250 ft. to 330 ft. The gradient of the slope break along the profile (i.e., approximately 1 ft./180 ft.), represents a 0.6% slope, or an increase of about 0.3° in the southward dip of the land surface toward the Gulf of Mexico. The surface projection of growth fault Matagorda GMO is approximately 13 ft. west of the west end of profile.

Profile STP L4

This approximately 2000-ft.-long profile was measured adjacent to a north-south-trending dirt road along the western side of the STPEGS STP 1 & 2 cooling water reservoir (Figure 2.4S.1-45 [References 2.5S.1-7, 2.5S.1-124, and 2.5S.1-151]). The profile traversed two cultivated fields separated by a dirt road. Profile STP L4 exhibits short-wavelength irregularity similar to that of profile STP L1, which is characteristic of the relatively natural, un-graded land surface compared to that of profiles STP L2 and STP L3 as well as local surface irregularities due to agricultural activities (Figure 2.5S.1-46). There is an abrupt, up-to-the-north increase in land surface elevation of about 2 ft. between horizontal distances of 0 ft. and 500 ft. No anomalous, laterally continuous slope break was observed associated with the up-to-the-north increase in land surface elevation between horizontal distances of 0 ft. and 500 ft. This topographic break most likely reflects the difference in elevation between the two fields and local grading associated with the dirt road between the fields. North of horizontal distance 500 ft., the land surface decreases southward about 0.75 ft. over a horizontal distance of about 1500 ft. Due to the irregularity of the land surface, it is not possible to unequivocally identify a discrete south-facing slope break in the section of the profile between horizontal distances 500 ft. and 2000 ft. Given that the maximum relief on any slope break within this reach is 0.75 ft., there is no south-facing slope break comparable in magnitude (1.5 ft. to about 5 ft.) to those documented in profiles STP L1, STP L2 and STP L3. The average slope between horizontal distances 500 ft. and 2000 ft. along profile STP L4 is 0.05%, or a gradient of 0.03° toward the south. This is an order of magnitude lower than the gradients of the relatively well-defined south-facing slope breaks in profiles STP L1, STP L2, and STP L3. There is no topographic break associated with the surface projection of growth fault Matagorda GMO of STP12I.

Despite the uncertainty in the location of the projection of GMO, which generally encompasses an area greater than the extent of the topographic profiles and extends beyond the ends of the topographic profiles, there is a strong spatial association between the observed, localized down-to-the-south flexure of the land surface and the projection of fault GMO. The additional spatial association between the lineations and the flexure (Figure 2.5S.1-45) as well as the projection of STP12I and the flexure (Figure 2.5S.1-45) provide *prima facie* evidence that the flexure is related to activity along growth fault GMO/STP12I. If the south-facing slope breaks are genetically related to displacement on the fault at depth, then the surface deformation is characterized by broad monoclinal tilting or flexure that is approximately uniform over

horizontal distances ranging from about 180 feet to 500 feet. Evidence for discrete surface fault rupture resulting in a well-defined fault scarp, as is commonly observed along active normal faults in the western United States, was not observed. Monoclinal tilting observed along profiles STP L1, STP L2, and STP L3 is tentatively attributed to fault-propagation folding of the ground surface above the buried tip of growth fault Matagorda GMO and STP12I at depth.

In contrast, profile STP L4 does not exhibit clear evidence for a discrete, well-defined, down-to-the-south break in topography similar to that of profiles STP L1, STP L2, and STP L3. Although it is possible that the slope break at the south end of profile STP L4 is related to movement on growth fault Matagorda GMO and STP12I, it is not part of a spatially extensive and noticeable geomorphic feature. The topographic break between 0 and 500 ft. is attributed to a combination of non-growth-fault related natural variation and cultural modification of the land surface. This interpretation is consistent with the results of explorations described the UFSAR for STP 1 & 2 (Reference 2.5S.1-7), which documented exposures of laterally continuous, undeformed Beaumont Formation strata in shallow excavated exposures along the western margin of the cooling water reservoir.

As shown on Figure 2.5S.1-45 (References 2.5S.1-7, 2.5S.1-124 and 2.5S.1-151), growth fault Matagorda GMO projects beneath the southwestern corner of the cooling water reservoir and is inferred to obliquely cross the southern dike of the reservoir. Given the spatial association between growth fault Matagorda GMO and slope breaks west of the cooling reservoir, the area south of the reservoir was investigated for similar features (Figure 2.5S.1-44). No laterally continuous topographic breaks within this region were observed. An east-west cross section of correlated borehole data was prepared along the southern margin of the reservoir, and was assessed to determine whether there is discernable southwest-side-down offset of textural facies in the Beaumont Formation across the updip projection of growth fault Matagorda GMO (cross section C-C' in Figure 2.5S.1-45 [References 2.5S.1-7, 2.5S.1-124 and 2.5S.1-151] and Figure 2.5S.1-47 [Reference 2.5S.1-155]). The data is from McClelland Engineers (Reference 2.5S.1-155) and was used in the UFSAR for STP 1 & 2 (Reference 2.5S.1-7). The textural facies identified in the boreholes include lenses of sand and clay, which are typical and characteristic of the late Pleistocene Beaumont Formation (Reference 2.5S.1-38). The correlated data show lateral variation and interfingering of the sand and clay facies in the vicinity of the updip projection of the growth fault, but no positive evidence for systematic displacement or offset. Given the extremely low relief across the slope breaks that is tentatively associated with growth fault Matagorda GMO and STP12I to the west (i.e., about 1.5 ft. to 5 ft.), it is possible that comparable displacements at depth would not be discernable if present in cross section C-C'.

2.5S.1.2.4.3 Summary

New subsurface data compiled for the STP 3 & 4 COL (Figure 2.5S.1-42 [References 2.5S.1-29, 2.5S.1-124, 2.5S.1-150, 2.5S.1-151, 2.5S.1-152 and 2.5S.1-153] and Figure 2.5S.1-43 [References 2.5S.1-7, 2.5S.1-124 and 2.5S.1-151]) do not significantly change the state of knowledge regarding the locations of growth faults in

the STP 3 & 4 site area. The most detailed subsurface mapping of growth faults in the site area remains the work documented in the UFSAR for STP 1 & 2 (Reference 2.5S.1-7). The mapping and data listed in Table 2.5S.1-1 are taken from studies that are more regional in scope and thus less detailed at the scale of the site area.

Among the growth faults in the site area not recognized in the UFSAR for STP 1 & 2 but identified within the Geomap data, is fault GMP (Reference 2.5S.1-124), whose surface projection is shown as trending north-northwest at the southern part of the cooling reservoir and is the fault with the closest surface projection to STP 3 & 4 (approximately 1.4 miles) (Figure 2.5S.1-43 [References 2.5S.1-7, 2.5S.1-124, and 2.5S.1-151]). The surface projection of GMP shown in Figure 2.5S.1-43 suggests that the fault could extend north towards the STP 3 & 4 site. However, subsurface relations documented in the Geomap data demonstrate that the fault curves to the west and trends away from the STP 3 & 4 site. Within the Geomap structural contour maps, growth fault GMP is mapped as a short splay of the extensively mapped growth fault GMO that initiates at approximately the same longitude as the STP 3 & 4 site. Within the upper horizon of the Geomap data, GMP is mapped as a splay to the north of GMO that trends westward, subparallel to GMO, for a total distance of approximately 3 miles, ending west of the STP 3 & 4 site. Therefore, the mapping within the upper horizon clearly shows that the fault trends away from and does not approach the STP 3 & 4 site. Within the lower horizon of the Geomap data, however, GMP is only shown as an approximately 1 mile long splay, initiating at the same location and trending predominately northwest. The trace of the fault in the lower horizon does not extend far enough to the northwest to depict the change to a more westerly strike, as documented in the map of the upper horizon.

As described in Subsection 2.5S.1.2.4.2.2.1, the surface projection for any given fault is derived from the location of the fault within both Geomap horizons. Therefore, the extent of the GMP surface projection is limited to the mapped length of GMP as documented in the lower Geomap horizon. Because the mapped extent of GMP in the lower horizon is limited to the short reach trending to the northwest, and does not extend to where the trend bends westward subparallel to GMO, the surface projection of GMP shows only this northwest-trending reach. This short reach accurately reflects the surface projection of GMP over the reach, but it does not reflect the full behavior of GMP evident in the upper horizon data where the fault curves westward and follows the trend of GMO well beyond the longitude of the STP 3 & 4 site. The subsurface Geomap data support the conclusion that fault GMP trends west past the northwestern end of the surface projection shown in Figure 2.5S.1-43 and not towards the STP 3 & 4 site.

The UFSAR for STP 1 & 2 (Reference 2.5S.1-7) also identified several approximately west-southwest-striking growth faults at the latitude of the STP 3 & 4 site footprint at depths ranging from 6000 ft. to 11,000 ft. (i.e., growth faults Matagorda STP12D, STP12E and STP12H). One or more of these structures likely correlates with growth faults Matagorda GML and GMK (Reference 2.5S.1-124), which strike into the site area from the west (Figure 2.5S.1-42 [References 2.5S.1-29, 2.5S.1-124, 2.5S.1-150, 2.5S.1-151, 2.5S.1-152, and 2.5S.1-153]) and are mapped to within approximately 5 miles or less of STP 3 & 4 (Figure 2.5S.1-43 [References 2.5S.1-7, 2.5S.1-124, and

2.5S.1-151]). The growth faults identified within the UFSAR for STP 1 & 2 (Reference 2.5S.1-7) cannot be directly correlated with growth fault GML or GMK because the seismic reflection lines from the UFSAR for STP 1 & 2 (Reference 2.5S.1-7) do not cross the Geomap fault traces for growth faults GML and GMK. However, the reflection lines from the UFSAR for STP 1 & 2 (Reference 2.5S.1-7) combined with the new studies presented here support the conclusion that there are no shallow growth faults that intersect either the site or the cooling reservoir.

The UFSAR for STP 1 & 2 (Reference 2.5S.1-7) also identified several approximately west-southwest-striking growth faults at the latitude of the STP 3 & 4 site footprint at depths ranging from 6000 ft. to 11,000 ft. (i.e., growth faults Matagorda STP12D, STP12E and STP12H). One or more of these structures may be correlative with growth faults Matagorda GMI and GMK (Reference 2.5S.1-124), which strike into the site area from the west (Figure 2.5S.1-42 [References 2.5S.1-29, 2.5S.1-124, 2.5S.1-150, 2.5S.1-151, 2.5S.1-152, and 2.5S.1-153]) and are mapped to within about 4 miles or less of STP 3 & 4 (Figure 2.5S.1-43 [References 2.5S.1-7, 2.5S.1-124, and 2.5S.1-151]). Direct comparison of the UFSAR for STP 1 & 2 (Reference 2.5S.1-7) mapping with the Geomap (Reference 2.5S.1-124) projections in Figure 2.5S.1-43 (References 2.5S.1-7, 2.5S.1-124, and 2.5S.1-151) is problematic. The growth fault locations from the two studies were developed from different datasets using different techniques (see Subsection 2.5S.1.2.4.1.2.2.1).

New topographic profiles and other data acquired for this study provide *prima facie* evidence for very low relief deformation of the upper surface of the Beaumont Formation above growth fault Matagorda GMO and STP12I both outside and just within the site area. The deformation is expressed as south-facing monoclinal flexures with about 1.5 ft. to 6 ft. of total relief over horizontal distances ranging from about 180 ft. to 500 ft. Topographic profile STP L4 surveyed adjacent to the western margin of the cooling water reservoir documents either no deformation above the updip projection of growth fault Matagorda GMO and STP12I, or that any deformation is below the limit of resolution due to the variability in land surface elevation along profile STP L4. These results are consistent with the conclusion of the UFSAR for STP 1 & 2 (Reference 2.5S.1-7), which reported no deformation of laterally continuous stratigraphic contacts along the southwestern margin of the cooling water reservoir above the projection of growth fault Matagorda STP12I.

2.5S.1.2.4.3.1 Conclusions

Compilation of data on growth faults at the scale of the site vicinity and site area for this study demonstrates that no new information has been developed to alter the conclusion of the UFSAR for STP 1 & 2 (Reference 2.5S.1-7) that no growth faults project to the surface through the STP site (Figure 2.5S.1-43 [References 2.5S.1-7, 2.5S.1-124 and 2.5S.1-151]).

There is *prima facie* evidence for localized, low relief tilting of the upper surface of the Beaumont Formation above growth fault Matagorda GMO/STP12I, just within the site area (5-mile radius) yet outside the site (0.6-mile radius). The deformation is characterized by south-down monoclinal flexure of the land surface, and is distributed

across horizontal distances of 180 feet to 500 feet. Data acquired for this study clearly document the absence of discrete surface rupture above growth fault Matagorda GMO/STP12I. Topographic profiles surveyed at intervals over a distance of several miles document significant variability in the magnitude and width of the zone of tilting, suggesting that activity is not uniform along strike. Surface deformation above growth fault Matagorda GMO/STP12I does not approach within the 0.6-mile site radius of STP 3 & 4.

2.5S.1.2.5 Site Area Geologic Hazard Evaluation

No geologic hazards have been identified within the STP site area. No geologic units at the site are subject to dissolution. No deformation zones were encountered in the exploration or excavation for STP 1 & 2, and none have been encountered in the site investigation for STP 3 & 4.

Volcanic activity typically is associated with subduction zones or “hot spots” in the earth's mantle, neither of which are present within the STP site region. Therefore, no volcanic activity is anticipated in the region.

2.5S.1.2.6 Site Engineering Geology Evaluation

2.5S.1.2.6.1 Engineering Soil Properties and Behavior of Foundation Materials

Engineering soil properties, including index properties, static and dynamic strength, and compressibility, are discussed in Subsection 2.5S.4. Evaluation and mapping of the variability and distribution of properties for the foundation bearing soils are included as the excavation is completed.

Settlement monitoring includes analyses performed for the final design.

2.5S.1.2.6.2 Zones of Alteration, Weathering, and Structural Weakness

No unusual weathering profiles have been encountered during the site investigation. No dissolution is expected to affect foundations. Mapping of any noted desiccation, weathering zones, joints, or fractures is performed and evaluated during excavation.

2.5S.1.2.6.3 Deformational Zones

No deformation zones were encountered in the exploration or excavation for STP 1 & 2, and none have been encountered in the site investigation for STP 3 & 4. Excavation mapping and evaluation is required during construction. No capable tectonic sources as defined by RG 1.165 exist in the STP site region. Field investigations for the STP 3 & 4 COL application verify the conclusions from STP 1 & 2 that no growth faults project to the surface through the STP site (Subsection 2.5S.1.2.4.3).

2.5S.1.2.6.4 Prior Earthquake Effects

Studies of the STP 1 and 2 excavation did not indicate any evidence for prior earthquake activity that affected Pleistocene deposits (e.g., paleoliquefaction and lateral spreading). As part of the STP 3 & 4 COLA, additional investigations were

conducted to identify the presence or absence of paleoliquefaction features within the site region.

As described in Sections 2.5S.1 and 2.5S.2, an extensive review of published literature, government agency reports, and other materials was conducted for the STP 3 & 4 COLA. One focus of this review was the identification of any reported liquefaction features within the site region. This review of available literature (e.g., References 2.5S.1-49, 2.5S.1-50, 2.5S.1-158, and 2.5S.1-136) discovered no reported liquefaction features within the site region. The lack of any previously reported liquefaction features, as well as the absence of any moderate to large earthquakes within the site region within the historical record (see discussion in Section 2.5S.2) (e.g., References 2.5S.1-157, 2.5S.1-113, and 2.5S.1-115), suggest that the probability of liquefaction features present within the site region is small.

Despite the small likelihood of any liquefaction features existing within the site vicinity, investigations were carried out for the STP 3 & 4 COLA to identify the presence or absence of paleoseismic features within the greater site area. These investigations include the analysis of stereo-paired aerial photography and field reconnaissance. Analysis of the aerial photography focused on identifying any evidence of liquefaction (e.g., tonal variations from sand ejected during liquefaction, filling of contemporary fissures, and stream bank failure). All potentially anomalous geomorphic features identified in the aerial photos were further investigated (see Figures 2.5S.1-44 and 2.5S.1-45), and none of these features provided evidence of liquefaction.

During geologic field reconnaissance within the greater site area, exposures of Quaternary sediments were investigated for the presence of liquefaction features. The best exposures of sediments within the site vicinity were of the Pleistocene Beaumont Formation and associated younger deposits (Reference 2.5S.1-38) along the banks of the Colorado River. Over 15 miles of riverbank along the Colorado River were investigated within the greater site vicinity for the presence of liquefaction features (see Figure 2.5S.1-44).

Riverbank exposures on both sides of the Colorado River were relatively continuous at the time of the field reconnaissance. Recent flooding and associated high stream flows had removed vegetation and produced fresh river-cut, near-vertical banks several meters high in many places. Because of the recent erosion, the riverbanks generally were well exposed with the exception of some areas with active slumping, man-made bank reinforcement, and undisturbed vegetation.

The riverbank exposures generally consisted of subhorizontal layers of interbedded silts and silty sand, with subordinate layers of coarser material including medium to fine-grained sand. These sandy layers likely correspond to point bar and channel bar deposits associated with well-developed channelbelts along the Colorado River. The sediments exposed in the riverbanks were sufficiently coarse and had low enough fines content to allow for liquefaction to occur during strong ground shaking. In addition, seepage and springs were observed in several locations along the banks indicating that the shallow groundwater conditions necessary for liquefaction also were present.

Exposures were investigated for evidence of sand boils and other cross-cutting relationships typical of sub-surface liquefaction. The laterally continuous, layered stratigraphy was well-suited for identification of the presence or absence of paleo-liquefaction features. No features consistent with liquefaction at depth or near the surface were observed to truncate or cross-cut the laterally continuous, sub-horizontal stratigraphic boundaries between exposed layers indicating an absence of liquefaction.

Exposures also were investigated for the presence of relict lateral spreads, particularly within exposures of buried stream channels distinguished by tabular sand bodies and internal cross-beds. Several major slumps were observed along the Colorado River but these features were associated with recent, wholesale failure of the riverbanks based on the presence of fresh looking margins and translocated vegetation within the headscarp areas of the failures. As such, these features are likely the result of lateral erosion and not strong ground shaking.

Smaller streams and tributaries along the Colorado River within the site vicinity were heavily vegetated and/or inaccessible by boat. The absence of observable outcrops and difficult access precluded examination of many of these secondary waterways during field investigation. However, several streams in the site vicinity were investigated by vehicle and foot access. Where exposures were visible, no evidence for liquefaction was found.

In summary, the investigations undertaken for the STP 3 & 4 COLA uncovered no evidence of prehistoric strong ground shaking (e.g, liquefaction, lateral spreading).

2.5S.1.2.6.5 Effects of Human Activities

Subsidence is known to be the result of withdrawal of fluids such as petroleum and/or groundwater over a long period of time. The weight of the overlying sediments is supported, in part, by the fluids in the underlying rock. The fluid loss in the sand has effects on the interbedded clays because the gradient from the clay into the sand increases and dewaters the clay as well. Lithostatic pressure compact the clays irrevocably so that even if groundwater levels are restored to pre-pumping levels, the clays will not rehydrate. Subsidence is common in many parts of the country with the common connection found in long-term pumping of groundwater from unconsolidated sands and gravels with clay interbeds. Ratzlaff stated that in northwestern Matagorda County, the land surface subsided more than 1.5 ft. due to groundwater withdrawals over a period of 30 years (1943-1973) (Reference 2.5S.1-156).

A general rule of thumb in calculating subsidence is that the compression (ΔB) is equal to the dimensionless storage coefficient (S) multiplied by the change in head (Δf) due to pumping.

$\Delta B = S \times \Delta f$

At STP, S has been determined to range between .0004 to .0005 and the maximum drawdown due to construction dewatering is expected to be 100 ft. Therefore, the maximum anticipated subsidence at STP due to construction dewatering is between

.04 and .05 ft. Because there are other considerations, such as infiltration by storm water, which will replace some of the water in the aquifer, it is unlikely that subsidence will reach these levels.

No mining operations or excessive injection of groundwater has occurred within the site area that can affect geologic conditions. The MCR impoundment does appear to affect groundwater flow direction of the Shallow Aquifer at the STP site, but evidence suggests that this influence in flow direction is localized and effectively controlled by the drainage system on site. A detailed discussion of the MCR and its effect on groundwater is provided in Subsection 2.4S.12.

2.5S.1.2.7 Site Groundwater Conditions

A detailed discussion of groundwater conditions is provided in Subsection 2.4S.12.

2.5S.1.3 References

2.5S.1-1 “Identification and Characterization of Seismic Sources and Determination of Safe Shutdown Earthquake Ground Motion,” United States Nuclear Regulatory Commission (NRC), Regulatory Guide 1.165, March 1997.

2.5S.1-2 “Physical Divisions of the United States,” Fenneman, N.M., and Johnson, D.W., United States Geological Survey, 1946.

2.5S.1-3 “Plate 1: Bathymetric Chart,”, The Gulf of Mexico Basin, v. J, The Geology of North America, Bryant, W. R., and Bryant, J. R., Geological Society of America, 1991.

2.5S.1-4 “USGS Seguin Quadrangle (2000), Houston Quadrangle (1999), Bay City Quadrangle (1999), and Beeville Quadrangle (2000) Topographic Maps (1:250,000),” United States Geological Survey (USGS).

2.5S.1-5 “USGS Port Lavaca Quadrangle (2000) and Freeport Quadrangle (1999) Topographic Maps (1:100,000),” United States Geological Survey (USGS).

2.5S.1-6 “USGS Blessing SE Quadrangle Topographic Map (1:24,000)” United States Geological Survey (USGS), 1995.

2.5S.1-7 STPEGS Updated Final Safety Analysis Report, STP 1 & 2, Revision 13, April 2006

2.5S.1-8 “Geologic map of the United States (exclusive of Alaska and Hawaii),” King, P.B., and Beikman, H.M., United States Geological Survey, 1974.

2.5S.1-9 “Geology of the Conterminous United States at 1:2,500,000 Scale -- A Digital Representation of the 1974 P.B. King and H.M. Beikman Map,” Digital Data Series DDS-11, Schruben, P.G., Arndt, R.E., Bawiec, W.J., King, P.B., and Beikman, H.M., U.S. Geological Survey, 1994.

2.5S.1-10 "Gulf Coast Geology (GCG) Online-Miocene of Southern Louisiana," Data Series 90-A, version 1.0, Huffman, A.C., Kinney, S.A., Biewick, L.R.H., Mitchell, H.R., and Gunther, G.L., United States Geological Survey, 2004.

2.5S.1-11 "Map Showing Geology, Oil and Gas Fields, and Geologic Provinces of the Gulf of Mexico Region," Open File Report 97-470-L, French, C.D., and Schenk, C.J., United States Geological Survey, 2005.

2.5S.1-12 "Physiographic Map of Texas," Bureau of Economic Geology, The University of Texas at Austin, 1996. http://www.lib.utexas.edu/geo/maps.html, accessed April 6, 2007.

2.5S.1-13 "Late Quaternary sedimentation," The Gulf of Mexico Basin: Boulder, Colorado, Geological Society of America, The Geology of North America, v. J, pp. 325-352, Coleman, J. M., Roberts, H. H., and Bryant, W.R., 1991.

2.5S.1-14 "Tectonic evolution of the southern Laurentian Grenville orogenic belt," Geologic Society of America Bulletin, v. 10, pp. 1357-1375, Mosher, S., 1998.

2.5S.1-15 "Kinematic constraints on Rodinia reconstructions from the core of the Texas Grenville Orogen," Journal of Geology, v. 112, pp. 185-205, Reese, J. F., and Mosher, S., 2004.

2.5S.1-16 "Geological Highway Map of Texas," American Association of Petroleum Geologists Map Series 7, Renfro, H.B., Feray, D.E., Dott, R.H., Sr., Bennison, A.P., 1979.

2.5S.1-17 "Probabilistic Seismic Hazard Evaluation at Nuclear Plant Sites in the Central and Eastern United States: Resolution of the Charleston Earthquake Issue," EPRI NP-6395-D, Electric Power Research Institute, April 1989.

2.5S.1-18 "Tectonic inheritance at a continental margin," GSA Today, v. 16, no. 2, pp. 4-11, Thomas, W.A., 2006

2.5S.1-19 "Stratigraphy, sedimentology, and depositional setting of pre-orogenic rocks of the Ouachita Mountains, Arkansas and Oklahoma," The Appalachian-Ouachita Orogen in the United States, v. F-2, The Geology of North America, pp. 575-590, Lowe, D.R., Geological Society of America, 1989.

2.5S.1-20 "Tectonic synthesis of the Ouachita orogenic belt," The Appalachian-Ouachita orogen in the United States, v. F-2, The Geology of North America, pp. 695-728, Viele, G.W., and Thomas W. A., Geological Society of America, 1989.

2.5S.1-21 "Ouachita thrust belt and Arkoma basin," The Appalachian-Ouachita orogen in the United States, v. F-2, The Geology of North America, pp.621-634, Arbenz, J. K., Geological Society of America, 1989.

2.5S.1-22 "Origin and development of the Gulf of Mexico Basin," The Gulf of Mexico Basin, v. J, The Geology of North America, pp.389-444, Salvador, A., Geological Society of America, 1991.

2.5S.1-23 "Plate 6: Cross sections of the Gulf of Mexico Basin," The Geology of North America, v. J, The Gulf of Mexico Basin, Salvador, A., Geological Society of America, 1991.

2.5S.1-24 "Pre-Triassic," The Geology of North America, v. J, The Gulf of Mexico Basin, pp.109-129, Woods, R.D., Salvador, A., and Miles, A.E., Geological Society of America, 1991.

2.5S.1-25 "Plate 5: Stratigraphic correlation chart," The Geology of North America, v. J, The Gulf of Mexico Basin, Geological Society of America, Salvador, A., 1991.

2.5S.1-26 "Plate 3: Structure at base and subcrop below Mesozoic marine section," The Geology of North America, v. J, The Gulf of Mexico Basin, Salvador, A., Geological Society of America, 1991.

2.5S.1-27 "Plate 2: Principal structural features, in The Gulf of Mexico Basin," The Geology of North America, v. J, The Gulf of Mexico Basin, Geological Society of America, Ewing, T. E., and Lopez, R. F., 1991.

2.5S.1-28 "Geologic Map Database of Texas," Open Data Series DS 170, Stoeser, D.B., Shock, N., Green, G.N., Dumonceaux, G.M., and Heran, W.D., United States Geological Survey, 2005.

2.5S.1-29 "Status and trends of wetland and aquatic habitats on Texas barrier islands, Matagorda Bay to San Antonio Bay," White, W.A., Tremblay, T.A., Waldinger, R.L., and Calnan, T.R., 2002. Final Report prepared for the Texas General Land Office and NOAA under GLO contract No. 01-241-R.

2.5S.1-30 "Geologic Atlas of Texas Beeville-Bay City Sheet," Barnes, V.E., Bureau of Economic Geology, University of Texas, 1987.

2.5S.1-31 "Lower Cretaceous" The Geology of North America, v. J, The Gulf of Mexico Basin, pp.181-204, McFarlan, E., Jr., and Menes, L.S., Geological Society of America, 1991.

2.5S.1-32 "Upper Cretaceous," The Geology of North America, v. J, The Gulf of Mexico Basin, p.205-244, Sohl., N.F., Martinez, R.E., Salmeron-Urena, P., and Soto-Jaramillo, F., Geological Society of America, 1991.

2.5S.1-33 "Cenozoic" The Geology of North America, v. J, The Gulf of Mexico Basin, p.245-324, Galloway, W.E., Bebout, D.G., Fisher, W.L., Dunlap, J.B., Jr., Cabrera-Castro, R., Lugo-Rivera, J.E., and Scott, T.M., Geological Society of America, 1991.

2.5S.1-34 "Cenozoic depositional history of the Gulf of Mexico basin," v. 84, no. 11, pp 1743-1774, Galloway, W.E., Ganey-Curry, P.E., Xiang Li, and Buffler, R.T., AAPG Bulletin, 2000.

2.5S.1-35 "Program on Technology Innovation: Assessment of a Performance-Based Approach for Determining Seismic Ground Motions for New Plant Sites," v. 2, Seismic Hazard Results at 28 Sites, EPRI Report TR-1012045, Final Report, Electric Power Research Institute and U.S. Department of Energy, August 2005

2.5S.1-36 "Regional stratigraphy and subsurface geology of Cenozoic deposits, Gulf Coastal Plain, south-central United States," U.S. Geological Survey Professional Paper 1416-G, 34 p. Hosman, R. L., 1996.

2.5S.1-37 "Geology of the Gulf Coast Aquifer, Texas in Proceedings of the Gulf Coast Aquifer Conference, Corpus Christi," Texas Water Development Board Report 365, pp. 23-50, Chowdhury, A.H., and Turco, M.J., 2006.

2.5S.1-38 "Signatures of climate vs. sea-level change within incised valley-fill successions: Quaternary examples from the Texas Gulf Coast," Sedimentary Geology, Volume 190, pp. 177-211, Blum, M. D., and Aslan, A., 2006.

2.5S.1-39 "Seismic hazard Methodology for the Central and Eastern United States (NP-4726)," Electric Power Research Institute (EPRI), 1986.

2.5S.1-40 "The earthquakes of stable continental regions," v. 1, assessment of large earthquake potential, Final Report TR-102261-V1, Johnston, A.C., Coppersmith, K.J., Kanter, L.R., and Cornell, C.A., 1994. Prepared for Electric Power Research Institute (EPRI).

2.5S.1-41 "Earthquakes in the eastern Great Lakes Basin from a regional perspective," Ebel, J.E., and Tuttle, M., Tectonophysics, v. 353, pp. 17-30, 2002.

2.5S.1-42 "Earthquakes and the cratonward limit of Iapetan faulting in eastern North America," Geology, v. 23, pp. 105-108, Wheeler, R.L., 1995.

2.5S.1-43 "Land and Marine Gravity CD-ROMS," Dater, D., Metzger, D., and Hittelman, A., United States Department of Commerce, National Oceanic and Atmospheric Administration, National Geophysical Data Center, 1999.

2.5S.1-44 "The crust under the Gulf of Mexico basin," The Geology of North America: The Gulf of Mexico Basin, v. J, pp. 53-72, Sawyer, D.S., Buffler, R.T., and Pilger, R.H., Geological Society of America, 1991.

2.5S.1-45 "Gravity Anomaly Map of North America (1:5,000,000)" Gravity Anomaly Map Committee, 1987.

2.5S.1-46 "Magnetic Anomaly Map of North America," Open-File Report 02-414 accompanying booklet, Bankey, V., Cuevas, A., Daniels, D., Finn, C.A., Hernandez, I., Hill, P., Kucks, R., Miles, W., Pilkington, M., Roberts, C., Roest, W., Rystrom, V., Shearer, S., Snyder, S., Sweeney, R., and Velez, J., United States Geological Survey, 2002.

2.5S.1-47 "Digital data grids for the magnetic anomaly map of North America," USGS Open-File Report 02-414, Bankey, V., Cuevas, A., Daniels, D., Finn, C.A., Hernandez, I., Hill, P., Kucks, R., Miles, W., Pilkington, M., Roberts, C., Roest, W., Rystrom, V., Shearer, S., Snyder, S., Sweeney, R., Velez, J., Phillips, J.D., and Ravat, D., United States Geological Survey (USGS), 2002.

2.5S.1-48 "Geothermal heat flow in the northeast margin of the Gulf of Mexico," AAPG Bulletin, Volume 89, pp. 821-831, Nagihara, S., and Jones, K.O., 2005.

2.5S.1-49 "Data for Quaternary faults, liquefaction features, and possible tectonic features in the Central and Eastern United States, east of the Rocky Mountain front," Open-File Report 00-260, Crone, A.J., and Wheeler, R.L., United States Geological Survey, 2000.

2.5S.1-50 "Known or Suggested Quaternary Tectonic Faulting, Central and Eastern United States-New and Updated Assessments for 2005," USGS Open-File Report 2005-1336, Wheeler, R.L., United States Geological Survey, 2005.

2.5S.1-51 "Structural framework," The Geology of North America, v. J, The Gulf of Mexico Basin, pp. 31-52, Ewing, T.E., Geological Society of America, 1991.

2.5S.1-52 "The Appalachian-Ouachita orogenic belt: Episodes," v. 10, pp. 259-266, Rodgers, J., 1987.

2.5S.1-53 "The Ouachita orogenic belt," The Geology of North America, v. F-2, The Appalachian-Ouachita orogen in the United States, pp.555-561, Viele, G. W., Geological Society of America, 1989.

2.5S.1-54 "Alleghanian Orogen," The Geology of North America, v. F-2, The Appalachian-Ouachita orogen in the United States, pp. 233-318, Hatcher, R. D., Thomas, W.A, Geiser, P. A., Snoke, A. W., Mosher, S., and Wiltschko, D, V., Geological Society of America, 1989.

2.5S.1-55 "Phanerozoic development of the Llano Uplift," Tectonic history of southern Laurentia: a look at Mesoproterozoic, late-Paleozoic, and Cenozoic structures in central Texas," Austin Geological Society Field Trip Guidebook 24, pp. 25-37, Ewing, T. E., 2004.

2.5S.1-56 "The Appalachian-Ouachita orogen beneath the Gulf Coastal Plain between the outcrops in the Appalachian and Ouachita Mountains," The Geology of North America, v. F-2, The Appalachian-Ouachita orogen in the United States, pp. 537-553, Thomas, W. A., Geological Society of America, 1989.

2.5S.1-57 "Tectonic synthesis of the Ouachita-Marathon-Sonora orogenic margin of southern Laurentia: Stratigraphic and structural implications for timing of deformational events and plate-tectonic model," The Mojave-Sonora megashear hypothesis: Development, assessment, and alternatives, Special Paper 393, pp. 543-596, Poole, F.G., Perry, W.J., Madrid, R.J., and Amaya-Martinez, R., 2005.

2.5S.1-58 "Lithospheric structure of the south-central United States," Geology, v. 20, pp. 335-338, Mickus, K.L., and Keller, G.R., 1992.

2.5S.1-59 "Structure and evolution of the central Gulf of Mexico continental margin and coastal plain, southeast United States," v. 116, pp. 188-199, Harry, D.L., and Londono, J., GSA Bulletin, 2004.

2.5S.1-60 "The Paleozoic margin of North America in west Texas and northern Mexico," Geofisica Internacional, v. 28, pp. 897-906, Keller, G.R., and Dyer, R., 1989.

2.5S.1-61 "Foreland Structure Adjacent to the Ouachita Foldbelt," The Geology of North America, v. F-2, The Appalachian-Ouachita orogen in the United States, pp. 681-688, Denison, R. E., Geological Society of America, 1989.

2.5S.1-62 "Triassic-Jurassic," The Geology of North America, v. J, The Gulf of Mexico Basin, pp.131-180, Geological Society of America, 1991.

2.5S.1-63 "Gulf of Mexico tectonic history: Hotspot tracks, crustal boundaries, and early salt distribution," AAPG Bulletin, v. 89, pp. 311-328, Bird, D., Burke, K., Hall, S.A., and Casey, J.F., 2005.

2.5S.1-64 "Implications of continental crust extension for plate reconstruction: an example from the Gulf of Mexico," Tectonics, Volume 6, pp. 739-755, Dunbar, J.A., and Sawyer, D.S., 1987.

2.5S.1-65 "Continental oceanic crustal transition in the Gulf Coast geosyncline," Ibrahim, A.K., and Uchupi, E., AAPG Memoir, v. 34, pp. 155-165, 1982.

2.5S.1-66 "Jurassic reconstruction of the Gulf of Mexico basin," Marton, G., and Buffler, R.T., International Geology Review," v. 36, pp. 545-586, 1994.

2.5S.1-67 "Early Mesozoic faults of the northern Gulf Coastal Plain in the context of opening of the Atlantic Ocean," Developments in Geotectonics," v. 22, pp. 463-476, Thomas, W.A., 1988.

2.5S.1-68 "Crustal structure in Gulf of Mexico from OBS refraction and multichannel reflection data," v. 65, pp. 1207-1229, Ibrahim, A.K., Carye, J., Latham, G., and Buffler, R.T., AAPG Bulletin, 1981.

2.5S.1-69 "Cenozoic structural evolution and tectono-stratigraphic framework of the northern Gulf Coast continental margin," Salt Tectonics: A Global Perspective, AAPG Memoir 65, pp. 109-151, Diegel, F., Karlo, J., Schuster, D., Shoup, R., and Tauvers, P., 1995.

2.5S.1-70 "Fault number 924, Gulf-margin normal faults, Texas," in Quaternary fault and fold database of the United States, Wheeler, R.L., 1999. http://earthqakes.usgs.gov/regional/qfaults, USGS, accessed January 11, 2007.

2.5S.1-71 "Deep structure of the Texas Gulf passive margin and its Ouachita Precambrian basement: results of the COCORP San Marcos Arch survey," AAPG Bulletin, v. 76, pp. 270-283, Culotta, R., Latham, T., Sydow, M., Oliver, J., Brown, L., and Kaufman, S., 1992.

2.5S.1-72 "Summary of the Balcones fault zone, central Texas: a prominent zone of Tertiary normal faults marking the western margin of the Texas coastal plain," Field Trip Guidebook, v. 24, pp. 81-89, Collins, E., Austin Geological Society, 2004.

2.5S.1-73 "Quaternary alluvial plain construction in response to glacio-eustatic and climatic controls, Texas Gulf coastal plain, Relative Role of Eustacy, Climate, and Tectonism in Continental Rocks," Special Publication 59, pp. 31-48, Blum, M., and Price, D.M., Society for Sedimentary Geology, 1998.

2.5S.1-74 "Tectonic stress field of the continental United States, in Geophysical framework of the continental United States," Geological Society of America Memoir 172, pp. 523-539, Zoback, M.L., and Zoback, M.D., 1989.

2.5S.1-75 "Global patterns of tectonic stress," Nature, v. 341, pp. 291-297, Zoback, M.L., Zoback, M.D., Adams, J., Assumpcao, M., Bell, S., Bergman, E.A., Blumling, P., Brereton, N.R., Denham, D., Ding, J., Fuchs, J., Gay, N., Gregersen, S., Gupta, H.K., Gvishiani, A., Jacob, K., Klein, R., Knoll, P., Magee, M., Mercier, J.L., Muller, B.C., Paquin, C., Rajendran, K., Stephansson, O., Suarez, G., Suter, M., Udias, A., Xu, Z.H., and Zhizhin, M., 1989.

2.5S.1-76 "The release 2005 of the World Stress Map," Reinecker, J., Heidbach, O., Tingay, M., Sperner, B., and Müller, B., Heidelberg Academy of Sciences and Humanities, 2005. www.world-stress-map.org, accessed March, 13, 2007.

2.5S.1-77 "Stress field constraints on intraplate seismicity in eastern North America," Journal of Geophysical Research, v. 97, pp. 1,1761-1,1782, Zoback, M., 1992.

2.5S.1-78 "Statistical trends in the intraplate stress field," Journal of Geophysical Research, v. 100, pp. 20,245-20,255, Coblentz, D.D., and Richardson, R.M., 1995.

2.5S.1-79 "North American plate dynamics," Journal of Geophysical Research, v. 96, pp. 12,201-12,223, Richardson, R.M., and Reding, L.M., 1991.

2.5S.1-80 "State of stress in the northern Gulf Coast," Geology, v. 13, pp. 429-432, Nunn, J., 1985.

2.5S.1-81 "Origin of the lithospheric stress field," Journal of Geophysical Research, v. 109, Lithgow-Bertelloni, C., and Guynn, J.H., 2004.

2.5S.1-82 "North American dynamics and western U.S. Tectonics," Reviews of Geophysics, v. 45, Humphreys, E.D., and Coblentz, D.D., 2007.

2.5S.1-83 "Geodynamics," 2nd Edition, Cambridge University Press, 456 p., Turcotte, D.L., and Schubert, G., 2002.

2.5S.1-84 "Isostasy and the ambient state of stress in the oceanic lithosphere," Journal of Geophysical Research, v. 86, pp. 7,801-7,807, Dahlen, F.A., 1981.

2.5S.1-85 "Gravity anomaly map of the United States," Lyons, P.L., O'Hara, N.W., Aiken, C., Barnes, D.F., Chapman, R.H., Cook, K.L., Dehlinger, P., Ferris, C., Godson, R.H., Hammer, S.I., Hanna, W.A., Holmer, R.C., Kane, M.F., Keller, G.R., Lisle, G.W., McMahon, R.F., Meyers, H., Scheibe, D.M., Schwimmer, P.M., Strange, W.E., Wessels, C.W., and Wilcox, L.E., Society of Exploration Geophysicists, 1982.

2.5S.1-86 "Plate 10: Geophysical maps of the Ouachita Region," The Geology of North America, v. F-2, The Appalachian-Ouachita orogen in the United States, Keller, G.R., Geological Society of America, 1989.

2.5S.1-87 "Marine gravity anomaly from Geosat and ERS 1 satellite altimetry," Journal of Geophysical Research, v. 102, pp. 10,039-10,054, Sandwell, D.T., and Smith, W.H.F., 1997.

2.5S.1-88 "Marine Gravity from Satellite Altimetry," v. 10.1, Sandwell, D.T., and Smith, W.H.F., Scripps Institution of Oceanography, Univ. of California San Diego, 2002. Available at http://topex.ucsd.edu/WWW_html/mar_grav.html, accessed October 14, 2002.

2.5S.1-89 "NGDC Coastal Relief Model, Central and Western Gulf of Mexico," Divins, D.L., and Metzger, D., National Geophysical Data Center, Vol. 4 & 5, 2007, http://www.ngdc.noaa.gov/mgg/coastal/coastal.html, accessed May 2007.

2.5S.1-90 "The Geology of North America: The Gulf of Mexico Basin," v. J, Salvador, A., Geological Society of America, 1991.

2.5S.1-91 "The rotational origin of the Gulf of Mexico based on regional gravity data," AAPG Memoir, v. 34, pp. 115-126, Hall, D.J., Cavanaugh, T.D., Watkins, J.S., and McMillen, K.J., 1982.

2.5S.1-92 "Constraints on the tectonic development of the Gulf of Mexico provided by magnetic anomaly data," Journal of Geophysical Research, v. 99, pp. 7,161-7,175, Hall, S.A., and Najmuddin, I.J., 1994.

2.5S.1-93 "Digital integration of potential fields and geological datasets for plate tectonic and basin dynamic modeling - the first step towards identifying new play concepts in the Gulf of Mexico Basin," Leading Edge, v. 23, pp. 384-389, Jacques, J.M., Price, A.D., and Bain, J.E., 2004.

2.5S.1-94 "The Ouachita System, A Geophysical Overview," The Geology of North America, v. F-2, The Appalachian-Ouachita orogen in the United States, pp. 689-693, Keller, G. R., Kruger, J. M., Smith K., J., and Voight, W. M., Geological Society of America, 1989.

2.5S.1-95 "Extensional evolution of the Gulf of Mexico basin and the deposition of Tertiary deposits," Journal of Petroleum Geology, v. 26, pp. 403-428, Wilson, H.H., 2003.

2.5S.1-96 "Free-air gravity anomaly map of the Gulf of Mexico and its tectonic implications," 1963 edition, Geophysics, v. 30, pp. 102-110, Dehlinger, P., and Jones, B.R., 1965.

2.5S.1-97 "The composite magnetic-anomaly map of the conterminous United States, in The utility of regional gravity and magnetic anomaly maps," Society of Exploration Geophysicists, pp. 1-24, Hinze, W.J., and Zietz, I., 1985.

2.5S.1-98 "Crustal structure of the Texas Gulf coastal plain," v. 86, pp. 807-810, Keller, G.R., and Shurbet, D.H., GSA Bulletin, 1975.

2.5S.1-99 "Interpretation of Crustal Structure from Regional Gravity Anomalies, Ouachita Mountains Area and Adjacent Gulf Coastal Plain," AAPG, v. 70, pp. 667-689, Kruger, J.M., and Keller, G.R., 1986.

2.5S.1-100 "Magnetic total intensity anomalies (west of 90W long.)," Gulf of Mexico, Ocean Margin Drilling Program, Regional Atlas Series, Atlas 6, Sheet 3, Pilger, R.H., Rubin, D.S., and Kauth, L.M., Marine Science International, 1984.

2.5S.1-101 "A new isostatic residual gravity map of the conterminous United States: SEG Technical Program and Expanded Abstracts, SEG 55th Annual Meeting," Simpson, R.W., Jachens, R.C., Saltus, R.W., and Blakely, R.J., Society of Exploration Geophysicists, 1985.

2.5S.1-102 "Northern Gulf of Mexico basement architecture: crustal study to prospect leads (abstract), Society of Exploration of Geophysics 69th Annual Meeting Workshop: The Seismic Link: Reducing Risk," Society of Exploration Geophysicists, Alexander, M., 1999.

2.5S.1-103 "Origin of arches in the northwestern Gulf of Mexico basin," Geology, v. 18, pp. 595-598, Laubach, S.E., and Jackson, M.L.W., 1990.

2.5S.1-104 "Tectonic History of the Llano Uplift," Tectonic History of Southern Laurentia: A Look at Mesoproterozoic, Late-Paleozoic, and Cenozoic Structures in Central Texas, Mosher, S., Austin Geological Society, 2004.

2.5S.1-105 "Middle Proterozoic geologic evolution of Llano uplift, Texas: Evidence from U-Pb zircon geochronometry," GSA Bulletin, v. 104, pp. 494-504, Walker, N., 1992.

2.5S.1-106 "Improving geologic understanding with gravity and magnetic data: examples from Gabon, Nigeria, and the Gulf of Mexico," v. 21, pp. 57-62, Jacques, J.M., Parsons, M.E., Price, A.D., and Schwartz, D.M., First Break, 2003.

2.5S.1-107 "New Insights into Old Data," The Leading Edge, v. 17, pp. 71-72, Fairhead, J.D., and Somerton, I.W., 1998.

2.5S.1-108 "The Ouachita system in the subsurface of Texas, Arkansas, and Louisiana," The Geology of North America, v. F-2, The Appalachian-Ouachita orogen in the United States, pp. 661-672, Nicholas, R., L., and Waddell, D. E., Geological Society of America, 1989.

2.5S.1-109 "The Ouachita system," Publication 6120, Flawn, P.T., Goldstein, A., King, P.B., and Weaver, C.E., University of Texas, Bureau of Economic Geology, 1961.

2.5S.1-110 "Ouachita overthrust: a new look at old data," Contributions to the Geology of South Texas, pp. 453-466, Sams, R., South Texas Geological Society, 1986.

2.5S.1-111 "Seismic stratigraphy of the deep Gulf of Mexico basin and adjacent margins," The Geology of North America, v. J, The Gulf of Mexico Basin, pp. 353-387, Buffler, R.T., Geological Society of America, 1991.

2.5S.1-112"Genetic structural provinces and salt tectonics of the Cenozoic offshore U.S. Gulf of Mexico: a preliminary analysis, in Salt Tectonics: a Global Perspective," Peel, F., Travis, C., and Hossack, J., AAPG Memoir 65, pp. 153-175, 1995.

2.5S.1-113"A compendium of earthquake activity in Texas, University of Texas at Austin, Bureau of Economic Geology," Geological Circular 89-3, Davis, S.D., Pennington, W.D., and Carlson, S.M., 1989.

2.5S.1-114"Seismicity of the central Gulf of Mexico," Geology, v. 10, pp. 103-106, Frohlich, C., 1982.

2.5S.1-115"Texas Earthquakes," University of Texas Press, Austin, 275p. Frohlich, C., and Davis, S.D., 2002.

2.5S.1-116"Putting it all together again," AAPG Explorer, v. 21, Pindell, J., Kennan, L., and Barrett, S., October, 2000.

2.5S.1-117"Foundations of Gulf of Mexico and Caribbean evolution: eight controversies resolved," v. 4, pp. 303-341, Pindell, J., Kennan, L., Stanek, K.P., Maresch, W.V., and Draper, G., Geologica Acta, 2006.

2.5S.1-118"Salt tectonics and listric-normal faulting," The Geology of North America: The Gulf of Mexico basin, v. J, pp. 73-89, Nelson, T., Geological Society of America, 1991.

2.5S.1-119"Fault tectonics of the east Texas basin," Geological Circular, No. 82-4, Jackson, M.P.A., University of Texas at Austin, Bureau of Economic Geology, 1982.

2.5S.1-120"Currie field (Smackover), East Texas Basin" The Jurassic of east Texas: Tyler, Texas, pp. 32-42, Locklin, A.C., East Texas Geological Society, 1984.

2.5S.1-121"Quaternary faulting in east Texas," Geological Circular 80-1, Collins, E., Hobday, D., and Kreitler, C., University of Texas at Austin, Bureau of Economic Geology, 1980.

2.5S.1-122"Geologic Map of Texas," Barnes, V.E., University of Texas at Austin, Bureau of Economic Geology, 1992.

2.5S.1-123"Dynamics of intra-plate compressional deformation: the Alpine foreland and examples," Tectonophysics, v. 252, pp. 7-59, Ziegler, P.A., Cloetingh, S., and van Wees, J.D., 1995.

2.5S.1-124"Upper Texas Gulf Coast Mapping Service maps 327 and 328," Geomap, 2007. Licensed from Geomap Company to William Lettis and Associates, Inc. from February 1, 2007 to January 31, 2008.

2.5S.1-125"Salt domes in the Gulf Coast aquifer, in Aquifers of the Gulf coast of Texas," Texas Water Development Board Report 365, pp. 217-230, Hamlin, H.S., Texas Water Development Board, 2006.

2.5S.1-126"Structural styles of the Wilcox and Frio Growth Fault Trends in Texas: Constraints on Geopressured Reservoirs," Bureau of Economic Geology Report of Investigations No. 154, Ewing, J., Bureau of Economic Geology, 1986.

2.5S.1-127"The Vicksburg Formation of Texas: depositional systems distribution, sequence stratigraphy, and petroleum geology;" AAPG Bulletin, v. 77, pp. 1,942-1,970, Combes, J.M., 1993.

2.5S.1-128"Structural setting and sequence architecture of a growth-faulted lowstand subbasin, Frio Formation, south Texas," Gulf Coast Association of Geological Societies Transactions, v. 54, pp. 237-246, Hammes, U., Loucks, R.G., Brown, L.F., Trevino, R.H., Remington, R.L., and Montoya, P., 2004.

2.5S.1-129"Characterization of fractures in limestones, northern segment of the Edwards Aquifer and Balcones fault zone, central Texas," Gulf Coast Association of Geological Societies Transactions, v. 37, pp. 43-54, Collins, E., 1987.

2.5S.1-130"Horst blocks and regional antithetic faults within the Balcones Fault zone, south-central Texas (Abstract)," Geological Society of America Abstracts with Programs, v. 37, pp. 8-8, Ewing, T.E., 2005.

2.5S.1-131"Structural style in an en echelon fault system, Balcones fault zone, central Texas: geomorphic and hydrologic implications," The Balcones Escarpment, central Texas, pp. 71-76, Grimshaw, T.W., and Woodruff, C.M., Geological Society of America, 1986.

2.5S.1-132"Stream piracy and evolution of the Edwards aquifer along the Balcones escarpment, central Texas," The Balcones Escarpment, central Texas, pp. 77-90, Woodruff, C.M., and Abbott, P.A., Geological Society of America, 1986.

2.5S.1-133"Syntectonic depositional systems within the Mt. Enterprise Fault zone," Lee, G.C., Stephen F. Austin State University, 2005.

2.5S.1-134"Faults and fractures of the Balcones fault zone, Austin region, central Texas," Guidebook 13, Collins, E.W., Laubach, S.E., Vendeville, B.C., and Muehlberger, W.R., 1990.

2.5S.1-135"Seismic Hazard Methodology for the Central and Eastern United States," Tectonic Interpretations, v. 5-10, Electric Power Research Institute (EPRI), July 1988.

2.5S.1-136"Known and suggested Quaternary faulting in the mid-continent United States," Engineering Geology, v. 62, pp. 51-78, Wheeler, R.L. and Crone, A.J., 2001.

2.5S.1-137"On the Modified Mercalli intensities and magnitudes of the 1811-1812 New Madrid earthquakes," Journal of Geophysical Research, v. 105, no. B10, pp. 23,839-23,864, Hough, S.E., Armbruster J.G., Seeber, L., and Hough, J.F., 2000.

2.5S.1-138"Seismic moment assessment of earthquake in stable continental regions - III. New Madrid 1811-1812, Charleston 1886 and Lisbon 1755," A.C., Geophysical Journal International, v. 126, pp. 314-344, Johnston, 1996.

2.5S.1-139"Magnitudes and locations of the 1811-1812 New Madrid, Missouri and the 1886 Charleston, South Carolina, earthquakes," Bulletin of the Seismological Society of America, v. 94, no. 1, pp. 64-75, Bakun, W.H. and Hopper, M.G., 2004.

2.5S.1-140"The enigma of the New Madrid earthquakes of 1811-1812," Annual Review of Earth and Planetary Sciences, v. 24, pp. 339-384, Johnston, A.C. and Schweig, G.D., 1996.

2.5S.1-141"Northern extension of the Tennessee Reelfoot scarp into Kentucky and Missouri," Seismological Research Letters, v. 66, n. 5., pp. 57-62, Van Arsdale, R.B., Kelson, K.I., and Lurnsden, C.H., 1995.

2.5S.1-142"Multiple late Holocene earthquakes along the Reelfoot fault, central New Madrid seismic zone," Journal of Geophysical Research, v. 101, no. B3, pp. 6151-6170, Kelson, K.I., Simpson, G.D., Van Arsdale, R.B., Haraden, C.C., and Lettis, W.R., 1996.

2.5S.1-143"Displacement history and slip rate on the Reelfoot fault of the New Madrid seismic zone," Engineering Geology, v. 55, pp. 219-226, Van Arsdale, R.B., 2000.

2.5S.1-144"The Earthquake Potenial of the New Madrid seismic zone," Bulletin of the Seismological Society of America, v. 92, no. 6, pp. 2080-2089, Tuttle, M.P., Schweig, E.G., Sims, J.D., Lafferty, R.H., Wolf, L.W., and Haynes, M.L., 2002.

2.5S.1-145"Evidence for New Madrid earthquakes in A. D. 300 and 2350 B. C.," Seismological Research Letters, v. 76, no. 4, pp. 489-501, Tuttle, M.P., Schweig, E.S., Campbell, J., Thomas, P.M., Sims, J.D., and Lafferty, R.H., 2005.

2.5S.1-146"Late Pleistocene and Holocene paleoseismology of an intraplate seismic zone in a large alluvial valley, the New Madrid seismic zone, central USA," Tectonophysics, v. 408, pp. 237-264, Guccione, M.J., 2005.

2.5S.1-147"Documentation for the 2002 update of the national seismic hazard maps," United States Geological Survey Open-File Report 02-420, Frankel, A.D., Petersen, M.D., Mueller, C.S., Haller, K.M., Wheeler, R.L., Leyendecker, E.V., Wesson, R.L., Harmsen, S.C., Cramer, C.H., Perkins, D.M., and Rukstales, K.S., 2002.

2.5S.1-148"National seismic-hazard maps: documentation," United States Geological Survey Open-File Report 96-532, Frankel, A.D., Barnhard, T., Perkins, D.M., Leyendecker, E.V., Hanson, K.L., and Hopper, M.G., 1996.

2.5S.1-149"Soil survey of Matagorda County, Texas, United States Department of Agriculture, Natural Resources Conservation Service," Hyde, H.W., 2001. In cooperation with Texas Agricultural Experiment Station.

2.5S.1-150"Reference high-resolution correlation cross sections, Paleogene section, Texas coastal plain," Galloway, W.E., Liu, X., Travis-Neuberger, D., and Xue, L, University of Texas, Bureau of Economic Geology, 1994.

2.5S.1-151"Structural cross sections, Tertiary formations, Texas Gulf coast," 32 plates, Dodge, M.M., and Posey, J.S., University of Texas, Bureau of Economic Geology, 1981.

2.5S.1-152"Structural Cross Section, Miocene Series, Texas Continental Shelf," Morton, R.A., Jirik, L.A., and Foote, R.Q., Texas Bureau of Economic Geology, 1985.

2.5S.1-153"Sediment distribution, bathymetry, faults, and salt diapirs, submerged lands of Texas," McGowen, J.H., and Morton, R., University of Texas, Bureau of Economic Geology, 1979.

2.5S.1-154Woolridge, M. Personal communication, Texas Department of Transportation, March 26, 2007.

2.5S.1-155"Geotechnical Study Cooling Water Reservoir South Texas Project: Volume IV Field and Labratory Data, Embankment, Dikes and Borrow Areas," STP report CSN BR-HL-2245, McClelland Engineers, 1975. Prepared for STPEGS STP 1 & 2.

2.5S.1-156"Land-Surface Subsidence in the Texas coastal Region," Texas Water Development Board Report 272, Ratzlaff, Karl W., 1982.

2.5S.1-157Davis, D.M., Pennington, W., and Carlson, S., 1985, Historical seismicity of the state of Texas: a summary: Gulf Coast Association of Geological Societies Transactions, v. 35, p. 39-44.

2.5S.1-158Wheeler, R.L., 2006, Quaternary tectonic faulting in the eastern United States: Engineering Geology, v. 82, p. 165-186.

Table 2.5S.1-1 Growth Faults within the Greater Site Vicinity

Growth Fault Name [1]	Source [2]	Dip Direction [3]	Depth of Projection (ft.) [4]	Surface Expression [5]
Matagorda BW1	White et al. (Reference 2.5S.1-29)	Unknown	NA	Yes
Matagorda BW2	White et al. (Reference 2.5S.1-29)	South	NA	Yes
Matagorda BW3	White et al. (Reference 2.5S.1-29)	Unknown	NA	Yes
Matagorda BW4	White et al. (Reference 2.5S.1-29)	Unknown	NA	Yes
Matagorda GMA	Geomap (Reference 2.5S.1-124)	South	7,200-8,600	No
Matagorda GMB	Geomap (Reference 2.5S.1-124)	North	7,900-8,030	No
Matagorda GMD	Geomap (Reference 2.5S.1-124)	South	7,300-7,400	No
Matagorda GMF	Geomap (Reference 2.5S.1-124)	South	8,100-9,300	No
Matagorda GMG	Geomap (Reference 2.5S.1-124)	South	7,500-7,900	No
Matagorda GMH	Geomap (Reference 2.5S.1-124)	South	7,000-8,400	No
Matagorda GMI	Geomap (Reference 2.5S.1-124)	South	8,100-8,700	No
Matagorda GMJ	Geomap (Reference 2.5S.1-124)	South	7,300-7,800	No
Matagorda GMK	Geomap (Reference 2.5S.1-124)	South	7,400-7,700	No
Matagorda GML	Geomap (Reference 2.5S.1-124)	South	7,300-7,700	No
Matagorda GMM	Geomap (Reference 2.5S.1-124)	North	7,400-7,600	No
Matagorda GMN	Geomap (Reference 2.5S.1-124)	North	7,700-7,900	No
Matagorda GMO	Geomap (Reference 2.5S.1-124)	South	4,400-5,400	Yes
Matagorda GMP	Geomap (Reference 2.5S.1-124)	West	4,300-4,500	No
Matagorda GMQ	Geomap (Reference 2.5S.1-124)	South	3,900-4,500	No
Matagorda GMR	Geomap (Reference 2.5S.1-124)	North	4,400-4,800	No
Matagorda GMS	Geomap (Reference 2.5S.1-124)	South	4,500-4,800	No
Matagorda GMT	Geomap (Reference 2.5S.1-124)	South	4,400-5,000	No
Matagorda GMU	Geomap (Reference 2.5S.1-124)	South	4,500-5,500	No

Table 2.5S.1-1 Growth Faults within the Greater Site Vicinity (Continued)

Growth Fault Name [1]	Source [2]	Dip Direction [3]	Depth of Projection (ft.) [4]	Surface Expression [5]
Matagorda GMV	Geomap (Reference 2.5S.1-124)	East	4,000-5,300	No
Matagorda GMX	Geomap (Reference 2.5S.1-124)	South	4,000-5,200	No
Matagorda GMY	Geomap (Reference 2.5S.1-124)	South	4,000-4,700	No
Matagorda GMZ	Geomap (Reference 2.5S.1-124)	South	6,600-8,500	No
Matagorda GMAA	Geomap (Reference 2.5S.1-124)	South	7,000-9,400	No
Matagorda GMAB	Geomap (Reference 2.5S.1-124)	South	7,000-9,600	No
Matagorda GMAC	Geomap (Reference 2.5S.1-124)	South	8,000-9,500	No
Matagorda GMAD	Geomap (Reference 2.5S.1-124)	South	8,100-8,600	No
Matagorda GMAE	Geomap (Reference 2.5S.1-124)	South	7,800-8,300	No
Matagorda GMAF	Geomap (Reference 2.5S.1-124)	South	7,500-8,000	No
Matagorda GMAG	Geomap (Reference 2.S5.1-124)	South	6,200-7,500	No
Matagorda GMAH	Geomap (Reference 2.5S.1-124)	South	7,000-7,200	No
Matagorda GMAI	Geomap (Reference 2.5S.1-124)	South	6,700-7,500	No
Matagorda GMAJ	Geomap (Reference 2.5S.1-124)	South	6,400	No
Matagorda GMAK	Geomap (Reference 2.5S.1-124)	South	5,500-6,500	No
Matagorda GMAL	Geomap (Reference 2.5S.1-124)	North	5,500-7,100	No
Matagorda GMAM	Geomap (Reference 2.5S.1-124)	North	5,500-6,400	No
Matagorda GMAN	Geomap (Reference 2.5S.1-124)	West	5,200	No
Matagorda GMAO	Geomap (Reference 2.5S.1-124)	East	5,100	No
Matagorda GMAP	Geomap (Reference 2.5S.1-124)	North	8,100-10,000	No
Matagorda GMAQ	Geomap (Reference 2.5S.1-124)	West	9,600-9,800	No
Matagorda DP1	Dodge and Posey (Reference 2.5S.1-151)	Unknown	7,300	No
Matagorda DP2	Dodge and Posey (Reference 2.5S.1-151)	Unknown	8,900	No

Table 2.5S.1-1 Growth Faults within the Greater Site Vicinity (Continued)

Growth Fault Name [1]	Source [2]	Dip Direction [3]	Depth of Projection (ft.) [4]	Surface Expression [5]
Matagorda DP3	Dodge and Posey (Reference 2.5S.1-151)	Unknown	6,600	No
Matagorda DP4	Dodge and Posey (Reference 2.5S.1-151)	Unknown	6,900	No
Matagorda DP5	Dodge and Posey (Reference 2.5S.1-151)	Unknown	6,400	No
Matagorda DP6	Dodge and Posey (Reference 2.5S.1-151)	South	6,900	No
Matagorda DP7	Dodge and Posey (Reference 2.5S.1-151)	North	6,600	No
Matagorda DP8	Dodge and Posey (Reference 2.5S.1-151)	South	6,400	No
Matagorda DP9	Dodge and Posey (Reference 2.5S.1-151)	South	6,300	No
Matagorda DP10	Dodge and Posey (Reference 2.5S.1-151)	South	5,300	No
Matagorda DP11	Dodge and Posey (Reference 2.5S.1-151)	South	4,700	No
Matagorda DP12	Dodge and Posey (Reference 2.5S.1-151)	South	7,000	No
Matagorda DP13	Dodge and Posey (Reference 2.5S.1-151)	South	7,300	No
Matagorda DP14	Dodge and Posey (Reference 2.5S.1-151)	South	7,000	No
Matagorda DP15	Dodge and Posey (Reference 2.5S.1-151)	South	6,500	No
Matagorda DP16	Dodge and Posey (Reference 2.5S.1-151)	North	5,800	No
Matagorda DP17	Dodge and Posey (Reference 2.5S.1-151)	South	5,200	No
Matagorda G1	Galloway et al. (Reference 2.5S.1-150)	South	8,600	No
Matagorda G2	Galloway et al. (Reference 2.5S.1-150)	South	8,400	No
Matagorda G3	Galloway et al. (Reference 2.5S.1-150)	South	7,200	No
Matagorda G4	Galloway et al. (Reference 2.5S.1-150)	South	6,200	No
Matagorda G5	Galloway et al. (Reference 2.5S.1-150)	South	4,400	No
Matagorda MJF1	Morton et al. (Reference 2.5S.1-152)	South	2,400	No
Matagorda MJF2	Morton et al. (Reference 2.5S.1-152)	South	200	No
Matagorda MJF3	Morton et al. (Reference 2.5S.1-152)	South	800	No

Table 2.5S.1-1 Growth Faults within the Greater Site Vicinity (Continued)

Growth Fault Name [1]	Source [2]	Dip Direction [3]	Depth of Projection (ft.) [4]	Surface Expression [5]
Matagorda MJF4	Morton et al. (Reference 2.5S.1-152)	South	1,000	No
Matagorda MJF5	Morton et al. (Reference 2.5S.1-152)	South	2800	No
Matagorda MM1	McGowen and Morton (Reference 2.5S.1-153)	West	NA	Unknown
Matagorda MM2	McGowen and Morton (Reference 2.5S.1-153)	South	NA	Unknown
Matagorda MM3	McGowen and Morton (Reference 2.5S.1-153)	South	NA	Unknown
Matagorda MM4	McGowen and Morton (Reference 2.5S.1-153)	South	NA	Unknown
Matagorda MM5	McGowen and Morton (Reference 2.5S.1-153)	South	NA	Unknown
Matagorda MM6	McGowen and Morton (Reference 2.5S.1-153)	South	NA	Unknown
Matagorda MM7	McGowen and Morton (Reference 2.5S.1-134)	South	NA	Unknown
Matagorda MM8	McGowen and Morton (Reference 2.5S.1-153)	North	NA	Unknown
Matagorda MM9	McGowen and Morton (Reference 2.5S.1-153)	South	NA	Unknown
Matagorda MM10	McGowen and Morton (Reference 2.5S.1-153)	North	NA	Unknown
Matagorda MM11	McGowen and Morton (Reference 2.5S.1-153)	North	NA	Unknown
Matagorda MM12	McGowen and Morton (Reference 2.5S.1-153)	North	NA	Unknown
Matagorda MM13	McGowen and Morton (Reference 2.5S.1-153)	North	NA	Unknown
Matagorda MM14	McGowen and Morton (Reference 2.5S.1-153)	South	NA	Unknown
Matagorda MM15	McGowen and Morton (Reference 2.5S.1-153)	South	NA	Unknown
Matagorda MM16	McGowen and Morton (Reference 2.5S.1-153)	East	NA	Unknown
Matagorda MM17	McGowen and Morton (Reference 2.5S.1-153)	South	NA	Unknown
Matagorda STP12A	STPEGS UFSAR 1 & 2 (Reference 2.5S.1-7)	South	800-1,700	No
Matagorda STP12B	STPEGS UFSAR 1 & 2 (Reference 2.5S.1-7)	South	7,500-8,000	No
Matagorda STP12C	STPEGS UFSAR 1 & 2 (Reference 2.5S.1-7)	South	8,000-10,000	No
Matagorda STP12D	STPEGS UFSAR 1 & 2 (Reference 2.5S.1-7)	South	11,000-11,500	No

Table 2.5S.1-1 Growth Faults within the Greater Site Vicinity (Continued)

Growth Fault Name [1]	Source [2]	Dip Direction [3]	Depth of Projection (ft.) [4]	Surface Expression [5]
Matagorda STP12E	STPEGS UFSAR 1 & 2 (Reference 2.5S.1-7)	South	10,500	No
Matagorda STP12F	STPEGS UFSAR 1 & 2 (Reference 2.5S.1-7)	South	9,500-13,000	No
Matagorda STP12H	STPEGS UFSAR 1 & 2 (Reference 2.5S.1-7)	North	6,000	No
Matagorda STP12I	STPEGS UFSAR 1 & 2 (Reference 2.5S.1-7)	South	900	Yes

[1] Growth fault naming convention used here.

[2] Source of growth fault location and description.

[3] Direction of growth fault dip.

[4] Depth from which growth fault surface trace was projected. For Geomap (2007) growth faults the range of depths of the upper structural horizon within which the growth fault was identified is given. Growth faults of McGowen and Morton (1979) are traces of growth faults observed to offset strata within 50 feet of the surface, and no projections were made. Growth faults of White et al. (2002) were identified in aerial photographs, so no projections were made. For all other growth faults, the depth is the approximate shallowest observed depth of the fault tip as determined from published cross sections.

[5] Whether or not surficial expression of the growth fault was observed in the field or has been reported by other research.

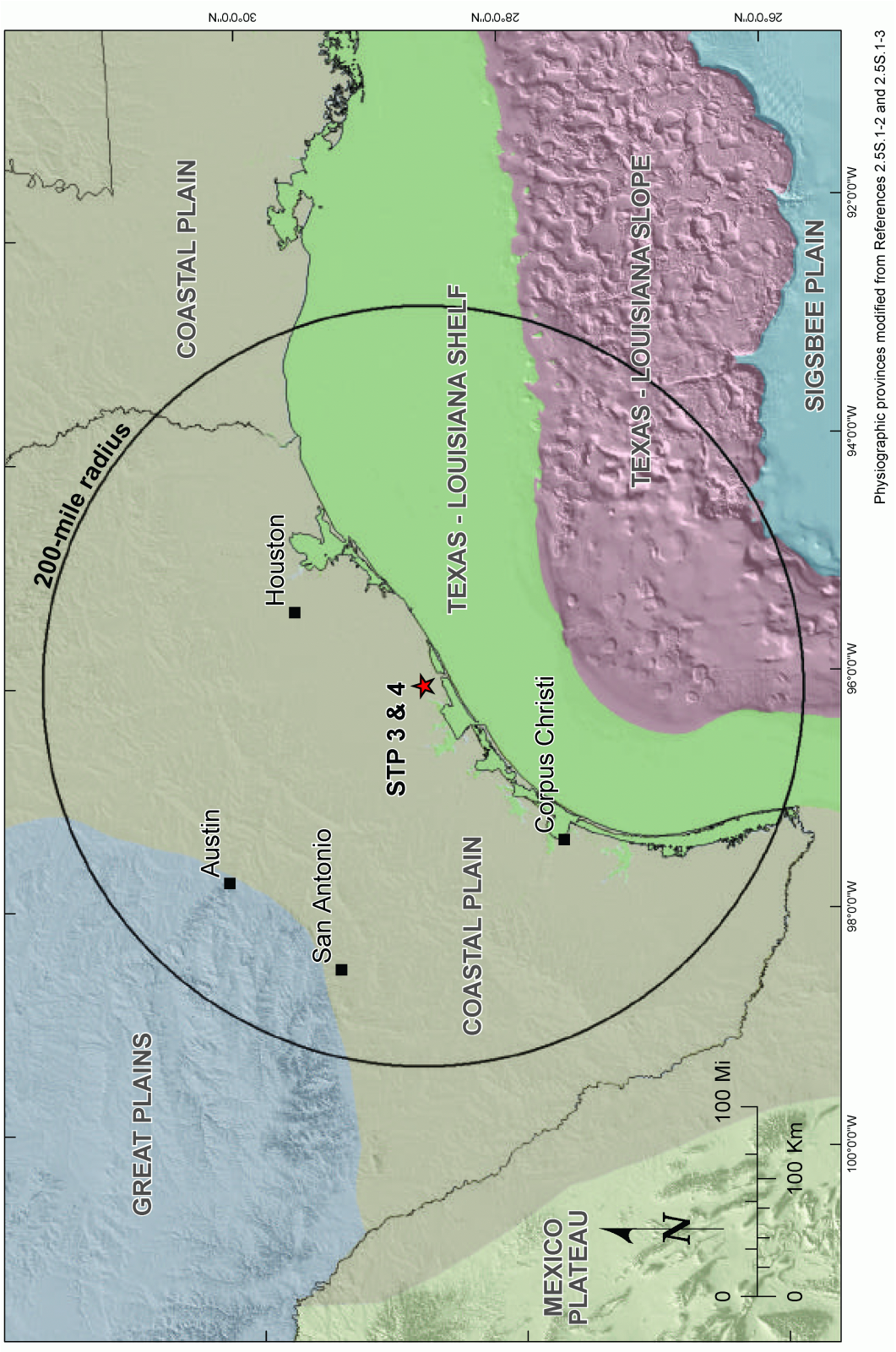

Figure 2.5S.1-1 Map of Physiographic Provinces